

TOPICAL REVIEW • OPEN ACCESS

Structural chirality and related properties in periodic inorganic solids: review and perspectives

To cite this article: Eric Bousquet *et al* 2025 *J. Phys.: Condens. Matter* **37** 163004

View the [article online](#) for updates and enhancements.

You may also like

- [Topological chiral phonons in center-stacked bilayer triangle lattices](#)
Xifang Xu, Wei Zhang, Jiaojiao Wang et al.
- [Phonon chirality tuned through interface transmission in a one-dimensional atomic junction model](#)
Jiaojiao Wang, Hao Chen, Guohuan Xiong et al.
- [Spinless topological chirality from Umklapp scattering in twisted 3D structures](#)
Cong Chen, Xu-Tao Zeng and Wang Yao

Topical Review

Structural chirality and related properties in periodic inorganic solids: review and perspectives

Eric Bousquet^{1,*} , Mauro Fava¹ , Zachary Romestan² , Fernando Gómez-Ortiz¹ , Emma E McCabe^{3,*}  and Aldo H Romero^{2,*} 

¹ Physique Théorique des Matériaux, Q-MAT, Université de Liège, Sart-Tilman B-4000, Belgium

² Department of Physics and Astronomy, West Virginia University, Morgantown, WV 26505-6315, United States of America

³ Department of Physics, Durham University, South Road, Durham DH1 3LE, United Kingdom

E-mail: eric.bousquet@uliege.be, emma.mccabe@durham.ac.uk and aldo.romero@mail.wvu.edu

Received 30 June 2024, revised 15 October 2024

Accepted for publication 14 February 2025

Published 18 March 2025



Abstract

Chirality refers to the asymmetry of objects that cannot be superimposed on their mirror image. It is a concept that exists in various scientific fields and has profound consequences. Although these are perhaps most widely recognized within biology, chemistry, and pharmacology, recent advances in chiral phonons, topological systems, crystal enantiomorphic materials, and magneto-chiral materials have brought this topic to the forefront of condensed matter physics research. Our review discusses the symmetry requirements and the features associated with structural chirality in inorganic materials. This allows us to explore the nature of phase transitions in these systems, the coupling between order parameters, and their impact on the material's physical properties. We highlight essential contributions to the field, particularly recent progress in the study of chiral phonons, altermagnetism, magnetochirality between others. Despite the rarity of naturally occurring inorganic chiral crystals, this review also highlights a significant knowledge gap, presenting challenges and opportunities for structural chirality mostly at the fundamental level, e.g. chiral displacive phase transitions, possibilities of tuning and switching structural chirality by external means (electric, magnetic, or strain fields), whether chirality could be an independent order parameter, and whether structural chirality could be quantified, etc. Beyond simply summarizing this field of research, this review aims to inspire further research in materials science by addressing future challenges, encouraging the exploration of chirality beyond traditional boundaries, and seeking the development of innovative materials with superior or new properties.

* Authors to whom any correspondence should be addressed.



Original Content from this work may be used under the terms of the [Creative Commons Attribution 4.0 licence](https://creativecommons.org/licenses/by/4.0/). Any further distribution of this work must maintain attribution to the author(s) and the title of the work, journal citation and DOI.

Keywords: chirality, crystallography, symmetry, magneto-chiral, chiral phonons, order parameter, phase transition

Contents

| | | | |
|------------------------------------------------------------------------------------------|----|-----------------------------------------------------------------------------|----|
| 1. Definitions of chirality | 4 | Data availability statement | 34 |
| 2. Crystallography and symmetry requirements for chirality in crystals | 5 | Acknowledgments | 34 |
| 3. Chirality and the origins of optical activity | 7 | Appendix A. Chirality in polar nanostructures | 34 |
| 3.1. Chiral axis and absolute chirality | 8 | Appendix B. Chirality in twisted bilayers | 35 |
| 4. Examples of structural chirality and associated phase transitions | 9 | Appendix C. Toroidal Monopole and other potential chirality order parameter | 35 |
| 4.1. MgTi_2O_4 | 9 | C.1. Multipole expansion and electric toroidal monopole | 35 |
| 4.2. K_3NiO_2 | 9 | References | 36 |
| 4.3. CsCuCl_3 | 10 | | |
| 4.4. $\text{Na}_2\text{Ca}_2\text{Si}_3\text{O}_9$ and $\text{Ag}_4\text{P}_2\text{O}_7$ | 11 | | |
| 4.5. $\text{Pb}_5\text{Ge}_3\text{O}_{11}$ | 11 | | |
| 4.6. $\text{Ba}(\text{TiO})\text{Cu}_4(\text{PO}_4)_4$ | 12 | | |
| 4.7. CsSnBr_3 | 12 | | |
| 4.8. Crystallographic databases and data mining for chiral crystals | 13 | | |
| 5. Chirality and its relationship to other properties | 14 | | |
| 5.1. Magnetism | 14 | | |
| 5.1.1. Magneto-Optical phenomena | 14 | | |
| 5.1.2. Magnetic chirality | 15 | | |
| 5.1.3. Electronic magneto chiral anisotropy (eMChA) | 15 | | |
| 5.1.4. Languite $\text{Ba}_3\text{NbFe}_3\text{Si}_2\text{O}_{14}$ | 16 | | |
| 5.1.5. MnSb_2O_6 | 16 | | |
| 5.1.6. $\text{Cr}_{1/3}\text{NbS}_2$ | 17 | | |
| 5.1.7. MnSi | 17 | | |
| 5.1.8. Mn_3Sn | 18 | | |
| 5.1.9. $\text{CaMn}_7\text{O}_{12}$ | 18 | | |
| 5.1.10. BaCoSiO_4 | 19 | | |
| 5.1.11. Altermagnetism | 19 | | |
| 5.2. Topological chiral materials | 20 | | |
| 5.3. Electric properties | 21 | | |
| 5.4. Strain | 23 | | |
| 6. Chiral phonons | 23 | | |
| 7. Chiral order parameter and control of structural chirality | 25 | | |
| 7.1. Definition of a chiral order parameter | 26 | | |
| 7.1.1. Enantioselectivity mediated by physical effects | 26 | | |
| 7.2. Chirality coupled with other order parameters | 27 | | |
| 7.2.1. Coupling with other structural deformations | 28 | | |
| 7.2.2. Coupling with strain | 28 | | |
| 7.2.3. Coupling with magnetism | 29 | | |
| 7.2.4. Coupling with electronic degrees of freedom | 29 | | |
| 7.2.5. Additional sources of chirality inversion through lasers | 29 | | |
| 8. Chirality measure and quantification | 30 | | |
| 9. Discussion and perspectives | 32 | | |
| 10. Conclusion | 33 | | |

‘C’est la dissymétrie qui crée le phénomène (dissymmetry creates the phenomenon)’,
Pierre Curie [1]

Our left and right hands are prototypical examples of chiral objects, as they are non-superimposable mirror images of each other. It is from this observation that the name ‘handedness’ was historically given to define this mirror image property and the term chirality was coined for the first time by Lord Kelvin in 1894 [2–4] as it is constructed from the Greek word *keir* = hand. Chirality emerges from a structure’s specific symmetry characteristics, or the lack of them, which reflects the impossibility of an object coincident with its mirror reflection.

The history of chirality is marked by significant milestones, from the early observations of optical activity to its profound implications in various scientific disciplines, including chemistry, biology, and medicine [7, 8], some selected events are shown in figure 1. Jean-Baptiste Biot first observed the rotation of plane-polarized light by chiral substances in 1812 [9] and in 1848, Louis Pasteur suggested a molecular origin for this phenomenon [2, 3, 10]. After this observation on crystal chirality, Pierre Curie highlighted the fundamental link between physical properties and the crystal structure and symmetry of materials [1]. ‘Dissymmetry’ refers to the lack of improper rotation symmetry elements, which is the formal requirement for chirality; this was perhaps expressed more tangibly by Lord Kelvin in terms of the non-superimposable nature of mirror images of chiral objects [4] (such as left and right hands, specific molecules and crystals, see figure 2). Hence, Pasteur’s crucial breakthrough became the foundation of molecular and crystal chirality and led to many discoveries in material science, physics, chemistry, and biology. The term ‘chirality’ itself was coined by Lord Kelvin in 1894 [11] while different enantiomers or diastereomers of a compound were formerly called optical isomers due to their different optical properties. Initially, chirality was considered restricted to organic chemistry, but further advancements in the field overthrew this misconception. Chirality was again discussed mainly around 1891 when Emil Fischer published his famous paper concerning the configuration of glucose and its isomers, an article dealing with the stereochemistry of the monomeric building block glucose, a real milestone [12]. This led to a recognition of the importance of molecular chirality in

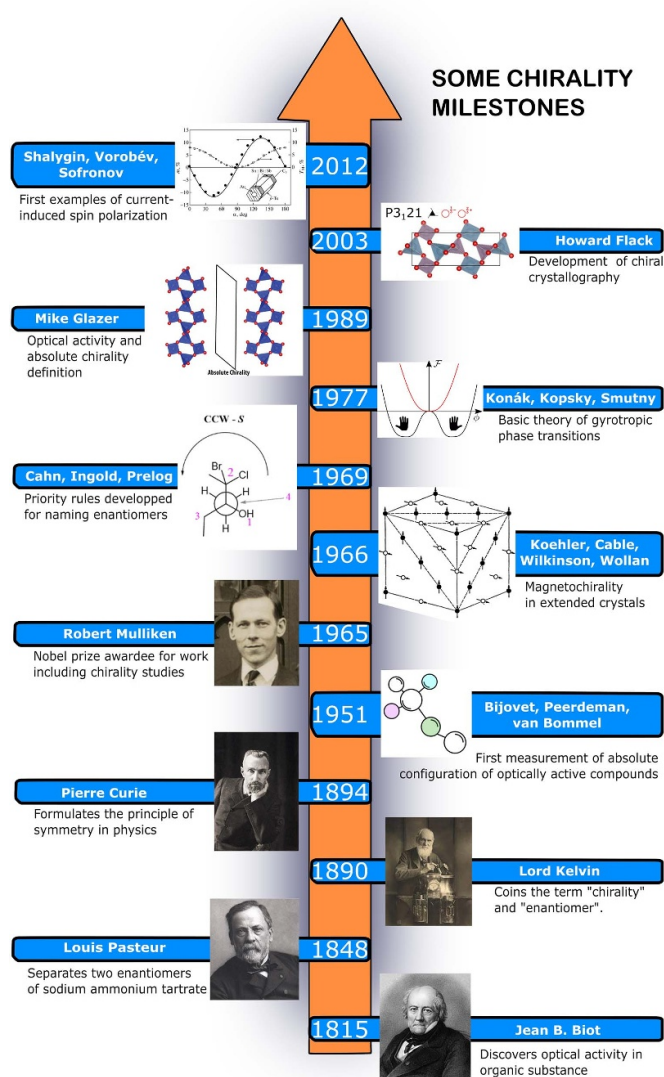


Figure 1. Timeline sketch highlighting important contributions to chirality and structural chirality. (1966) Reprinted figure with permission from [6], Copyright (2015) by the American Physical Society. (1984) This [Pierre Curie] has been obtained by the author(s) from the Wikimedia website, where it is stated to have been released into the public domain. It is included within this article on that basis. (1848) This [Louis Pasteur] has been obtained by the author(s) from the Wikimedia website, where it is stated to have been released into the public domain. It is included within this article on that basis. (1815) This [Jean Baptiste Biot] has been obtained by the author(s) from the Wikimedia website, where it is stated to have been released into the public domain. It is included within this article on that basis. (1890) This [Sir William Thomson, Baron Kelvin] has been obtained by the author(s) from the Wikimedia website, where it is stated to have been released into the public domain. It is included within this article on that basis. (1965) This [Mulliken, Robert 1929 Chicago] has been obtained by the author(s) from the Wikimedia website, where it is stated to have been released into the public domain. It is included within this article on that basis. (2012) Reproduced from [5], with permission from Springer Nature. The other panels at 2003, 1989, 1977, 1969 and 1951 are original figures.

biological systems and the concept of homochirality, a term introduced by Kelvin in 1904 [13]. Homochirality describes a process or system's preference for one enantiomer over the other, and it has significant implications for the origin of life and the emergence of biological homochirality [14]. Indeed, the concept of chirality is so crucial and fundamental in natural sciences that it appears at the root of many diverse fields like cosmology, particle physics, astrophysics, chemistry reactions, liquid crystals, optics, medicine or life itself; chirality is a trans-disciplinary property which manifests at any length scale in nature [15].

Despite its broad interest and extensive study in biology, chemistry, and pharmaceutical medicines, chirality is relatively under-explored in solid-state extended crystals. Some seminal works exploring the origins of optical activity explained chirality in terms of helices in the crystal structures of extended solids [16]. This insight gave a much deeper understanding of the optical activity and absolute configuration of chiral materials (e.g. α -TeO₂ [17], KLiSO₄ [18] or α -LiIO₃ [19]) but also illustrated the challenges in determining the absolute configuration of a material and therefore understanding its consequences for physical properties. A recent revival of chirality studies has taken place in high-impact topics like topological insulators [20–22], spin-Hall effect [23], spin/orbit chirality [24], Skyrmions [25, 26] or valleytronics [27], i.e. mostly linked to the electrons and their spins (e.g. fermions). This clearly shows that the shape of the electronic structure of chiral materials can be indirectly linked to chiral structural distortions [22], i.e. the amplitude of the structural distortion from achiral to chiral phases can dictate the electronic band dispersion and density of states. Still, these latter are not dependent on the handedness and, hence, are not chiral [28]. On the other hand, in topological materials, the Berry curvature of the electronic structure is a hint of the topology and it is linked to handedness, though it cannot be a measure of the chirality itself [28]. Another aspect of this revival is the very recent observations of chiral phonons (bosons) in 2D materials [29–31], in kagome lattices [32] or in the potential for orbital magnetic moments to be carried by chiral phonons [33]. Studies of bulk chiral multiferroics [34, 35] or superlattices [36] have been carried out, but their findings have yet to be applied widely concerning chirality. A very recent review (that became available while our manuscript was under review) explores the chiral structures adopted by naturally-occurring minerals [37].

Chirality is critical to developing and understanding the properties of these new and technologically important functional materials. These recent developments have motivated this review in which we aim to discuss the state of the art of crystal chirality at the structural level and the consequences for physical properties, highlighting the related shortcomings in our understandings/widespread applications and posing open questions of high interest for materials science and technological applications. This paper is focused on bulk inorganic

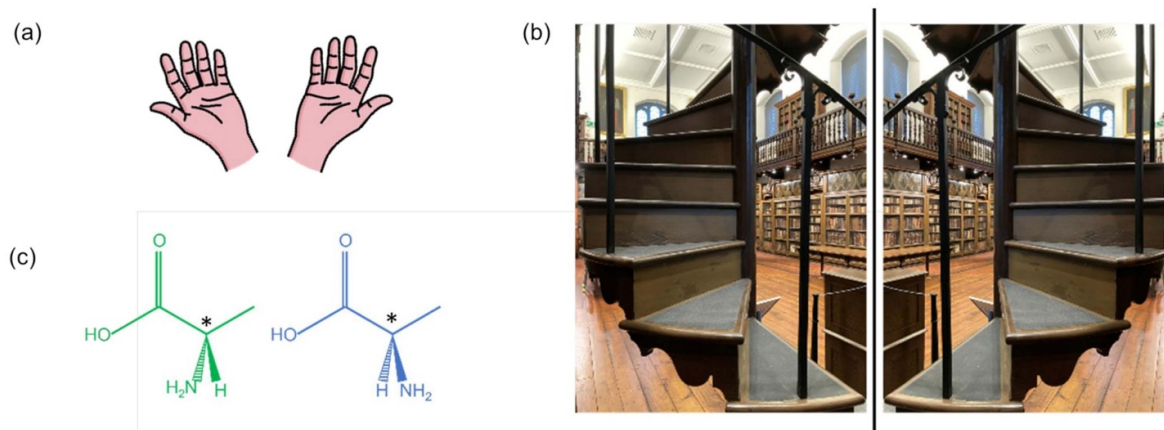


Figure 2. Illustration of the chiral nature of (a) left and right hands, (b) a spiral (helical) staircase (left) and its mirror image (right) (Cosin's Library, Durham University); helices are hallmarks of structural chirality (section 3), and (c) L- (green) and D- (blue) enantiomorphs of alanine (an essential amino acid) with chiral carbon noted *.

periodic chiral crystals, e.g. we will not address chirality in molecular, hybrid [38, 39], or biological systems or at surfaces [40] or in nano-hetero structures [41–45] or in 2D materials [46], despite the importance of chirality in these fields. Here, we focus on chiral bulk periodic inorganic crystals and their related response properties.

We will start this review with a first section looking at how chirality is defined in different fields of research (section 1). In the second section (section 2), we give an overview of the general symmetry requirements in periodic solids as viewed through group theory and crystallography, with the distinction between crystals described by a chiral and enantiomorphic space group, and chiral crystals that are not described by one of these groups (Sohncke groups). Because chirality is intimately linked to optical activity, we dedicate the following section to the field of optical activity (section 3). After these general overviews, we will give a few examples of structural chirality and associated structural phase transitions (section 4) to illustrate the key concepts described in these sections. We also review the chiral crystals reported in existing inorganic crystal structure databases (ICSDs), demonstrating the relative scarcity of these inorganic chiral crystals and possible explanations for this. This leads us on to explore the different responses of chiral crystals under applied magnetic fields (magneto chirality, chiral magnetostriction, chiral magnetogyraton, etc), applied electric fields (electroporation, gyrotropy), and strain in section 5. In each case, we will describe several crystal examples to illustrate the different responses that can be observed. Structural chirality can naturally be extended to phonons that carry chirality, for which we dedicate an entire section (section 6) with all the associated and unique properties that emerge from them. This allows us to consider displacive (and order-disorder) chiral phase transitions and, hence, how a chiral order parameter could be defined together with possibilities to control and flip chirality (ferrochirality) in section 7. Afterward (section 8), this notion of a chiral order parameter and displacive chiral phase transitions will bring us to discuss the open question regarding the quantification and measure of chirality in a periodic solid.

Lastly, before concluding remarks, we give some original and unexplored perspectives and properties of chiral crystals that would be promising and appealing to explore further in section 9.

We note that a review on chirality in the solid state was recently published by Fecher *et al* [28]. Its focus on chiral vs achiral space groups gives an excellent overview of the chiral structures of some elements and binary systems (as well as some more complex materials) and some consequences for electronic structure. Our review builds on this and goes beyond it, discussing structural phase transitions, the possibility of tuning chirality by applied fields, chiral phonons, quantification of chirality, and the consequences for topological and electronic structures. As such, these reviews are somewhat complementary, and their timing reflects the current interest in chiral extended solids.

1. Definitions of chirality

Given the wide-ranging significance of chirality across numerous branches of physics, multiple definitions have been established, each tailored to the particular field of study. While historically intertwined, it is now clear that chirality and handedness convey separate concepts. As outlined in the introduction, chirality refers to the lack of mirror symmetry in an object. Handedness, however, deals with categorizing these non-superimposable chiral entities into right or left orientations. To respect this distinction, mainly when referring to the traditional use of 'handedness' raised by Lord Kelvin it is advisable to use quotation marks, as we will do in this review.

In this section, we shall discuss the different interpretations of chirality used in physics aiming to clarify and differentiate them, thus outlining the specific focus and scope of this review.

For instance, chirality is often encountered in magnetism and magnetic materials [47, 48]. A paradigmatic example is the monoaxial helimagnetic order (along the c axis) with associated Dzyaloshinskii–Moriya (DM) energy gain reads $\mathbf{D} \cdot (\mathbf{S} \times \nabla_j \mathbf{S})$ [49]. Since \mathbf{D} and $\mathbf{S} \times \nabla_j \mathbf{S}$ are (time-even) axial

and polar vectors respectively, their product can constitute a chiral quantity. Similarly, a vector chirality κ can be defined as the sum of the cross products of neighboring spins,

$$\kappa_{ij} = S_i \times S_j. \quad (1)$$

The resulting vector is helpful to quantify the chirality of a group or network of spins [50]. However, this vector chirality may not be a good indication of proper chirality [51–54] (and instead reflects ‘false chirality’ in the notation of Barron; it is even concerning time-reversal symmetry.) [54]. Nevertheless, since it reflects the spin dynamics, it can give insight into the spin current and other transport properties (see below) [52, 55, 56]. On the other hand, scalar spin chirality χ_{ijk} is defined as follows:

$$\chi_{ijk} = S_i \cdot (S_j \times S_k) \quad (2)$$

and can be thought of in terms of the solid angle between three neighboring spins. It is non-zero for non-co-planar spin arrangements and changes signs under time reversal but is invariant under spin rotation [57] (important for coupling to polarization in multiferroics) [58]. This language is useful for describing, for example, the spin arrangement with uniform scalar chirality of the spin ice arrangement of Pr^{3+} moments $\text{Pr}_2\text{Ir}_2\text{O}_7$ and its anomalous Hall effect (AHE) [59].

In other disciplines like particle physics, chirality assumes a more mathematical characterization. There, particle chirality is discerned through its transformation within either a right- or left-handed representation of the Minkowski space-time isometries [60]. Furthermore, a clear differentiation between helicity, defined as the projection of a particle’s spin in the direction of its motion, and chirality is delineated. For massless particles, both definitions coincide, and handedness and chirality are thus equivalent. Recently, some authors have leveraged this precise definition of helicity, employing Pauli matrices to mathematically describe chirality in odd-frequency Cooper pairs [61], as well as to quantify chirality polarizations in topological insulators and superconductors [62]. Furthermore, in [63] this definition of the helicity operator has been extended to the space of solutions of Fourier-transformed Maxwell’s equations expressed as $\frac{1}{k} \nabla \times$. Subsequently, they achieved a general distinction between enantiomers through an investigation of light–matter interaction.

Lastly, in topological materials, chiral crystals are identified as belonging to one of the 65 Sohncke space groups, which exclusively contain orientation-preserving operations, allowing them to be classified by a specific handedness. In these space groups, structural chirality imbues the materials with various intriguing properties, including natural optical activity (NOA), negative refraction in metamaterials, non-reciprocal effects like magneto chiral birefringence of light or electronic magneto chiral anisotropy, and the formation of chiral magnetic textures such as helices and skyrmions. As we discuss

in this review, the idea of handedness should not be identified as absolute chirality and the existence of enantiomorphic pairs. For example, Schröter *et al* [20] the presence of Weyl fermions in recently discovered Weyl semimetals (WSMs) are discussed, where the crystal structure and the electronic wavefunctions exhibit chirality at point-like two-band crossings of the quasiparticle dispersion, and chirality is used in the sense of handedness.

On the other hand, in crystallography and condensed matter physics, which will be the focus of this review, a more geometric approach akin to that employed in chemistry has been adopted. Under this framework, a crystal is deemed chiral if it cannot be perfectly overlaid onto its mirror image. This requires the object to be ‘dissymmetric’, i.e. lacking proper rotation symmetry elements, as discussed in section 2. Additionally, a distinction between handedness, rotational direction, and chirality has been elucidated, as extensively discussed in section 8. Subsequently in section 2, we will explore the prerequisites of symmetry for a crystal to exhibit chirality and detail experimental methodologies for their characterization in the ensuing sections. In section 7 we shall also discuss different sources of chirality as according to Hlinka, chirality may also arise as the product between a vector \mathbf{V} and an axial \mathbf{A} representation. Consequently, it is reasonable to consider such a product as an interesting quantity to track chirality.

2. Crystallography and symmetry requirements for chirality in crystals

Given the importance of chirality in extended solids for functionality, relatively little attention has been paid to this ‘structural chirality’ especially compared with molecular systems with discrete point symmetry. The formal definition of chirality in terms of dissymmetry given by Curie [1] is worth expanding upon: whether considering point group or space group symmetry, this requirement means the object must possess no improper rotation symmetry elements. Mirror planes and centers of inversion symmetry can be described by improper rotations (e.g. considering the operations of crystallographic space groups, the inversion operation could be described by a $\bar{1}$ rotation-inversion operation; the mirror plane by a $\bar{2}$ roto-inversion operation) [64], leading to the (often used but incomplete) statement that a requirement for chirality is the absence of mirror planes and inversion symmetry. A consequence of this lack of improper rotation symmetry elements is that when two chiral objects (referred to as enantiomorphs in extended systems) are considered, their mirror images are non-superimposable, hence the ‘handedness’ referred to by Lord Kelvin [4].

Crystallographic symmetry operations can be categorized into those that preserve handedness (i.e. map a right-handed helix onto a right-handed helix) referred to as ‘operations of the first kind’ and those that reverse handedness (i.e. map a right-handed helix onto a left-handed helix) ‘operations of the

Table 1. Acentric crystal classes compatible with optical activity; the 65 Sohncke space groups are highlighted in grey; the 22 enantiomorphic (chiral) space groups are listed in the right-hand column.

| Classes compatible with optical activity | | |
|------------------------------------------|-------------------------------------------------------------------------------------------------------------------------------------------------------------------------------------------------------------------------------------------------------------------------------------|----------------------------------------------------------------------------------------------------------------------------------------------|
| $\bar{4}$ | | |
| m | | |
| $mm2$ | | |
| $\bar{4}2m$ | | |
| Classes compatible with chirality | Non-enantiomorphic space groups | Enantiomorphic (chiral) space groups |
| 1 | <i>P</i> 1 | |
| 2 | <i>P</i> 2, <i>P</i> 2 ₁ , <i>C</i> 2 | |
| 3 | <i>P</i> 3, <i>R</i> 3 | <i>P</i> 3 ₁ , <i>P</i> 3 ₂ |
| 4 | <i>P</i> 4, <i>P</i> 4 ₂ , <i>I</i> 4, <i>I</i> 4 ₁ | <i>P</i> 4 ₁ , <i>P</i> 4 ₃ |
| 6 | <i>P</i> 6, <i>P</i> 6 ₃ | <i>P</i> 6 ₁ , <i>P</i> 6 ₅ , <i>P</i> 6 ₂ , <i>P</i> 6 ₄ |
| 422 | <i>P</i> 422, <i>P</i> 42 ₁ 2, <i>P</i> 4 ₂ 22, <i>P</i> 4 ₂ 2 ₁ 2, <i>I</i> 422, <i>I</i> 4 ₁ 22 | <i>P</i> 4 ₁ 22, <i>P</i> 4 ₃ 22 <i>P</i> 4 ₁ 2 ₁ 2, <i>P</i> 4 ₃ 2 ₁ 2 |
| 222 | <i>P</i> 222, <i>P</i> 222 ₁ , <i>P</i> 2 ₁ 2 ₁ 2, <i>P</i> 2 ₁ 2 ₁ 2 ₁ , <i>C</i> 222, <i>C</i> 222 ₁ , <i>F</i> 222, <i>I</i> 222, <i>I</i> 2 ₁ 2 ₁ 2 ₁ | |
| 622 | <i>P</i> 622, <i>P</i> 6 ₃ 22 | <i>P</i> 6 ₁ 22, <i>P</i> 6 ₅ 22, <i>P</i> 6 ₂ 22, <i>P</i> 6 ₄ 22 |
| 32 | <i>P</i> 312, <i>P</i> 321, <i>R</i> 32 | <i>P</i> 3 ₁ 12, <i>P</i> 3 ₂ 12 <i>P</i> 3 ₁ 21, <i>P</i> 3 ₂ 21 |
| <i>T</i> | <i>P</i> 23, <i>F</i> 23, <i>I</i> 23, <i>P</i> 2 ₁ 3, <i>I</i> 2 ₁ 3 | |
| <i>O</i> | <i>P</i> 432, <i>F</i> 432, <i>I</i> 432, <i>P</i> 4 ₂ 32, <i>F</i> 4 ₁ 32, <i>I</i> 4 ₁ 32 | <i>P</i> 4 ₁ 32, <i>P</i> 4 ₃ 32 |

second kind' [65]. Of the 230 crystallographic space groups, 165 contain improper symmetry operations (operations of the second kind) and describe achiral crystals. An achiral crystal described by one of these 165 space groups could be grown from a racemic mixture (i.e. a mixture containing both enantiomer forms), and the improper rotation operations of the space group would relate the two enantiomeric molecules in the crystal structure, giving a structure with no overall chirality [66].

The Sohncke groups include 11 pairs of enantiomorphic space groups, i.e. 22 chiral space groups (table 1). These chiral space groups are characterized by each containing a screw axis of the form n_p or n_{n-p} (but not both!) where $p \neq \frac{n}{2}$ [66].

For example, of the cubic class *O*, space groups *P*4₁32 and *P*4₃32 are an enantiomorphic pair containing 4₁ and 4₃ screw axes, respectively. Space group *P*4₂32 does not have an enantiomorphic pair: it contains a 4₂ screw axis and $4_{(4-2)} = 4_2$, and so opposite enantiomorphic structures would be described by the same space group. Combining the 4₁ screw axis with centering (e.g. *F*, *I*) gives the 4₃ axis, so these two screw axes of opposite handedness coexist, incompatible with chirality. Hence, space groups *I*4₁32 and *F*4₁32 are not enantiomorphic [66].

These screw axes of opposite handedness, giving helices in the crystal structure, are a hallmark of the structures described by these 22 chiral symmetries—so much so that developing spirals at the nanoscale in inorganic materials is a recent development towards preparing functional chiral materials [67].

A necessary consequence for functional materials using chirality, is that the crystal packing in structures described by one of the 22 enantiomorphic space groups is chiral, meaning that either chiral or achiral objects (molecules or structural building units) can be packed in a chiral fashion (i.e. about one of the chiral helices) to give a chiral crystal [65, 66]. The term 'structural chirality' describes this chirality due to the crystal packing, distinguishing it from any chirality inherent in a discrete object (e.g. a molecular crystal made of chiral molecular building blocks) [68]. A pair of enantiomorphic space groups will describe the two enantiomorphs of opposite chirality for the same chemical composition and stoichiometry.

The remaining 43 Sohncke space groups that are not enantiomorphic will preserve the chirality of a chiral object (e.g. pack a chiral object such as a molecular enantiomorph) without symmetry operations generating the opposite enantiomorph, giving a chiral crystal. However, the packing in these 43 Sohncke space groups will not give chirality for achiral

objects. Switching the sense of chirality of a crystal described by one of these 43 non-enantiomorphic Sohncke space groups does not change the space group symmetry; two equivalent crystals of opposite chirality are described by the same space group (see, for example, $\text{Pb}_5\text{Ge}_3\text{O}_{11}$ described in section 4).

3. Chirality and the origins of optical activity

Chirality and optical activities are intimately linked. Indeed, the history of chirality dates back to the early 19th century, when the first observation of optical activity, the ability of a chiral substance to rotate the plane of polarization of light, was made by the French physicist Jean-Baptiste Biot in 1812 [69]. He discovered that certain organic substances, such as tartaric acid and its salts, could rotate the plane of polarized light [9]. A similar observation was reported the year before by Arago [70], who noticed that polarized sunlight gave color changes on an image when an analyzer crystal was rotated. However, the significance of this discovery was not recognized at the time because of the lack of a microscopic mechanism for the phenomenon. Indeed, at that time, the atomic theory of matter was still under development, and the concept of molecular structure was not yet fully elaborated. The significance of optical activity went beyond a mere curiosity in the interaction of light with matter, pointing towards a fundamental asymmetry in nature at the molecular level. Pasteur's work, some decades later, demonstrated the connection between the rotation of polarized light and the molecular structure of the substances causing this rotation [69]. Pasteur's separation of the two forms of tartaric acid crystals and his subsequent experiments showed that the ability to rotate light was related to the shape of the molecules and their three-dimensional (3D) arrangement. He manually separated the two types of crystals with a microscope and found that solutions of each of the two types of crystal rotated polarized light in opposite directions. This experiment proved to be the first time someone had separated two enantiomers or mirror-image forms of a molecule.

Pasteur's work laid the foundation for understanding that the molecules in living organisms are chiral and that this chirality is critical to how they function. For example, in biochemistry, the chirality of amino acids is crucial because only one enantiomer of amino acids is used to make proteins in living organisms [71, 72]. Thus, while Biot's discovery was significant, its full importance was not appreciated until the underlying principles of molecular chirality were understood.

The theoretical explanation for optical activity and chirality was developed further in the late 19th and early 20th centuries, which we depict in figure 3.

NOA arises from the spatial dispersion of the dielectric response or optical conductivity for conductors. This results from finite light speed, allowing currents generated at nonzero wavevectors to affect the local response dependent on frequency. By expanding the non-local dielectric response in powers of q to first order, the NOA can be seen to arise as a third-rank tensor as

$$\epsilon_{ij}(\omega, \mathbf{q}) = \epsilon_{ij}(\omega, \mathbf{q} = 0) + i\lambda_{ijk}(\omega)q_k + \dots \quad (3)$$

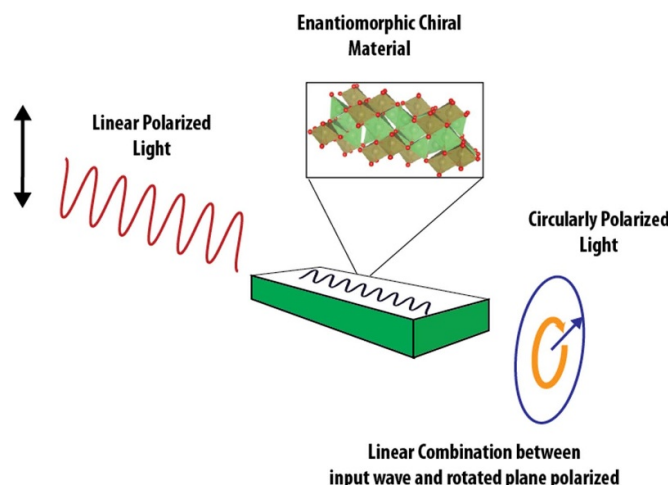


Figure 3. Illustration of optical activity through light rotation in chiral crystals.

Thus the NOA can be obtained from:

$$\lambda_{ijk}(\omega) = -i \left. \frac{\partial \epsilon_{ij}(\omega, \mathbf{q})}{\partial q_k} \right|_{\mathbf{q}=0}. \quad (4)$$

Sometimes the NOA is written as a rank two tensor called the gyration tensor as

$$g_{ij}(\omega) = \frac{1}{2} \epsilon_{kli} \lambda_{klj}(\omega). \quad (5)$$

Considering the non-negligible contribution to the dielectric response, the crucial role in stereochemistry, and the potential for applications, several theoretical efforts have been made to provide accurate predictive tools to compute the NOA. Early theoretical efforts to understand the phenomenon based on semiclassical theories of electromagnetism [73]. First principles methods have been developed from these theories using sum over states formulas [74], linear response [75], and real-time propagation [76]. While these approaches are successful in molecules, the origin dependence of the theory is unsuitable for crystalline materials. Band theory formalism in the long-wavelength limit and neglecting local field effects [77–80] combined with a first principles sum over states approach [81] extended the theory of optical activity to crystals. While this approach is successful for some materials, it significantly underestimates the optical activity when local field effects cannot be ignored [82]. A framework based in density functional perturbation theory has been proposed recently [83] to address these issues.

In 1874, Jacobus Henricus van't Hoff and Joseph Le Bel independently proposed that the carbon atom could form four bonds directed toward the corners of a tetrahedron with the potential to bond to four different species. This pseudo-tetrahedral arrangement could create two different spatial arrangements (isomers) of atoms, which explains the existence of enantiomers [84]. The recognition that many biological molecules are chiral led to the development of stereochemistry, which studies the spatial arrangement of atoms in molecules and their impact on their behavior and reactions. In

pharmacology, the chirality of drugs is paramount because different enantiomers of a drug can have very different biological activities (one may be therapeutic, while the other could be inactive or even harmful, as was tragically demonstrated in the case of thalidomide in the 1950s and 1960s) [85]. In the case of periodic systems, the history of optical activity is strongly tied to the development of crystallography, and an understanding of symmetry through the application of group theory (see section 2). Experimental crystallographic methods allowed scientists to determine the arrangement of atoms within a crystal and understand how this arrangement affects the crystal's properties, including optical activity. A good review of the approaches to describe optical activity can be found in [16].

Following the Neumann [86] symmetry principle, optical activity can only be exhibited by non-centrosymmetric structures. This is because an inversion center in a crystal structure would negate the conditions necessary to manifest optical activity. Therefore, optical activity can demonstrate the lack of inversion symmetry in a crystal structure (and these measurements can be complemented by anomalous x-ray scattering to determine the absolute configuration of the structure [87]). Of the 21 acentric crystal classes, 15 are compatible with optical activity, but four of these classes ($\bar{4}$, m , $mm2$, $\bar{4}2m$) contain symmetry operations that are not compatible with chirality. Of the 15 classes consistent with optical activity, 11 are compatible with chirality and give the 65 Sohncke space groups, which contain only operations of the first kind (table 1) [88–90], and so the optical activity we associate with chirality is not confined to only symmetries compatible with enantiomorphism [88, 91]. Crystals possessing D_{2d} ($\bar{4}2m$) symmetry, or any of its non-enantiomorphic subgroups such as S_4 ($\bar{4}$), C_{2v} ($2mm$), or C_s (m), can rotate the plane of polarized light when it is incident in a general direction [91].

Optically active materials interact with light and have distinct refractive indices for left-handed circularly polarized light (LCP) and right-handed circularly polarized light (RCP). Generally, the refractive index of a material can be expressed as $n = n_0 \pm \gamma_1 + i(n_2 \pm \gamma_2)$, where γ_1 and γ_2 depend on the product of the light's frequency and the gyrotropic constant of the material. Consequently, each circular polarization state, LCP, and RCP is characterized by different refractive indices, denoted as n^L and n^R , respectively. From these refractive indices, one can define the optical rotation angle $\phi = (2\pi/\lambda)(n_0^L - n_0^R)d$, where λ represents the wavelength of the incident light, and d is the optical path length through the material. The terms n_0^L and n_0^R refer to the real parts of the refractive indices for LCP and RCP light, respectively. Similarly, the ellipticity Ψ , which quantifies the extent to which the polarization of light becomes elliptical after passing through an optically active material, can be defined as $\Psi = (\pi/\lambda)(n_2^L - n_2^R)$, with n_2^L and n_2^R being the imaginary parts of the refractive indices corresponding to LCP and RCP light absorption. In most cases, the ellipticity is small enough for the rotation to be measured as if the light were still plane-polarized, and what is measured experimentally is the optical rotatory dispersion (ORD). The effects of the imaginary parts of the index of refraction are usually determined by measuring the absorption of LCP and RCP radiation separately and

calculating the ratio as

$$\frac{I_R - I_L}{I_R + I_L},$$

where I_R and I_L are the intensities of right and left handed polarized light, respectively. As a function of frequency, this quantity is known as circular dichroism (CD). ORD measures the change in a substance's optical rotation as a function of the wavelength of light. At the same time, CD is a spectroscopic technique that measures the difference in the absorption of LCP versus RCP as it passes through a chiral substance.

Therefore, optical activity can be used to distinguish between enantiomorphs of chiral materials as opposite enantiomorphs will give opposite rotations of the plane of polarization, as in SiO_2 (quartz), HgS (cinnabar), NaClO_3 (which is a chiral crystal), AlPO_4 (Berlinite) [16], Te [92], Bi and many different chiral magnetic crystals such as MnSi , FeGe , Cu_2OSeO_3 [93], $\text{Fe}_{(1-x)}\text{Co}_x\text{Si}$, CrNb_3S_6 , $\beta\text{-Mn}$, [16] etc. Chiral crystals are being actively researched for their nonlinear optical properties, which are of significant interest in the field of nonlinear optics, in particular, due to the recent observation of large chiral-specific second harmonic generation (SHG) response [94, 95]. One of the most innovative applications of optical activity lies in chiral catalysis [96–98]. Here, heterogeneous catalysts exploit the chiral surfaces of crystal materials to drive enantioselective reactions, which are directly influenced by the material's optical activity. This underscores the importance of optical activity in catalysis and provides further motivation for synthesizing enantiomerically pure compounds, a critical aspect of drug development and various chemical manufacturing processes.

In industrial contexts, the measurement of optical activity is employed for quality control, particularly in the manufacturing of optical devices [99–101]. Furthermore, manipulating light's polarization state in optoelectronic devices leverages the unique properties of chiral crystals, enhancing the performance of optical sensors in communication devices and other applications that empower a two-fold improvement of the rate of information transport through polarization multiplexed fiber optic waveguides [102], quantum communication [103–105], optical integrated circuits [106, 107], on chip photodetectors [108–110] and quantum computing [111, 112]. Furthermore, these magneto-optical (MO) effects and the use of CPL form the basis for technological breakthroughs, such as all-optical switching in spintronic devices [113–115], CPL LEDs [116–120], photoresponsive displays [121, 122], and bioresponsive imaging [123, 124]. Other devices also use MO effects like Faraday rotation and Kerr rotation. While these rotate the plane of polarization, these effects are unrelated to the material structure or symmetries (see section 5.1 for magnetic-symmetry dependent effects).

3.1. Chiral axis and absolute chirality

The optical activity of a material (its ability to rotate the plane of polarized light) is defined by its magnitude and its sign i.e. the direction of rotation: viewed along the beam direction towards the light source, if the sense of rotation of the

polarization is clockwise, the material is described as left-handed (levorotatory), and right-handed (dextrorotatory) if the sense of rotation is anticlockwise, as discussed in section 3. The sense of rotation should be related to the structural helix of the most polarizable atoms in the crystal structure [16, 68]. However, it can be challenging to determine the true chirality (i.e. the ‘absolute configuration’ of molecular systems, or ‘absolute structure’ or ‘absolute chirality’ for crystalline materials [68, 90]) of a crystal structure [125], leading to some ambiguity in reported structures and confusion in the link between the chiral crystal structure and its measured physical properties (including optical activity, and polarization where relevant) [16, 68]. This has undoubtedly contributed to the difficulty of quantifying chirality (see section 8). Glazer and Stadnicka reported that chiral axes for relevant crystal classes were analogous to polar directions in polar structures [68]. This concept is perhaps most relevant when exploring electrogyration, the change in the optical activity of a ferroelectric crystal by the application of an electric field (see section 5.3) [126]. This practical meaning of absolute chirality and the resulting link between structure (and its handedness) and the resulting physical properties should not be confused with the mathematical concepts of ‘absolute’ and ‘relative’ chirality derived from graph theory by Le Guennec [127–129]. See also [52] for a detailed discussion about the experimental determination of the absolute chirality via neutron scattering probes.

4. Examples of structural chirality and associated phase transitions

In this section, we give specific examples of crystals exhibiting non-reconstructive phase transitions involving structural chirality, discussing their optical activity where relevant. We discuss MgTi_2O_4 , K_3NiO_2 , CsCuCl_3 , $\text{Na}_2\text{Ca}_2\text{Si}_3\text{O}_9$ and $\text{Ag}_4\text{P}_2\text{O}_7$ with low symmetry (chiral) structures described by enantiomorphic space groups, and $\text{Pb}_5\text{Ge}_3\text{O}_{11}$ and $\text{Ba}(\text{TiO})\text{Cu}_4(\text{PO}_4)_4$ with low symmetry structures described by a non-enantiomorphic Sohncke space groups.

4.1. MgTi_2O_4

Above 260 K, MgTi_2O_4 adopts a normal spinel structure of cubic symmetry ($Fd\bar{3}m$). On cooling, it undergoes a transition from a metallic state to a spin-singlet insulating state, driven by the dimerization of pairs of $3d^1$ Ti^{3+} ions. This metal–insulator transition is accompanied by a cubic to tetragonal phase transition [130]. Variable temperature synchrotron and neutron diffraction experiments indicate that the symmetry is lowered to $P4_12_12$ (or its enantiomorphic pair $P4_32_12$), with a change in the size of the unit cell to accommodate ordering of Ti–Ti dimers with shorter bonds. This symmetry lowering gives helical chains of long and short Ti–Ti bonds (figure 4). Variable temperature neutron powder diffraction data indicates that this is an abrupt transition, suggesting that it is of a first-order kind [131].

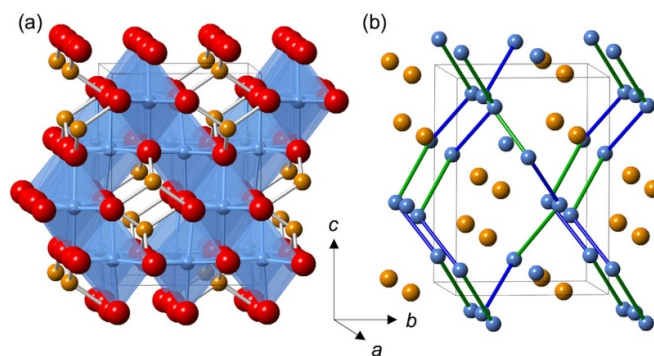


Figure 4. Schematic showing the crystal structure of the chiral $P4_12_12$ phase of spinel MgTi_2O_4 showing (a) TiO_6 octahedra (blue) and MgO_4 units and (b) highlighting shortest (dimerized) and longest Ti–Ti bonds in blue and green (with oxide ions omitted for clarity); Mg, Ti and O sites are shown in orange, blue and red, respectively. Adapted from [131].

The structural phase transition can be described by the higher-dimensional X_4 irrep and as both enantiomorphs must be degenerate, the transition from the achiral phase to either enantiomorph must be described by the same irrep. The transitions to the two enantiomorphs differ by the order parameter direction: $(0, a; 0, 0; 0, 0)$ gives the $P4_12_12$ enantiomorph, whilst $(a, 0; 0, 0; 0, 0)$ gives the $P4_32_12$ enantiomorph [132, 133]. In summary for MgTi_2O_4 :

- the phase transition from achiral structure to a structure described by an enantiomorphic space group is first order and is accompanied by a change in unit cell volume;
- the phase transition is described by an irrep (X_4) that is at least two-dimensional (2D) [134];
- the transition to the two enantiomorphs (described by a pair of enantiomorphic space groups) are described by the same irrep but with different order-parameter directions.

4.2. K_3NiO_2

On cooling below 410 K, K_3NiO_2 undergoes a first-order phase transition from a centric structure of $P4_2/mnm$ symmetry to a non-centrosymmetric and chiral phase of $P4_12_12$ (or $P4_32_12$) symmetry. As for MgTi_2O_4 described above, the structures of the two enantiomorphs are described by an enantiomorphic pair of chiral space groups [135]. For these two structures to be degenerate, the distortion from the $P4_2/mnm$ phase to each enantiomorph must be described by the same 2D Z_3 irrep: the phase transition involves slight rotations of the NiO_2^{3-} units about the $[110]/[1\bar{1}0]$ directions and small displacements of potassium ions which breaks the linearity of the O–Ni–O–K–O–Ni–O chains [135] (see figure 5). The two enantiomorphs differ in the direction of this 2D irrep: the (a, a) and (\bar{a}, \bar{a}) order parameter directions give the $P4_12_12$ enantiomorph whilst (a, \bar{a}) and (\bar{a}, a) give the $P4_32_12$ enantiomorph [136]. For these enantiomorphic structures, whilst (a, a) and (a, \bar{a}) domains are related by a mirror plane, they are non-superimposable (they contain opposite structural helices) and so are described by different space groups. Recently, Fava

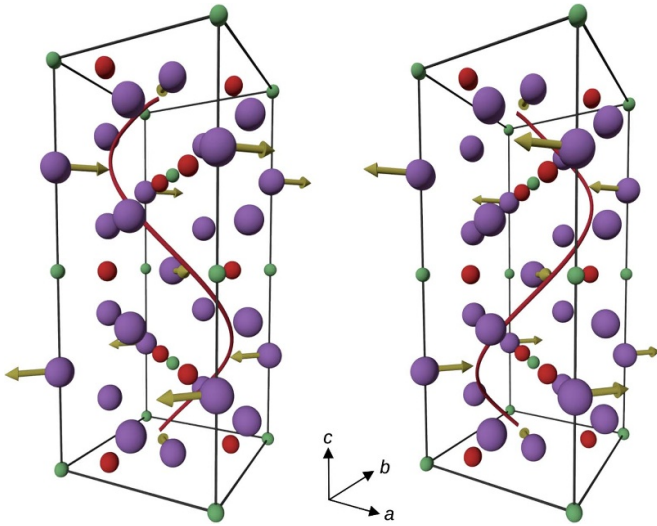


Figure 5. Schematic view of the symmetry allowed atom eigendirection of the (a), (a) chiral domain coming from the Z_3 irrep of the $P4_2/mmm$ space group of A_3BO_2 crystal family. The purple, green and red balls corresponds to A, B and O atoms, the displacements are represented by gold arrows and the spirals are highlighted by the red lines connecting each displacement arrows. Only the atom displacements creating the spiral are shown and all the arrows of allowed displacements are normalized to the same length for clarity. In the case of K_3NiO_2 , the Ni does not contribute much to the distortion, i.e. it is reduced to mostly K motion. From [136].

et al [136] have shown from first-principles calculations that the transition from the $P4_2/mmm$ high symmetry phase to the low chiral phases $P4_12_12$ and $P4_32_12$ can be explained from the condensation of a soft zone boundary mode of the Z_3 symmetry label. In summary, for K_3NiO_2 :

- the phase transition from achiral structure, to a structure described by enantiomorphic space group is first order and is accompanied by a change in unit cell volume;
- the phase transition is described by an 2D irrep (Z_3), with most of the displacement due to potassium and oxygen motion.
- the transition to the two enantiomorphs (described by a pair of enantiomorphic space groups) are described by the same irrep but with different order-parameter directions.

4.3. $CsCuCl_3$

At room temperature $CsCuCl_3$ adopts a chiral crystal structure described by enantiomorphic $P6_122$ or $P6_522$ symmetries [137]. Optical measurements reveal the domain structure of samples, with domains of the two opposite enantiomorphs rotating the plane of polarized light in opposite directions. On warming through 423 K, $CsCuCl_3$ undergoes a first-order phase transition to an achiral phase of $P6_3/mmc$ symmetry where the unit cell c axis is reduced by a third compared with the chiral crystal structure (see figure 6), and in which the optical rotatory power is lost [138] (a ‘gyrotropic’ phase transition). The $P6_3/mmc \rightarrow P6_122/P6_522$ phase transition

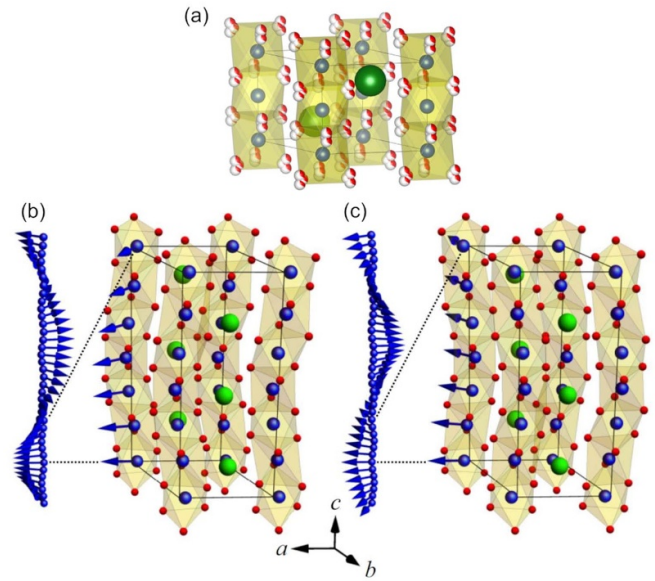


Figure 6. Crystal and magnetic structures of $CsCuCl_3$ showing (a) high-temperature achiral phase of $P6_3/mmc$ symmetry and below, low-temperature chiral phases of (b) $P6_122$ symmetry and (c) $P6_522$ symmetry, showing Cs, Cu and Cl sites in green, blue and red, with $CuCl_6$ octahedra in yellow, and Cu^{2+} moments in blue. The right-handed and left-handed helimagnetic structures for the right-handed ($P6_122$) and left-handed ($P6_522$) enantiomorphs are shown by the chains of blue arrows in panels (b) and (c). Reprinted figure with permission from [140], Copyright (2017) by the American Physical Society.

is due to a cooperative Jahn-Teller distortion of the $CuCl_6$ octahedra which share faces along c , leading to helical displacements of ions [139] to give either right-handed helices ($P6_122$ symmetry) or left-handed helices ($P6_522$ symmetry). The structural phase transition involves displacements of Cl^- ions described by the Δ_6 irrep with $(a, 0, 0, 0)$ order parameter direction giving the $P6_522$ enantiomorph, whilst the $(0, a, 0, 0)$ order parameter direction gives the $P6_122$ enantiomorph [132, 133, 139].

The Cu^{2+} $S = \frac{1}{2}$ moments order antiferromagnetically below $T_N = 10.5$ K with a triangular helical spin structure: moments lie in the ab plane but the direction within the plane modulates along c [141] (with a period of ~ 210 Å), figures 6(b) and (c). This helical structure results from intrachain ferromagnetic interactions between Cu^{2+} nearest-neighbors and antisymmetric DM interactions, [141] allowed for this non-centrosymmetric structure [142, 143]. The crystal chirality determines the DM axial vector (the sense of the Cu^{2+} helix along c). So the magnetic chirality depends directly on the crystal chirality [141]: the chiral vector (along c) has opposite directions for the two enantiomorphs [144].

- The gyrotropic phase transition from the achiral $P6_3/mmc$ phase to the enantiomorphic phases ($P6_122/P6_522$ symmetries) is first order and is accompanied by a change in unit cell volume;
- the phase transition is described by an irrep (Δ_6) that is at least 2D;

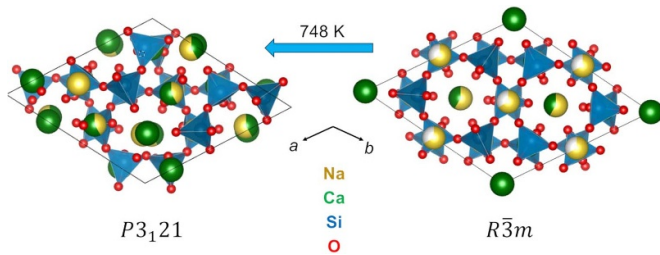


Figure 7. Crystal structures of combeite $\text{Na}_2\text{Ca}_2\text{Si}_3\text{O}_9$ showing SiO_4 tetrahedra in blue and Na, Ca and O sites in yellow, green and red, respectively. There is an origin shift of the unit cells in the phase transition, but the figure illustrates the twisting of SiO_4 tetrahedra to lower the symmetry of the Na/Ca sites on cooling, as the distribution of Na and Ca cations and vacancies over these sites changes through this phase transition.

- the chirality of the magnetic structure is determined by the crystal chirality.

4.4. $\text{Na}_2\text{Ca}_2\text{Si}_3\text{O}_9$ and $\text{Ag}_4\text{P}_2\text{O}_7$

The silicate combeite, $\text{Na}_2\text{Ca}_2\text{Si}_3\text{O}_9$, has been also reported to undergo a phase transition around 758 K from an achiral high symmetry ($R\bar{3}m$) structure to a low symmetry phase of either $P3_121$ or $P3_221$ enantiomorphic space groups [145–148]. The crystal structure of combeite can be described in terms of rings of corner-linked SiO_4 tetrahedra in its high symmetry phase which are distorted into ellipses in the low symmetry phase, concomitant with a change in the distribution of Na^+ , Ca^{2+} and vacancies over the cation sites (see figure 7) [147]. However, few studies have been carried out on combeite regarding its chiral phase transition.

The phosphate $\text{Ag}_4\text{P}_2\text{O}_7$ undergoes a similar structural chiral phase transition from the trigonal $R\bar{3}c$ achiral high temperature phase to enantiomorphic ($P3_121/P3_221$ or $P3_112/P3_212$) phases at 623 K [149]. Although this crystal has not been further characterized concerning its phase transition or its chiral properties, it is of interest as one of very few materials (including $\text{Na}_2\text{Ca}_2\text{Si}_3\text{O}_9$) to undergo a continuous achiral to chiral phase transition with enantiomorphic space groups.

4.5. $\text{Pb}_5\text{Ge}_3\text{O}_{11}$

The high-temperature ($T > 450$ K) crystal structure of $\text{Pb}_5\text{Ge}_3\text{O}_{11}$ is described by $P\bar{6}$ symmetry, and although it is non-centrosymmetric (it is piezoelectric and second-harmonic generation active), it is paraelectric. Its structure is related to the structures of apatite and nasonite, composed of GeO_4 tetrahedra and Ge_2O_7 dimers, with Pb^{2+} ions in interstitial sites arranged around a 6_3 screw axis (see figure 8(a)) [150]. At 450 K, $\text{Pb}_5\text{Ge}_3\text{O}_{11}$ undergoes a second-order (displacive) phase transition to a polar structure of $P3$ symmetry (figure 8(b)). This structural phase transition involves rotations of GeO_4 units and displacements of Pb^{2+} ions (including along the polar c axis) [150], described by the 1D irreducible representation (irrep) [Γ_2].

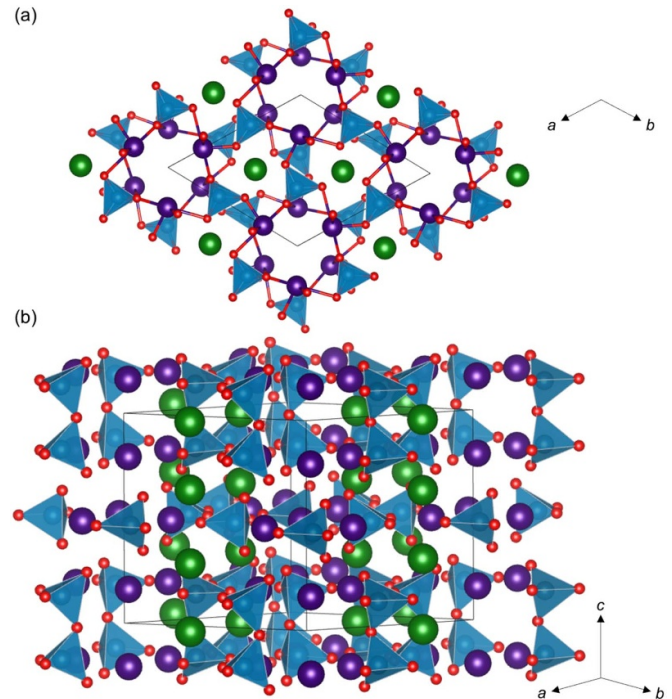


Figure 8. Illustration of the high-temperature $P\bar{6}$ symmetry crystal structure of $\text{Pb}_5\text{Ge}_3\text{O}_{11}$ showing projection down hexagonal channels (a) and perpendicular to the channels (b) illustrating the connectivity of GeO_4 tetrahedra. O^{2-} sites are shown in red, with Pb^{2+} ions on the sites arranged around the hexagonal channels in purple and lower symmetry Pb^{2+} sites shown in green, with GeO_4 tetrahedra in blue.

In addition to being polar, the low-temperature $P3$ phase of $\text{Pb}_5\text{Ge}_3\text{O}_{11}$ is chiral and optically active: the GeO_4 rotations are thought to contribute to the optical activity, whilst the polarization is predominantly due to the Pb^{2+} and Ge_2O_7 displacements [151]. The $P3$ space group is one of the 43 achiral Sohncke groups, and so both enantiomorphs are described by the same symmetry. Interestingly, as the sign of the polarization is changed by an applied electric field, similarly, the sense of chirality and the sign of optical rotation are also reversed by an applied electric field (a phenomenon called gyroelectricity, see section 5.3) [152, 153]. Recently, it has been shown from density functional theory (DFT) calculations and continuous symmetry measures [154] that the soft polar mode condensing into the $P6$ structure which is responsible for the ferroelectric phase transition is also chiral. This explains why the optical activity and the predicted spin-momentum locking [155] follow the change of polarization under an applied electric field as the polar distortions are also chiral in $\text{Pb}_5\text{Ge}_3\text{O}_{11}$ [156]. This study has also shown that when quantifying the chirality of each phonon mode of $\text{Pb}_5\text{Ge}_3\text{O}_{11}$, the mode chirality increases with the mode frequency.

In summary for $\text{Pb}_5\text{Ge}_3\text{O}_{11}$:

- the phase transition from achiral structure to a structure described by a Sohncke group is second order and there's little change in unit cell volume associated with this phase transition;

- the phase transition is described by a singly-degenerate polar irrep (Γ_2);
- the same space group symmetry describes both enantiomorphs (Sohncke group);
- the polarization and optical rotation are coupled, such that the ferroelectric polarization hysteresis loop is also observed for the optical activity, i.e. the gyroelectric effect;

4.6. $\text{Ba}(\text{TiO})\text{Cu}_4(\text{PO}_4)_4$

$\text{Ba}(\text{TiO})\text{Cu}_4(\text{PO}_4)_4$ crystallizes in the high symmetry tetragonal space group $P4/nmm$ and below 983 K it undergoes a structural phase transition to the low symmetry tetragonal space group $P4_212$. This phase transition is chiral where the low symmetry phase does not belong to one of the enantiomorphic space groups (the two chiral phases belong to the same space group). The crystal structure of $\text{Ba}(\text{TiO})\text{Cu}_4(\text{PO}_4)_4$ (see figure 9) is made of a Cu_4O_{12} building block composed of four corner shared square-planar CuO_4 units that are connected by PO_4 tetrahedra. In contrast to $\text{Pb}_5\text{Ge}_3\text{O}_{11}$, $\text{Ba}(\text{TiO})\text{Cu}_4(\text{PO}_4)_4$ does not involve ferroelectric polarization nor any other ferroic order such that the phase transition of $\text{Ba}(\text{TiO})\text{Cu}_4(\text{PO}_4)_4$ has been coined a ferrochiral phase transition [157]. This phase transition is of the second order kind and involves a combination of an antiferroaxial order together with an antipolar order, the combination of which induces chirality at the zone center as no cell doubling is at play. Other isostructural $A(\text{BO})\text{Cu}_4(\text{PO}_4)_4$ ($A = \text{Sr Pb}$ and $B = \text{Ti, V}$) crystals were reported to crystallize in the same low symmetry $P4_212$ space group but no high symmetry phases were reported at high temperatures such that they might not exhibit a similar ferrochiral phase transition [158–160]. An experimental study looking at the difference between the case of a non-accessible achiral phase of $\text{Sr}(\text{TiO})\text{Cu}_4(\text{PO}_4)_4$ and the case of $\text{Ba}(\text{TiO})\text{Cu}_4(\text{PO}_4)_4$ where it is observed when increasing the temperature shows that the domain formations are not the same, i.e. the Sr case shows predominant monodomain states while the Ba case shows predominant multidomain states [160].

In summary for $\text{Ba}(\text{TiO})\text{Cu}_4(\text{PO}_4)_4$:

- the phase transition from achiral structure to a structure described by a Sohncke group is second order;
- the same space group symmetry describes both enantiomorphs (Sohncke group);
- the phase transition is described by coupled antiferroaxial and antipolar distortions that induce chirality;
- it is the unique zone center ferrochiral structural phase transition that has been reported so far.

4.7. CsSnBr_3

Whilst preparing this review article, a very elegant study of the polar and chiral phase of CsSnBr_3 was published [161]. At intermediate temperatures ($85 \text{ K} < T < 269 \text{ K}$) it adopts the tilted perovskite structure ($a^-b^+a^-$ tilts of SnBr_6 octahedra) of $Pnma$ symmetry. At low temperatures, CsSnBr_3 adopts a

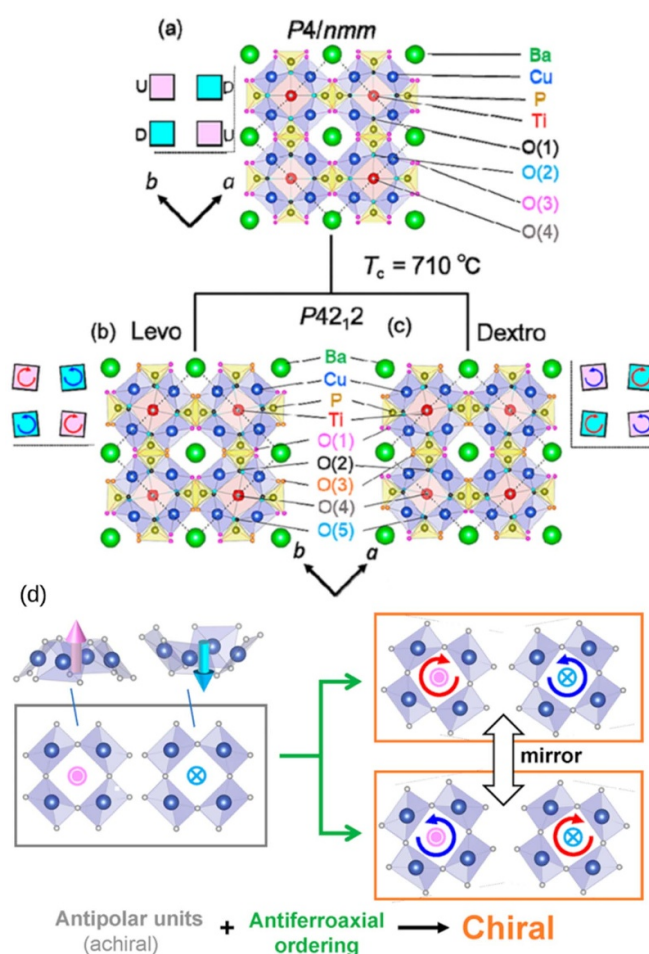


Figure 9. Illustration of the crystal structure of $\text{Ba}(\text{TiO})\text{Cu}_4(\text{PO}_4)_4$: (a) high symmetry phase above the critical temperature (around 983 K) viewed along the c axis. (b) Crystal structures of levo- and dextro- (c) domains below the critical temperature as viewed along the c axis. The squares in the insets of parts (a)–(c) schematically represent the axial rotations of Cu_4O_{12} units of up (magenta) and down (cyan). (d) shows how the combination of the antipolar distortions (left side with pink and light blue arrows) and the antiferroaxial distortions (right side with red and dark blue arrows) drives chirality in $\text{Ba}(\text{TiO})\text{Cu}_4(\text{PO}_4)_4$. Reprinted (adapted) with permission from [157]. Copyright (2021) American Chemical Society.

chiral and polar structure of $P2_1$ symmetry (one of the non-enantiomorphic Sohncke groups), but it reaches this low temperature phase via two continuous (second order) phase transitions. From the $Pnma$ phase, there's a second order phase transition at 85 K to a ferroaxial phase of $P2_1/m$ symmetry, with similar tilts to the $Pnma$ phase but with additional antipolar displacements of Sn^{2+} cations [161] (due to the $5s^2$ pairs of electrons) [162]. On cooling a little further to 77 K, the $P2_1/m$ phase undergoes a second order phase transition to the chiral and polar $P2_1$ phase, which now allows polar displacements of the Sn^{2+} cations. As observed for $\text{Pb}_5\text{Ge}_3\text{O}_{11}$ and $\text{Ba}(\text{TiO})\text{Cu}_4(\text{PO}_4)_4$, the achiral—chiral (non-enantiomorphic) phase transition is second order and driven by a zone-center polar distortion mode (Γ_1^-). In summary:

- the achiral to chiral phase transition is second order and involves little change in unit cell volume;
- the same space group symmetry (a non-enantiomorphic Sohncke group) describes both enantiomorphs;
- the transition is described by the polar zone-center irrep Γ_1^- .

4.8. Crystallographic databases and data mining for chiral crystals

After having presented a few specific examples of chiral crystals, we would like to discuss the following observation: of the 240 000 structures recorded in the ICSD by 2022, about 20% (i.e. around 8000 structures) are described by one of the 65 Sohncke space groups, and of these, only around 900 are described by one of the 22 chiral and enantiomorphic space groups. Hence, we can question whether the small number of crystals reported for the 11 pairs of enantiomorphic space groups are rare for a physical or chemical reason or have simply been overlooked.

The CSD is one of the pioneering digital databases, encompassing a comprehensive collection of organic and metal-organic crystal structures [163, 164]. In the 1990s, the ICSD was established, focusing on experimentally determined inorganic and mineral structures with around 200k compositions today [165, 166]. These crystal structure databases (alongside others including materials project (MP) [167], crystallography open database (COD) [168], AFLOW database [169], NOMAD repository [170]) allow the materials community to search for, analyze, and use this information to design new materials with desired properties. There has been a notable upsurge in efforts to use machine learning and data mining methodologies to examine and unveil novel crystal materials by harnessing existing crystal databases. This concept entails training a model using established structures to predict their chemical stability. With a suitable dataset, machine learning can anticipate the formation energies of hypothetical structures, presenting a powerful instrument for materials exploration and design. This methodology strives to predict properties or generate new crystal structures utilizing generative models, as exemplified in recent research endeavors [171, 172]. The methods used to populate the computational databases are high-throughput techniques that screen many systems fairly rapidly [169, 173, 174]. This is performed using DFT calculations to simulate crystal structures' electronic structure and stability. High-throughput DFT calculations can screen large numbers of crystal structures for desirable properties. This means that thousands of materials are computed and then analyzed to identify those with desirable properties such as stability or specific optical, electrical, or magnetic properties. This allows for a much more efficient and rapid identification of promising materials. Researchers can use these methods to screen large libraries of compounds for chiral properties or to systematically explore the structural and compositional variations of a particular class of chiral materials.

Here, we analyze the available chiral crystal structures from the following three prominent databases: MP [167], COD [175], and AFLOW [169]. The foundational data for these databases originates from the experimental ICSD [165,

Table 2. Number of structures existing in materials project (MP), AFLOW, and crystallographic open database (COD). The consolidated column is a constructed consolidated database without repeated structures. The last two columns refer to the number of structures with octahedra or tetrahedra.

| Space group | MP | AFLOW | COD | Consolidated | Octa. | Tetra. |
|-------------|-----|-------|-----|--------------|-------|--------|
| 76 | 55 | 79 | 317 | 421 | 85 | 218 |
| 78 | 22 | 2 | 295 | 309 | 67 | 171 |
| 91 | 37 | 23 | 31 | 78 | 49 | 46 |
| 92 | 152 | 64 | 544 | 604 | 159 | 356 |
| 95 | 63 | 5 | 42 | 98 | 74 | 72 |
| 96 | 72 | 22 | 466 | 503 | 139 | 303 |
| 144 | 55 | 17 | 236 | 262 | 49 | 146 |
| 145 | 63 | 7 | 234 | 284 | 69 | 191 |
| 151 | 15 | 10 | 12 | 25 | 13 | 13 |
| 152 | 144 | 141 | 284 | 410 | 129 | 217 |
| 153 | 8 | 2 | 7 | 14 | 3 | 4 |
| 154 | 43 | 18 | 225 | 241 | 78 | 134 |
| 169 | 24 | 10 | 199 | 219 | 43 | 131 |
| 170 | 10 | 2 | 212 | 219 | 37 | 143 |
| 171 | 3 | 0 | 13 | 16 | 2 | 7 |
| 172 | 2 | 0 | 11 | 13 | 3 | 9 |
| 178 | 22 | 8 | 70 | 87 | 32 | 46 |
| 179 | 2 | 2 | 65 | 65 | 18 | 39 |
| 180 | 50 | 171 | 59 | 217 | 10 | 67 |
| 181 | 39 | 18 | 29 | 54 | 5 | 39 |
| 212 | 2 | 35 | 27 | 54 | 15 | 30 |
| 213 | 67 | 37 | 33 | 86 | 40 | 28 |

[176]. These three databases have since been substantially expanded through the application of high-throughput methods. Our study encompassed data reported up until May 2023. Table 2 summarizes our screening and shows that fewer structures are reported for chiral space groups than for achiral space groups and even for other Sohncke crystals. COD contains structures with larger unit cells compared to the other databases. When constrained to 50 atoms per unit cell, the number of chiral structures in COD becomes similar to the other databases. To compile a comprehensive dataset, we merged all three databases into a single master database, eliminating repeated structures and excluding those in COD with incorrect crystallographic information file (CIF) format. Following this process, we obtained 4285 structures that belong to one of the 22 enantiomorphic space groups, of which only 1034 have unit cells with less than 50 atoms. For a visual representation, figure 10 illustrates the distribution of different chemical species present in the reported structures. In unrestricted unit cells, carbon emerges as the most frequently occurring element, with 3050 structures, followed by hydrogen and oxygen, with 2965 and 2990 structures, respectively. This is related to the abundance of organic crystals with large unit cells in the consolidated database. However, in unit cells with fewer than 50 atoms, the composition shifts, with oxygen constituting 38.5% of the reported structures in the joint database, followed by boron at 18.6% and carbon at 16.0%. Notably, 70% of the structures with less than 50 atoms contain transition metals. An analysis similar to that carried out by Halasyamani and Poeppelmeier [88], to seek to identify structural features that might be incorporated into design strategies for chiral materials, would be of interest. The relatively small number

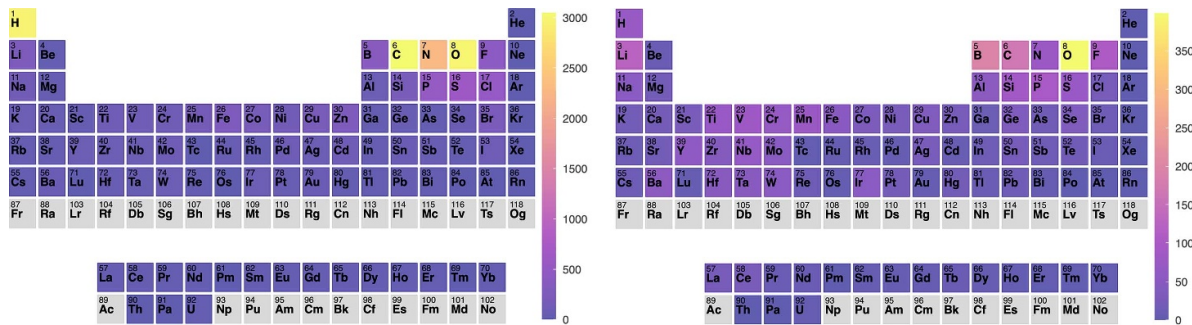


Figure 10. Color trend over the different periodic table elements as a function of the frequency of chiral crystals' appearance in the COD database. The top figure is 22 chiral materials overall, and the bottom figure only includes those with less than 50 atoms in the unit cell.

of chiral structures reported to date makes this challenging. However, proposed chiral structures from high-throughput and machine-learning computational work might soon make this more feasible.

We observed an unequal distribution of structures between enantiomorphic pairs, implying that either achieving synthesis control over specific enantiomorphic space groups has not yet been fully realized, or that experimentally there may be challenges with determining the absolute configuration of a system (see section 3.1). This discrepancy highlights the complexity and challenges in controlling chiral structure formation and determination, prompting further research and innovation. Using a high-throughput method to search for chiral materials would be an excellent strategy for rapidly identifying new chiral materials with specific functionalities. These high-throughput methods allow researchers to quickly test large numbers of potential chiral materials in parallel rather than individually. Such methods have the potential to uncover new chiral functional materials, adding to our understanding and meeting the demands of emerging technologies [177].

5. Chirality and its relationship to other properties

In this section, we will discuss how chirality can be tuned externally, i.e. by applied electric and magnetic fields or with strain. While chirality is not the property directly investigated, most of the responses that we discuss below are related to tuning optical activity as an indirect probe of change in chirality in the materials. A dedicated discussion about flipping chirality will be done further in section 7. We will also discuss the cases of topological materials and altermagnets as their properties can be related to chirality.

5.1. Magnetism

Harnessing the influence of an applied magnetic field on properties associated with chirality (including optical responses) holds promise for a range of functional materials applications, including electric power systems, magnetic field sensors, all-dielectric measurement devices, and broadband frequency responses [178, 179]. This has motivated research into materials capable of demonstrating magnetic-optical interactions,

including magneto-chiral materials that have appropriate symmetry (either as a result of their crystal or magnetic structures) for optical activity [180].

5.1.1. Magneto-Optical phenomena. Several magneto-optical (MO) phenomena do not rely on specific symmetries of the light-transmitting media (including the Faraday effect and magnetic circular dichroism (CD)), but instead rely on an applied magnetic field (or a magnetization of the medium) [89]. These phenomena contrast with NOA (see section 3), which depends on the symmetry of the spatial dispersion of the electric dipoles in the medium (alongside a generally weaker effect due to magnetic dipoles [181, 182]), giving rise to differences in propagation of oppositely polarized light. The Faraday rotation Ψ is given by

$$\Psi = V_{ij}tN_iH_j \quad (6)$$

where t is the path length, H_j are the components of the magnetic field, N_i the directions of the wave normal, and V_{ij} is the Faraday tensor (a polar second-rank tensor). In the inverse Faraday effect, a solid can be magnetized when exposed to intense circularly-polarized light [89]. Magnetic CD is related to the Faraday effect but relies on the different absorption coefficients for oppositely circularly polarized light in an applied magnetic field. This results in a phase difference between left- and right waves propagating through a medium [89].

As noted above, the magnetic optical activity observed in both the Faraday effect and magnetic CD result from the applied magnetic field breaking time-reversal symmetry and not from the intrinsic symmetry of the light-transmitting medium [183]. However, a magnetic phenomenon analogous to NOA exists, referred to as 'magnetochiral dichroism' (MChD), which relies on the symmetry of magnetic dipoles in the light-transmitting medium [183–185]. Barron and Vrbancich demonstrated that chiral systems should show different optical properties depending on whether the light propagates through the chiral medium either parallel or anti-parallel to the magnetic field direction, with opposite effects for the two enantiomers [186]. Atzori *et al* give excellent overviews of the experimental work in this field and introduce the implications of this effect for sound propagation, photochemistry, and electrochemistry (and even possible explanations for

the origins of homochiral life on earth!) [187, 188]. The MChD effect depends on the relative orientations of the wave vector and magnetic field and the different absorptions of light by opposite enantiomorphs arising from magneto-chiral anisotropy (MChA) [183, 187]. There's a growing body of work exploring the MChD effect in molecular systems and complexes, which typically takes advantage of molecular chirality to give a magnetized chiral system [189–191]. However, in this review focusing on structural chirality, it is relevant to consider possible magnetic and chiral extended solids, and the following sections explore 'magnetic chirality' i.e. chirality in spin-ordered states or textures [51].

5.1.2. Magnetic chirality. In addition to the structural chirality described in section 2, which arises from the crystal structure's symmetry, the symmetry of the magnetic order can give rise to additional physical properties [192, 193]. In terms of chirality, several possibilities can be considered:

- magnetic spins on a chiral crystal structure order with the magnetic chirality fixed by the chirality of the crystal structure (e.g. langasite $\text{Ba}_3\text{NbFe}_3\text{Si}_2\text{O}_{14}$);
- magnetic spins on a chiral crystal structure order in a non-centrosymmetric and chiral fashion (MnSi);
- magnetic spins on an achiral crystal structure order in a chiral fashion (e.g. Mn_3Sn).

Before discussing these phenomena in more detail, it is helpful to consider some aspects of magnetic symmetry that are distinct from purely structural crystallography, as well as their consequences. Although magnetic moments are often represented by arrows (similar to electric dipoles), it is important to note that they are described by axial vectors (rather than the polar vectors used to describe electric dipoles). The image of the magnetic moment arising from a current loop (figure 11) helps to visualize the effects of various symmetry operations acting on an axial vector (and the resulting magnetic moment), which is often quite different from the effects on polar vectors. Magnetic symmetry groups (to describe ordered magnetic structures) combine the geometric symmetry elements discussed in section 2 in addition to the non-spatial symmetry operation of 'time reversal': reversing time would reverse the current flow in a loop and, therefore reverse the direction of the magnetic moment (time reversal switches the sign of an axial vector) [89, 194]. However, magnetic chirality does not change under time reversal [51].

This understanding allows us to consider two types of chirality that emerge from non-collinear magnetic structures often associated with magnetic chirality: vector chirality and scalar chirality, as discussed in section 1.

Collinear magnetic structures are not chiral, and so in the search for magnetic chirality, non-collinear magnetic structures are needed [195], and the microscopic mechanisms that stabilize these more complex magnetic arrangements should be considered. Non-collinear magnetic structures arise from combinations of symmetric exchange with, for example, geometric frustration of symmetric (Heisenberg) exchange

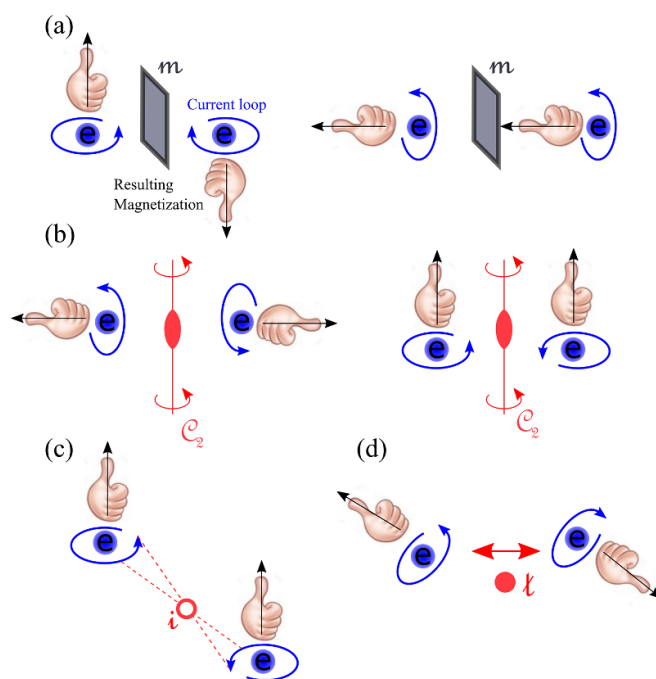


Figure 11. Visualizing magnetic moments as axial vectors resulting from a current loop. Panels show the effects of (a) a two-fold rotation, (b) reflection, (c) spatial inversion and (d) time reversal. Reproduced from [89].

interactions [196] (e.g. langasite $\text{Ba}_3\text{NbFe}_3\text{Si}_2\text{O}_{14}$ [197–199], magnetocrystalline anisotropy, and DM interaction (DMI, an antisymmetric exchange via a spin-orbit interaction, which may be non-zero if there's no inversion symmetry between the pair of magnetic sites) [142, 143] (e.g. CsCuCl_3) [141]. Several broad classes of non-collinear magnetic structures are frequently reported and it's useful to consider them concerning chirality:

- Cycloidal spin structures (e.g. $\text{Ca}_3\text{Ru}_2\text{O}_7$ [200]): although polar they are achiral.
- Helical spin structures (e.g. MnSi, $\text{Ba}_3\text{NbFe}_3\text{Si}_2\text{O}_{14}$): chiral (does not break time-reversal symmetry and so an example of true chirality) [51].
- Canted and toroidal spin structures (e.g. BaCoSiO_4): chiral (does not break time-reversal symmetry and so an example of true chirality) [51].

5.1.3. Electronic magneto chiral anisotropy (eMChA). A fundamental condition for observing eMChA is the absence of inversion symmetry and the presence of spin-orbit coupling, rendering the material non-centrosymmetric. While various transport parameters may undergo modifications in such materials, a particularly noteworthy consequence of this anisotropy is its effect on electrical resistance. This influence on resistance arises from the interaction between the orientation of magnetization and the direction of current flow within the material. Consequently, alterations in the relative alignment of these two vectors can influence the material's electrical characteristics, underscoring the intricate interplay between

its structural asymmetry and electrical behavior. In enantiomorphic crystals, this difference can be written as:

$$R^{L/R}(\mathbf{B}, \mathbf{I}) = R_0 \left(1 + \mu^2 R^2 + \gamma^{L/R} \mathbf{B} \cdot \mathbf{I} \right), \quad (7)$$

with $\gamma^R = -\gamma^L$ referring to the conductor's right- and left-handed enantiomer, μ is the electron mobility, and \mathbf{I} is the electrical current. This effect leads to the so-called eMChA, most commonly detected by the associated second-harmonic voltage generation under low-frequency a.c. as reported in chiral metals [201]. Though several applications can be overseen on materials with this effect (such as in rectifiers), the problem is that usually, γ is very small. Therefore, there is a need to search for new materials with larger electronic magnetochiral anisotropy. A potential path is to use Weyl materials, where chirality can induce a charge imbalance between Weyl fermions of different chirality as reported in TaAs [202]. A different direction is concerning identifying chiral magnetic materials with larger anisotropy, as in the case of CuB_2O_4 [203] or LiCoPO_4 [204].

Exploring some well-characterized magnetochiral materials may best illustrate these aspects of magnetic chirality and the origins of these phenomena.

5.1.4. Langanite $\text{Ba}_3\text{NbFe}_3\text{Si}_2\text{O}_{14}$. $\text{Ba}_3\text{NbFe}_3\text{Si}_2\text{O}_{14}$ crystallizes with a chiral structure of $P321$ symmetry, isostructural with the mineral langasite $\text{La}_3\text{Ga}_5\text{SiO}_{14}$. This space group is consistent with optical activity and piezoelectricity. It is one of the non-enantiomorphic Sohnke groups, meaning that crystals of opposite handedness are described by the same space group symmetry. Samples of opposite handedness (of their crystal structures) have been prepared, and their absolute chirality determined by anomalous x-ray scattering experiments [197, 198]. The structure consists of layers of equilateral triangles of FeO_4 tetrahedra with antiferromagnetic superexchange interactions between Fe^{3+} cations via oxide ions within the triangles (and super-superexchange interactions between triangles). $\text{Ba}_3\text{NbFe}_3\text{Si}_2\text{O}_{14}$ undergoes a (second order) magnetic ordering transition below $T_N = 27$ K to an (approximately) co-planar antiferromagnetic structure. However, there is suggested to be a small out-of-plane ferromagnetic moment [198].

The arrangement of Fe^{3+} ions in triangular units gives rise to frustration of the antiferromagnetic Fe–O–Fe superexchange interactions and results in Fe^{3+} moments within a triangle arranged at 120° to one another. This ‘triangular chirality’ is an example of vector chirality (see above), and analysis of results from inelastic neutron scattering experiments indicate that this vector chirality persists up to high temperatures, well above T_N [199]. Symmetric exchange interactions between triangles in successive layers result in the helical 3D magnetic order observed below T_N , with crystals of opposite

handedness switching the relative magnitudes of these interlayer exchange interactions and resulting in magnetic structures of opposite helices [197, 199]. Qureshi *et al* [197] showed this very elegantly by carrying out scattering experiments on two samples of opposite crystal chirality to show that both enantiomorphs had the same vector chirality within the Fe triangles but opposite magnetic chiralities overall due to the opposite sense of the magnetic helices (figure 12). $\text{Ba}_3\text{NbFe}_3\text{Si}_2\text{O}_{14}$ provides an exciting contrast to systems such as CsCuCl_3 (see section 4.3) because the helical magnetic structure of $\text{Ba}_3\text{NbFe}_3\text{Si}_2\text{O}_{14}$ is thought to arise from frustrated symmetric (Heisenberg) exchange interactions, without the need for antisymmetric exchange (such as the DMI) [197–199]. In summary for $\text{Ba}_3\text{NbFe}_3\text{Si}_2\text{O}_{14}$:

- The magnetic chirality is fixed by the crystal chirality.
- Magnetic chirality results from competing symmetric exchange interactions.

5.1.5. MnSb_2O_6 . MnSb_2O_6 also crystallizes in a chiral but non-enantiomorphic structure of $P321$ symmetry. The structure is built from layers of (distorted) MnO_6 and SbO_6 octahedra, with Mn^{2+} ions ordered into alternate layers to give distorted triangular networks of three MnO_6 octahedra around either an Sb^{5+} site or a vacancy [205]. On cooling, it undergoes an antiferromagnetic phase transition at 12.5 K (with approximately 3D-Heisenberg-like behavior) [205] and Johnson *et al* used single crystal neutron diffraction to investigate its magnetic ordering, characterized by co-rotating cycloids of Mn^{2+} moments [35]. This contrasts with $\text{Ba}_3\text{NbFe}_3\text{Si}_2\text{O}_{14}$ discussed above in that rather than a helical structure observed for $\text{Ba}_3\text{NbFe}_3\text{Si}_2\text{O}_{14}$, the spin plane has been rotated by 90° to give a cycloidal spin structure, probably favored by out-of-plane anisotropy in MnSb_2O_6 [35]. There's some ambiguity as to the exact orientation of the planes in which the spins rotate without an applied magnetic field [58, 206], but it is close to the (110) plane [35]. This cycloidal spin structure again results from several symmetric exchange interactions (and anisotropy). The relative magnitudes of interlayer exchange interactions are directly related to the crystal structure's handedness, which determines the magnetic domain configuration [35]. The DMI and cycloidal magnetic structure result in a polarization perpendicular to the [001] axis [35]. It seems that an applied magnetic field can tilt the plane of the spin cycloid (until a spin flop transition is reached at higher fields to give a helical spin structure), which can change the sign of the polarization [58, 206]. The opportunity to control electrical polarization by applying a magnetic field in this magnetoelectric material is particularly exciting. In summary for MnSb_2O_6 :

- The magnetic domain configuration of MnSb_2O_6 is directly related to the crystal chirality.
- The cycloidal spin structure alone is achiral, resulting in an electric polarization.

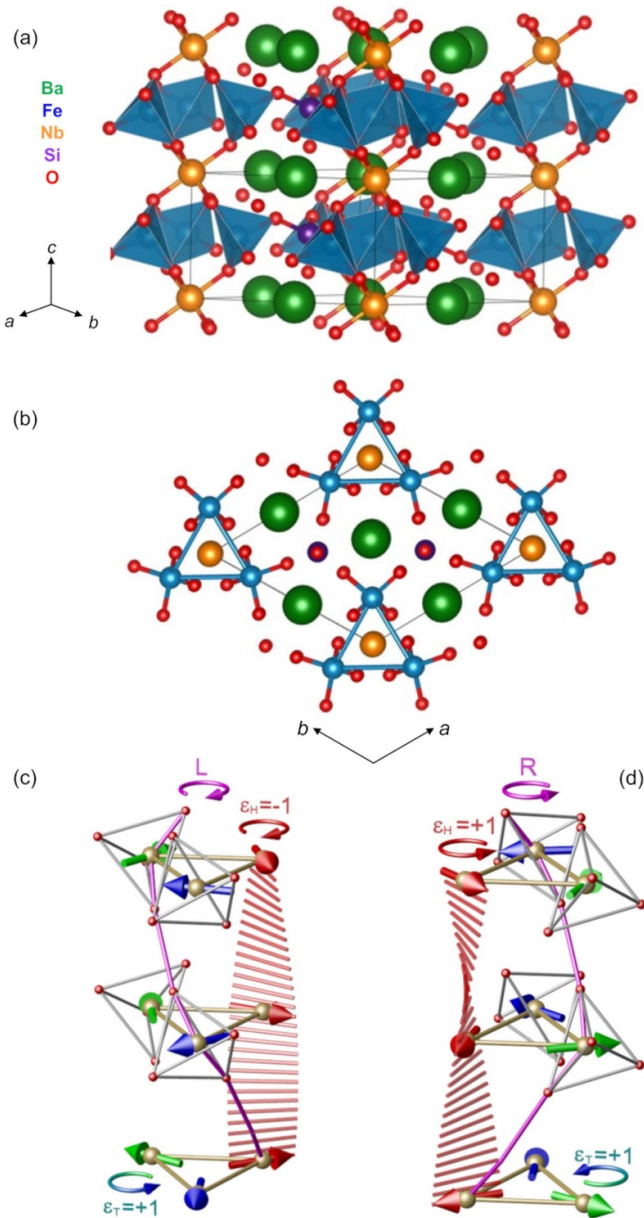


Figure 12. (a) Crystal structure of $\text{Ba}_3\text{NbFe}_3\text{Si}_2\text{O}_{14}$ showing FeO_4 tetrahedra in blue and Ba, Nb, Si and O ions in green, orange, purple and red, respectively; (b) shows the structure viewed perpendicular to the layers (down [001]) highlighting the triangles of Fe^{3+} cations in blue. Panels (c) and (d) show the left-handed magnetic helix for the left-handed enantiomorph and the right-handed magnetic helix for the right-handed enantiomorph, respectively; both magnetic helices have the same triangular chirality ($\epsilon_T = +1$ as shown in green), whilst their magnetic helices are of opposite handedness ($\epsilon_H = +1$ or -1 as shown in red). Reprinted figure with permission from [197], Copyright (2020) by the American Physical Society.

- An applied magnetic field can tilt the spin cycloid, switching the polarization and the ferroelectric domain configuration.

5.1.6. $\text{Cr}_{1/3}\text{NbS}_2$. The metallic ferromagnet $\text{Cr}_{1/3}\text{NbS}_2$ (also referred to as CrNb_3S_6) can be described as an intercalation product of the 2H disulfide NbS_2 , with $\text{Cr}_{1/3}\text{NbS}_2$

adopting a hexagonal structure composed of sheets of edge-linked NbS_6 trigonal prisms, with Cr^{3+} ions in octahedral sites between the layers. Depending on the precise stoichiometry and ordering of Cr^{3+} ions over these sites, the structure is described by either $P6_322$ or $P6_3$ symmetry (i.e. Sohncke but non-enantiomorphic space groups) [207, 208]. A range of magnetic ordering temperatures have been reported ($\sim 80\text{ K} \leq T_C \leq \sim 130\text{ K}$) [208–210] and neutron scattering work indicated that in zero-field, the ground state is a chiral, helical magnetic structure, with Cr^{3+} spins in the ab plane (i.e. within the layer plane). The spin helices propagate along the c axis (the direction perpendicular to the layers) with periodicity much longer than the unit cell dimensions (similar to the helical magnetic state observed in zero-field for MnSi discussed below). This helical spin structure results from several factors: the crystal field at the Cr^{3+} sites gives strong uniaxial anisotropy favoring spins in the ab plane, whilst intralayer symmetric ferromagnetic exchange and DMI give the helical spin structure [209]. As for MnSi , this combination of interactions means that $\text{Cr}_{1/3}\text{NbS}_2$ has a complex phase diagram [211]. In addition to the chiral helical magnetic ground state, an applied field along the helix propagation direction can give a helical conical spin state with spins tilting towards the field direction before a forced ferromagnetic state is reached at higher fields. On the other hand, applying a magnetic field perpendicular to the helical axis (i.e. within the plane) gives a chiral soliton lattice (figure 13), with kinks separating ferromagnetic regions. The lengths of the ferromagnetic regions grow (as does the period of the chiral soliton lattice) with increasing applied field strength until a forced ferromagnetic state is reached above some critical field [47, 212]. In summary for $\text{Cr}_{1/3}\text{NbS}_2$:

- Multiple factors give rise to the helical magnetic states observed for $\text{Cr}_{1/3}\text{NbS}_2$ including magnetic anisotropy, symmetric exchange interactions, and antisymmetric DMI.
- The long periodicity of the spin helices compared with the periodicity of the crystal lattice hints at the weaker coupling between magnetic and crystal structures and the potential for field control of the magnetic order.

5.1.7. MnSi . As noted in section 7, intermetallic MnSi crystallizes with the B20 structure described by the Sohncke (but non-enantiomorphic) space group $P2_13$ [214], with the absolute structure determined using resonant x-ray scattering [215]. It orders magnetically below 29 K with a helical magnetic ground state in zero-applied magnetic field with periodicity λ much larger than the lattice dimensions ($\lambda \approx 190\text{ Å}$; $a \approx 4.56\text{ Å}$), similar to observations of $\text{Cr}_{1/3}\text{NbS}_2$ described above [209]. The chiral helical state in MnSi is stabilized by ferromagnetic exchange and (weaker) DMI (allowed in this non-centrosymmetric crystal structure). The crystal field (anisotropic exchange) fixes the propagation vector of the helix along the [111] directions of the unit cell but the much longer periodicity compared with the unit cell dimensions reflects the relatively weak coupling between the magnetic and

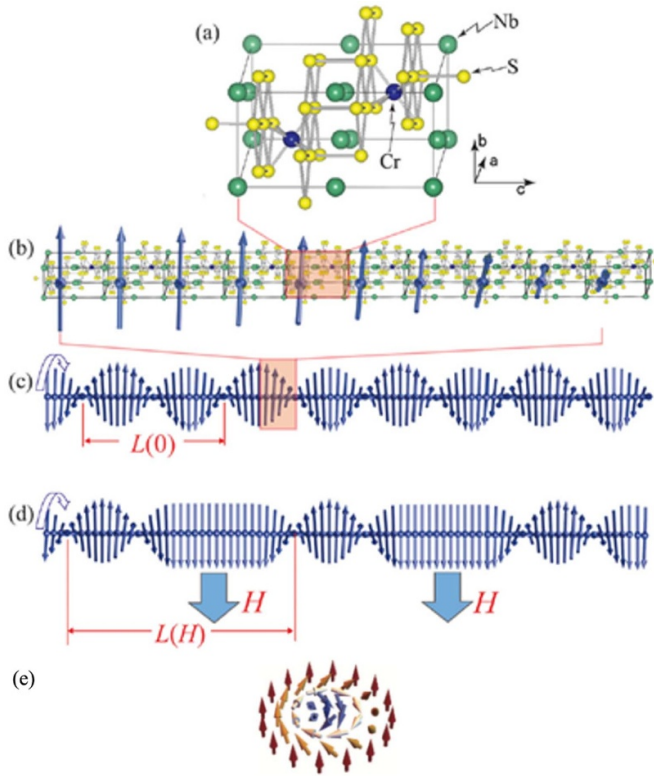


Figure 13. (a) Crystal structure of $\text{Cr}_{1/3}\text{NbS}_2$ showing Cr, Nb, and S ions in blue, green, and yellow, respectively; (b) shows a part of a left-handed chiral helix observed as the magnetic ground state in zero applied field, and (c) shows the whole left-handed spin helix; (d) shows the chiral soliton lattice in applied fields perpendicular to the helical axis. Reprinted figure with permission from [47], Copyright (2012) by the American Physical Society; (e) shows a Bloch skyrmion as observed in MnSi . Reprinted (adapted) with permission from [213]. Copyright (2021) American Chemical Society.

atomic structures [25]. The sense of the magnetic chirality is determined by the crystal chirality: left-handed crystals give left-handed magnetic helices [216]. The relative strengths of the symmetric ferromagnetic exchange and antisymmetric DMI change as a function of the applied magnetic field, giving a fascinating phase diagram [217, 218]. A conical magnetic structure is observed at low temperatures with applied field along [111] [219], before a ferromagnetic state emerges at higher fields. In a small region of the phase diagram in low applied fields and just below T_C , the ‘A phase’ was observed [217, 218]. Neutron scattering experiments showed that this A phase consists of topologically-protected magnetic vortices known as skyrmions (figure 13(e)) [25]. Proposed by mathematician Tony Skyrme [220, 221], these skyrmion particles are relevant to various fields of physics [213], but magnetic skyrmions were predicted by Bogdanov and Hubert to be metastable phases in acentric materials, stabilized by DMI [222]. Mechanisms that give rise to non-collinear magnetic structures are necessary for magnetic skyrmions, and therefore, much research has focused on chiral magnets with non-collinear magnetic structures stabilized by competing symmetric exchange and DMI. However, a wide variety of

skyrmion hosts are known, including those with achiral crystal structures, including [213]:

- the spinel GaV_4S_8 with achiral, but non-centrosymmetric crystal structure which hosts Néel skyrmions stabilized by DMI [223];
- centrosymmetric metallic magnet Gd_2PdSi_3 which hosts Bloch skyrmions that result from frustrated magnetic exchange interactions (and not DMI) [224];
- centrosymmetric $\text{Gd}_3\text{Ru}_4\text{Al}_{12}$ in which Bloch skyrmions are stabilized by a combination of magnetic frustration and RKKY interactions [225].

The observation of these complex non-collinear magnetic textures in materials with a range of crystal symmetries (both centric and acentric) highlights the possibility of achiral crystal structures hosting chiral magnetic structures that result from combinations of symmetric exchange with antisymmetric DMI, frustration or anisotropies, as illustrated by Mn_3Sn and $\text{CaMn}_7\text{O}_{12}$ discussed below.

5.1.8. Mn_3Sn . The metallic half-Heusler Mn_3Sn crystallizes in a centrosymmetric structure of $P6_3/mmm$ symmetry with Mn sites arranged in a Kagome-type lattice in the ab plane, with Sn sites within the hexagons. These Kagome layers are stacked along the c axis, with triangles stacked in a staggered fashion to give twisted triangular tubes. Below $T_N \approx 420$ K Mn_3Sn orders magnetically with Mn spins in-plane in an almost antiferromagnetic arrangement but with a small in-plane ferromagnetic component due to a slight canting of spins [226, 227]. The spin arrangement is referred to as an ‘inverse triangle’ configuration, which results from exchange interactions (which are geometrically frustrated as a result of the Kagome lattice), as well as the magnetic anisotropy of the Mn sites and the DMI [228]. This non-collinear (but co-planar) spin arrangement has vector chirality (i.e. opposite signs for ‘inverse’ and ‘normal’ triangle configurations), and these configurations are non-degenerate due to spin–orbit coupling [229]. This has consequences for the AHE observed in Mn_3Sn , with the sign of the AHE reversed by a small applied magnetic field [230].

5.1.9. $\text{CaMn}_7\text{O}_{12}$. The quadruple perovskite $\text{CaMn}_7\text{O}_{12}$ undergoes a series of phase transitions on cooling. The magnetic phases observed illustrate the delicate balance of interactions that can give rise to chiral magnetic order [231]. Starting from the $R\bar{3}$ phase below 400 K, charge ordering of Mn^{3+} and Mn^{4+} ions over the perovskite B sites occurs on cooling before orbital ordering is observed below 250 K giving an incommensurate structural modulation [232] associated with an orbital density wave [233]. Below $T_{N1} = 90$ K, $\text{CaMn}_7\text{O}_{12}$ orders antiferromagnetically and this magnetic phase transition induces a significant ferroelectric polarization [234]. Below T_{N1} , the Mn spins order in a chiral, in-plane helical structure [34] with periodicity related to the structural incommensurate modulation resulting from orbital ordering [231, 235]. Because the nearest-neighbor magnetic exchange interactions

are via Mn^{3+} 3d orbitals, these interactions are modulated by the orbital density wave which affects the spin helix giving regions with more ferromagnetic interactions (and reduced helicity) and regions with more antiferromagnetic interactions (and increased helicity) [231], and so the helix results from competition between these symmetric exchange interactions [233].

It's striking that this chiral magnetic order emerges from an achiral crystal structure but also that this magnetic ordering breaks inversion symmetry and gives rise to a large electric polarization. The polarization is perpendicular to the spin rotation plane, and the magnetoelectric coupling is thought to arise from ferroaxial coupling between the magnetic helix and the global rotation present in the crystal structure [233] (rotations of parts of a crystal structure concerning the rest, allowed by certain ferroaxial crystal classes) [236]. Spin-orbit interactions are needed for this coupling between the electrical polarization and the magnetic helicity, i.e. via the DMI, by which the helix's non-collinear spin arrangement stabilizes structural distortions. In $\text{CaMn}_7\text{O}_{12}$, these distortions result in a local polarization along c (perpendicular to the spin plane), and the global chirality of the magnetic structure means that these local polarizations sum to give a net polarization, with direction determined by the magnetic chirality [233].

5.1.10. BaCoSiO_4 . The stuffed tridymites often adopt chiral and polar crystal structures and, with their compositional flexibility, offer a promising field in which to explore magnetic chirality [237]. The chiral antiferromagnet BaCoSiO_4 shows coupling between several ferroic orders and helps illustrate the complex coupling between structural chirality, magnetic chirality, polarity, and ferrotoroidicity [238, 239]. The stuffed tridymite structure is built from corner-linked BO_4 and $\text{B}'\text{O}_4$ tetrahedra, with larger A cations in interstitial sites. Slight rotations of these tetrahedra give crystal structures of opposite handedness of $P6_322$ symmetry, while ordering of B and B' cations can give a polar axis, giving chiral and polar structures of $P6_3$ symmetry, as observed for BaCoSiO_4 (figure 14). Interestingly, $P6_3$ symmetry is of crystal class 6, which is pyroaxial [236] (allowing ferrotorotational order), and so, as discussed for $\text{CaMn}_7\text{O}_{12}$ above, this symmetry allows coupling between the structural chirality, magnetic chirality, and electric polarization via the DMI [238]. BaCoSiO_4 orders magnetically below $T_{\text{N}_1} \approx 3.2$ K with a chiral, triangular arrangement of Co^{2+} spins with a slight canting of spins towards the (polar) c axis. This arrangement results from frustrated antiferromagnetic interactions within the triangular units and strong easy-plane magnetic anisotropy, with ferromagnetic canting due to the DMI [239]. This ferromagnetic canting gives these triangular units ferrotoroidal moments, with the direction of the toroidal moment linked to the scalar chirality within each triangle (figure 14(c)). The antiferromagnetic exchange between triangular units is frustrated, so the ground state is ferritoroidal, but a small magnetic field applied along c can induce a transition to a ferrotoroidal phase [238, 239].

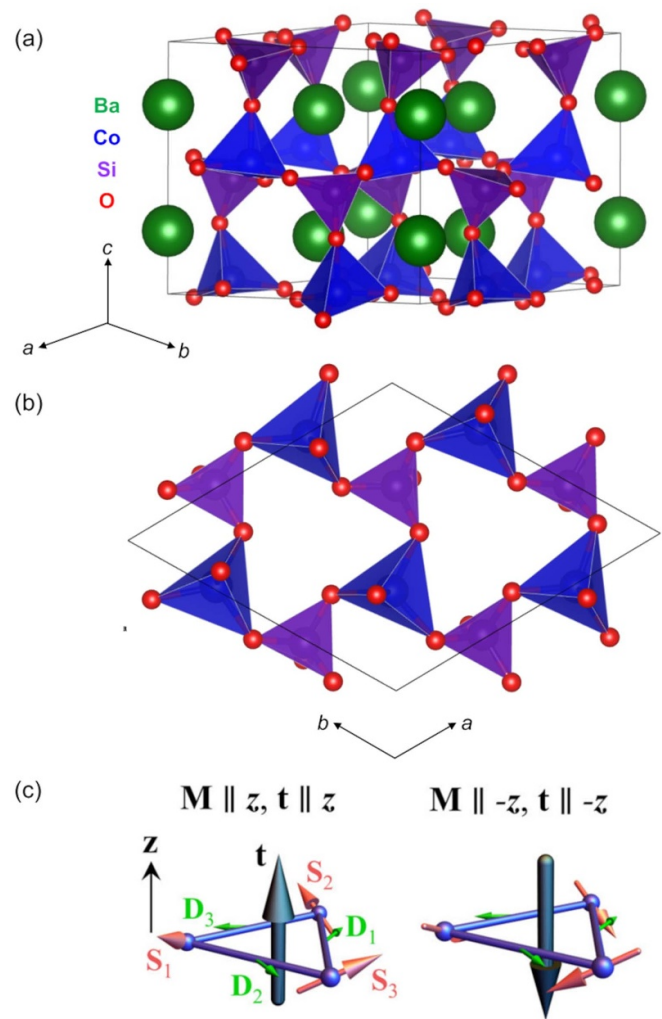


Figure 14. (a) Crystal structure of BaCoSiO_4 and (b) showing puckered rings of corner-linked SiO_4 and CoO_4 tetrahedra, with Ba, Co, Si and O sites shown in green, blue, purple and red, respectively. Panel (c) shows the arrangements of three Co^{2+} arranged in a triangle (spins shown by pink arrows) resulting from frustrated Heisenberg exchange, magnetic anisotropy, and DMI (DM vectors shown by green arrows), giving a toroidal moment (large black arrows) parallel to the magnetization of each triangle. Reproduced from [239]. CC BY 4.0.

5.1.11. Altermagnetism. While magnetochirality is a well-recognized effect with widespread applications, we aim to spotlight a novel form of magnetism that holds the potential to reshape our understanding of magnetic properties in chiral materials: altermagnetism [240].

These new altermagnetic materials share a lack of the nonrelativistic Kramer degeneracy at a general point in the Brillouin zone (BZ), finite anomalous Hall effect (AHE), and finite magneto-optical effect similar to ferromagnets. Typically, spin degeneracy is lifted by one of two means. The first is breaking inversion symmetry in relativistic spin-orbit coupling, which introduces momentum-dependent splitting of the band structure by spin. The second is breaking time-reversal

symmetry, which results in moment-independent spin splitting. This would seemingly indicate that collinear antiferromagnets must have spin degenerate non-relativistic bands. Spin degeneracy can be traced back to crystallography, mainly when nonrelativistic spin groups are employed instead of solely relativistic spin–orbit coupling symmetries. This approach involves two sequential transformations: the first targets the crystal structure, while the second manipulates the spin space, offering a novel perspective on the underlying mechanisms of these magnetic materials [240]. In this scheme, the spin sub-lattices of conventional antiferromagnets are connected through a spin rotation and a spatial translation, which preserves time-reversal symmetry, causing the band structure to have spin degeneracy. Nonetheless, time reversal symmetry can still be broken when the spin sub-lattices are connected by a spatial translation combined with a spatial rotation in addition to the spin rotation. The broken time-reversal symmetry results in spin splitting in the band structure, similar to ferromagnets, while there is zero net magnetization, which defines the new altermagnetic phase.

Given that the magnetic sublattices units can be connected by rotation (sometimes combined with other symmetry operations), it should be expected that some antiferromagnetic enantiomorphic chiral crystals should also manifest altermagnetism, as they can host the primary magnetic anticipated groups to show this effect [241–243]. Though this effect has not (yet) been reported in chiral crystal structures belonging to one of the enantiomorphic space groups, it has already been reported to be the case in the non-enantiomorphic Sohncke space groups [21, 22, 244], hence, this is calling for further studies.

5.2. Topological chiral materials

The intricate relationship between structural chirality and spin has garnered significant attention recently, as evidenced by several notable publications [20, 21, 245–247]. In particular, the work of Chang *et al* delves into the intriguing connection between these two facets of condensed matter physics [21]. They have elucidated how Kramers–Weyl fermions, a fascinating and universal topological electronic property, are inherent to non-magnetic chiral crystals characterized by spin–orbit coupling. This discovery is particularly intriguing because these Kramers–Weyl fermions are not merely coincidental but are intricately tied to structural chirality, lattice translation symmetries, and time-reversal symmetry. In particular, to realize Kramers–Weyl points, two criteria should be met: one breaks inversion symmetry, \mathcal{P} , but respects time-reversal symmetry, \mathcal{T} , whereas the other is the removal of double degeneracy at nontime reversal invariant points (TRIMs). Figure 15 presents a simple description of Weyl point classification in phonons, described in [248]. Therefore, a chiral lattice becomes a prime candidate for realizing Kramers–Weyl fermions as it inherently lacks inversion, mirror, or other roto-inversion symmetries, giving it a well-defined ‘handedness’.

Recognizing these interrelationships opens up exciting avenues for further exploration and understanding of chiral materials, their topological properties, and the intriguing role of chirality in governing electronic behavior. For example, it

has a unique spin texture, giant helicoid Fermi arcs, large topologically nontrivial energy windows, quantized circular photogalvanic effects, etc [249]. The emergence of these topological states represents a unique scenario in which traditional frameworks like the Landau–Ginzburg–Wilson theory fail to explain the transitions leading to these states. Notably, these are conditions where no symmetry is spontaneously broken. Instead, understanding these states relies on a concept known as topological invariance, commonly referred to as the Chern number [250, 251]. This Chern number serves as a global parameter that encapsulates the topological essence of the system and is determined by the structure of the manifold that encloses these states. This approach diverges from conventional theories and offers a more nuanced understanding of the topological properties of the system. In particular, Chang *et al* suggest several materials (where we only report the enantiomorphs) that can have Kramers–Weyl fermions: TiBO_2 ($P4_1$ space group 76), $\text{Sr}_2\text{As}_2\text{O}_7$ ($P4_3$ space group 78), Ag_3SbO_4 ($P4_122$ space group 91), MgAs_4 ($P4_12_12$ space group 92), $\text{H}_4\text{Ca}_2\text{AsF}_{13}$ ($P4_322$ space group 95), $\text{m-Cu}_2\text{S}$ ($P4_32_12$ space group 96), $\text{DyAl}_3\text{Cl}_{12}$ ($P3_112$ space group 151), IrGe_4 ($P3_121$ space group 152), SrIr_2P_2 ($P3_221$ space group 154), $\alpha\text{-In}_2\text{Se}_3$ ($P6_1$ space group 169), $\text{BaN}_2\text{O}_4\cdot\text{H}_2\text{O}$ ($P6_5$ space group 170), Hf_5Ir_3 ($P6_122$ space group 178), $\text{Na}_3\text{B}_4\text{O}_7\text{Br}$ ($P6_522$ space group 179), NbGe_2 ($P6_222$ space group 180), WAl_2 ($P6_422$ space group 181), $\text{Li}_2\text{Pd}_3\text{B}$ ($P4_332$ space group 212), Mg_3Ru_2 ($P4_132$ space group 213). From this list, we find semi-metals and small-gap insulators; some can also host unconventional four-fold-degenerate chiral fermions at TRIMs and may thus host the unconventional spin-3/2 chiral fermion [252] or even quantized photocurrent. Other materials also reported recently are, e.g. $\text{Li}_2\text{Pt}_3\text{B}$ ($P4_332$ space group 212), which is a s-wave superconductor with an antisymmetric spin–orbit coupling induced by the broken inversion symmetry that leads to the spin-splitting of the Fermi surface and gives to unique superconducting properties, such as the parity mixing of Cooper pairs; SrSi_2 is a nonmagnetic double WSM with a circular photogalvanic effect reported [253].

The low numbers of Kramers–Weyl fermion hosts reported for some chiral space groups (indeed, no reported structures for several chiral symmetries!) highlights the gaps in the landscape of chiral materials and motivates materials design and discovery (see section 4.8). According to [254], all the enantiomorphic groups should have materials with emergent particles. This last reference provides a comprehensive classification of emergent particles in time-reversal-invariant systems. The paper focuses on spinful and spinless particles in 3D systems and categorizes them based on the 230 space groups. For example, they report that most enantiomorphs (magnetic and nonmagnetic) have topological properties such as charge -2 , -3 , -4 Weyl points, can have nodal surfaces, and have Dirac points. Here we want to stress that the lack of known and reported chiral materials hinders the exploration of the topological materials in enantiomorphic groups as the list of enantiomorphic groups with representative compounds for emergent particles is incomplete.

On the other hand, we encounter a fascinating phenomenon in condensed matter physics: emerging particles or excitations

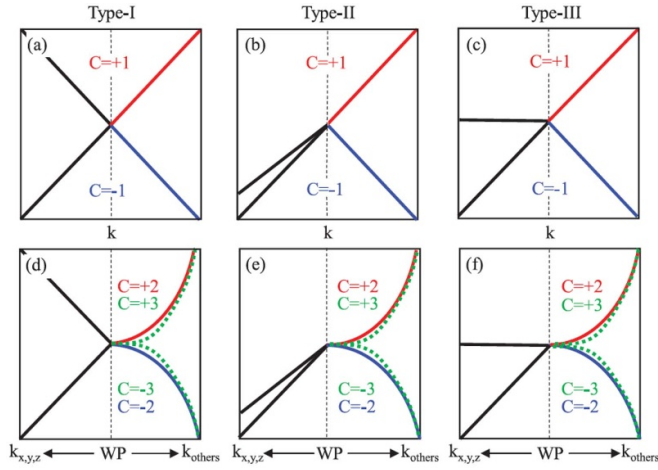


Figure 15. Three types of unconventional Weyl phonons (WPs) localized at HSLs. (a)–(c) Phononic dispersions along the $kx(y, z)$ -WP- k other path for type-I, and type-II and type-III charge-one WP. (d)–(f) Phononic dispersions along the $kx(y, z)$ -WP- k other path for type-I, type-II, and type-III CTWP and charge-three WP, where the solid red-blue and green-dashed lines denote the phononic dispersions of charge-three WP. Reproduced from [248].

CC BY 4.0.

owe their existence to degenerate band crossings within the dispersion relation. These band crossings can involve electrons, phonons, or magnons and are safeguarded by specific symmetries inherent to the system. Topological materials can typically be categorized based on the type of band crossing they exhibit. The first category consists of materials with zero-dimensional (0D) band crossings, commonly called nodes or nodal points. These include Dirac semimetals (DSMs) and WSMs, where either doubly or singly degenerate bands intersect at discrete points near the Fermi level (E_F). The second category features materials with one-dimensional (1D) band crossings, which occur along lines in momentum space. Such materials are generally termed topological nodal-line semimetals (TNLSMs) and exhibit four or twofold band crossings along these lines. Finally, the third category encompasses materials with 2D band crossings preserved on a surface within the 3D BZ. These materials are topological nodal-surface semiconductors and represent a more complex form of band crossing. An excellent discussion of the differences between these groups can be found in [247]. Weyl particles serve as a pioneering example of topological materials. In this context, these particles emerge due to the convergence of two distinct bands in the material's energy dispersion, one for each spin channel. What distinguishes Weyl particles is their unique status as symmetry-protected entities arising from the crystal's inherent symmetries. This symmetrical protection bestows these particles a distinctive topological charge, a quantized Berry flux residing in momentum space. Within Weyl particles, this topological charge is quantified by an integer known as the Chern number, as introduced before. This numerical value plays a pivotal role, imparting a sense of handedness to the electronic wavefunction associated with these particles and capturing the topology of the filled electron

bands. In essence, the Chern number encapsulates the topological properties of Weyl particles, dictating their behavior and providing an intrinsic link between their emergence and the underlying symmetries of the crystal lattice. The Chern number generally identifies the topological invariance of quantum Hall insulators. This connection between topology and symmetry is a profound revelation in condensed matter physics, offering a deeper understanding of how exotic particles like Weyl fermions come into existence and how they influence the electronic properties of materials.

Given the structural attributes of the chiral materials under discussion, it is evident that their unique topological properties and emergent particles extend to other excitations, such as in phonon band structures. For instance, KMgBO_3 has been reported to feature multifold and multidimensional topological phonons and charge-four Weyl phonons [255]. Similarly, TlBO_2 (space group 76) exhibits multi-Weyl points in its nonmagnetic crystals [256]. In the case of $\alpha\text{-TeO}_2$ (space group 92), non-symmorphic twist symmetries underlie phonon band anti-crossings and topological behaviors [257]. CsBe_2F_5 (space group 213) uniquely hosts type-I and type-II unconventional charge-two Weyl points with varying Chern numbers [248]. MgAs_4 ($P4_12_12$ space group 92) features topological Weyl points arising from twisting phonon symmetries that combine rotational and translational elements [258]. The coexistence of charge-2 Weyl and charge-2 Dirac points characterizes BaPt_2S_3 ($P4_12_12$ space group 92) [259]. In contrast, $\text{K}_2\text{Mg}_2\text{O}_3$ ($P4_32_12$ space group 96) and $\text{Nb}_3\text{Al}_2\text{N}$ ($P4_132$ space group 213) host isolated Weyl phonons with two or four Chern numbers in their acoustic branches [260]. Moreover, there are instances where topological phonons coexist with other topological particles, such as the reported coexistence between charge-2 Dirac points and Weyl phonons in enantiomorphic space groups 92, 94, and 96, specifically in $\text{Na}_2\text{Zn}_2\text{O}_3$ ($P4_32_12$ space group 96) [261]. This extensive work underscores chiral materials' rich topological landscape regarding emergent particles and complex phonon band structures.

5.3. Electric properties

While the change of optical activity of magnets (or diamagnetic substances) under an applied magnetic field was discovered by Faraday in 1845 (the Faraday effect, see section 5.1), the analysis of the analogous electric phenomenon, i.e. the change of optical activity under an applied electric field, came more than a century later [262–270]. The (linear) electrogyration tensor η can be defined as the change of optical activity under an applied electric field \mathbf{E} :

$$\gamma_{ijk} = \left. \frac{\partial g_{ij}}{\partial E_k} \right|_{\mathbf{E}=0}, \quad (8)$$

where i, j and k refer to the Cartesian directions and g is the gyration or optical activity tensor. Hence, as for the Faraday effect, a crystal not optically active can show electrogyration as an applied electric field can induce a non-zero optical activity. All crystals can exhibit linear electrogyration except those with symmetry $m3m$, $\bar{4}3m$ and 432 [267, 271]. Of course,

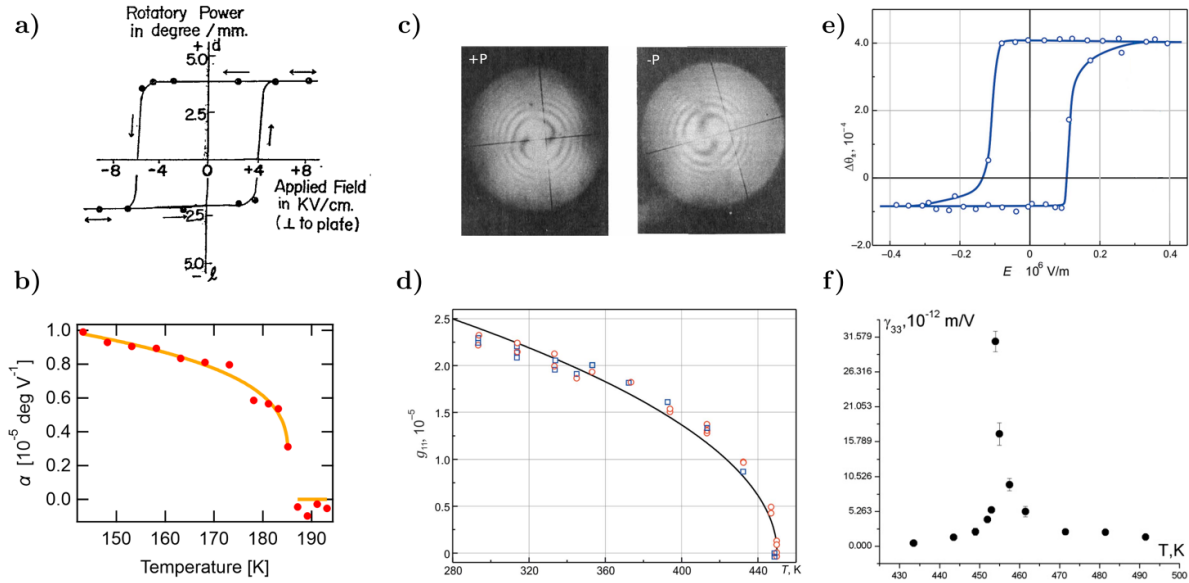


Figure 16. (a) Hysteresis loop of the optical activity rotation versus electric field as measured in $\text{LiH}_3(\text{SeO}_4)_2$. Reproduced with permission from [272]. © 1962 The Physical Society of Japan. (b) Temperature evolution of the absolute value of the electrogyration coefficient of a single domain of $\text{RbFe}(\text{MoO}_4)_2$. Reprinted figure with permission from [273], Copyright (2021) by the American Physical Society. (c) Airy's spirals of the ferroelectric $\text{Pb}_5\text{Ge}_3\text{O}_{11}$ crystal for the two polarized domains (+P and -P). [274] [10 June 2011], reprinted by permission of the publisher (Taylor & Francis Ltd, www.tandfonline.com). (d) Temperature dependence of the absolute value of the gyration component of $\text{Pb}_5\text{Ge}_3\text{O}_{11}$ as measured experimentally (red circles and blue squares), the black curve shows the theoretical evaluation. (e) Hysteresis flip of the optical activity angle versus electric of $\text{Pb}_5\text{Ge}_3\text{O}_{11}$. (d) and (e) Reproduced with permission from [275]. Copyright © International Union of Crystallography. (f) Temperature dependence of the electrogyration coefficient of $\text{Pb}_5\text{Ge}_3\text{O}_{11}:\text{Cr}$ crystal. Reproduced from [276]. © IOP Publishing Ltd. All rights reserved.

higher-order electrogyration responses (quadratic electrogyration) can exist if one treats higher derivatives of the optical activity tensor.

The special case where the optical activity is reversed by an applied electric field is called gyroelectricity [262, 277] or ferrogyrotropy [278, 279]. There is also the special case of hypergyroelectricity [262, 267]), which is defined as crystals where it is the electrogyration (vs the optical activity reversal for gyroelectrics) that can be reversed by an electric field. There is an intimate link between gyroelectricity and ferroelectricity, as reversing the optical activity under an electric field is done by reversing the polarization. Some of the first observations of gyroelectricity were made on $\text{Ca}_2\text{Sr}(\text{C}_2\text{H}_5\text{CO}_2)_6$ [280] and $\text{LiH}_3(\text{SeO}_4)_2$ [272] ferroelectric crystals in 1962. In these measurements, a hysteresis loop is observed when plotting the optical activity versus the applied electric field (see figure 16(a) for the case of $\text{LiH}_3(\text{SeO}_4)_2$). Having such a switchable optical activity under an applied electric field with a hysteresis loop shape raised the question of whether the optical activity can form or be associated with a new ferroic order [278]. However, as the optical activity tensor is mediated by the ferroelectric order, it has been defined as an implicit form of ferroicity, i.e. it can only be affected through an accompanying explicitly ferroic order [278]. Hence, in a gyroelectric crystal, the optical activity tensor evolution with temperature follows the ferroelectric polarization, i.e. evolves as a square root function below T_C (see, e.g. figure 16(b) for $\text{RbFe}(\text{MoO}_4)_2$ or figure 16(d) for $\text{Pb}_5\text{Ge}_3\text{O}_{11}$). Then, several crystals were reported for their

electrogyration and/or their gyroelectric response, such as the boracites $\text{Co}_3\text{B}_7\text{O}_{13}\text{I}$ and $\text{Cu}_3\text{B}_7\text{O}_{13}\text{Cl}$ [281], the sillenites $\text{Bi}_{12}\text{SiO}_{20}$ and $\text{Bi}_{12}\text{GeO}_{20}$ [282, 283], $\text{Sn}_2\text{P}_2\text{S}_6$ [284], Stolizite PbMoO_4 and PbWO_4 [285] or more recently in the ferroaxial phase transitions reported in NiTiO_3 [286] and $\text{RbFe}(\text{MoO}_4)_2$ [273] (see figure 16(b)). Among them, one of the most studied crystals for its large gyroelectric and electrogyration response is the aforementioned lead germanate $\text{Pb}_5\text{Ge}_3\text{O}_{11}$ (see sections 4.5, 7 and figure 16). Figure 16(c) shows the Airy's spirals of the two ferroelectric domains of $\text{Pb}_5\text{Ge}_3\text{O}_{11}$ where we can observe the change of the rotation direction in the two cases. Figure 16(d) shows the evolution of the temperature dependence of the gyration amplitude of $\text{Pb}_5\text{Ge}_3\text{O}_{11}$ which becomes non-zero at the ferroelectric phase transition and evolves as a square root function, i.e. like the polarization of the material. Figure 16(e) shows how the optical activity angle evolves under an applied electric field in $\text{Pb}_5\text{Ge}_3\text{O}_{11}$. Here again, we can see that the optical activity exhibits a hysteresis shape as it follows the switching of ferroelectric polarization under an applied electric field. Finally, figure 16(f) shows the evolution of the electrogyration coefficient of doped $\text{Pb}_5\text{Ge}_3\text{O}_{11}:\text{Cr}$ crystal when varying the temperature. Here again, at the critical temperature where the ferroelectric phase transition appears, we can observe the divergence of the electrogyroelectric response, with very large values compared with crystals that do not have such a phase transition. Recently, Fava *et al* [156], have shown from DFT calculations that the chirality of the ferroelectric phase comes from a polar soft mode that induces the phase transition. This offers

a microscopic understanding of why the optical activity follows the ferroelectric polarization in a one-to-one way, given that the polar distortion is also chiral.

We can see that electrogyration and gyroelectricity were topics put aside in the past 10 years. Still, they could be brought back to the forefront with the increase in interest in chiral crystals and the recent advance in photonic applications.

5.4. Strain

The study of elastic properties in chiral materials is an emerging field that has garnered increasing attention over the years. One of the pioneering works in this area can be traced back to the study by Ben-Haïm *et al* [287], which delved into the elastic constants of 30 nm chromatin fiber. The study examined the fiber's DNA elastic properties and geometric attributes and made significant inferences about how the inherent chirality of the chromatin fiber influences its mechanical characteristics.

In the context of structural chiral materials, the work by Huang *et al* [288], which delves into the atomic-scale sensitivity of elastic properties in chiral crystals, stands out in the field. The paper is particularly noteworthy for exploring the Dresselhaus effect in ferri-chiral crystals and specifically identifying NaCu_5S_3 as a material that exhibits this unique behavior. The study further discusses the potential for switching chirality, affecting the Dresselhaus spin splitting. This opens up new avenues for understanding the intricate relationship between chirality and spin in periodic crystals, offering a compelling alternative to the conventional Rashba spin textures.

On the other hand, the interplay between chirality and optical activity as influenced by strain remains a relatively unexplored area in materials science, however a good theoretical description of the phenomena is provided in [289]. While some studies have touched upon this subject, as seen in materials like NaCu_5S_3 [290] or $\text{Co}_3\text{Ni}_3\text{Ga}_8$ [291], they offer limited insights into how strain specifically alters the optical activity. One of the seminal studies in this field centers on dicalcium strontium propionate (DSP), $\text{Ca}_2\text{Sr}(\text{C}_3\text{H}_5\text{CO}_2)_6$ [278, 292, 293]. This unique material is both ferroelastic and ferroelectric, exhibiting gyrotropic behavior under the influence of uniaxial stress. The authors of these works provide an in-depth analysis of how mechanical strain impacts the optical properties of DSP across its various phases and domains. The material undergoes a subtle lattice distortion upon applying strain, transitioning from a high-symmetry phase with $m3m$ symmetry to a low-symmetry phase characterized by 422 symmetry. This phase transition occurs at a critical temperature of 281.7 K, leading to six distinct gyrotropic states, each defined by a unique gyration tensor. This structural phase transition can be generalized regarding macroscopic symmetry breaking, as discussed in [294].

The elastic properties of other chiral materials have also been studied, including TeO_2 [17], where $\alpha\text{-TeO}_2$ is noted for its acoustic-optic properties, which result

from its unusual elastic behavior and high birefringence; $(\text{C}_5\text{H}_{11}\text{NH}_3)_2\text{ZnCl}_4$ [295], where strain can break the symmetry of this electro-toroid system and the system becomes spontaneously optical active; Cu_2OSeO_3 [296, 297], where the dichroism extinction effect measured in this material which shows helical, conical, and skyrmion phases, and the sound velocity is affected by direction of an applied magnetic field CrNb_3S_6 [298], where the hybridization of the rotational and translational vibrational modes provides a unique response related to elastic response. (The effect on the optical activity of CrNb_3S_6 is not yet reported.)

Interestingly, the direction and magnitude of the applied stress can induce shifts in both the ferroelastic and gyrotropic states across different domains within the material [289]. This makes DSP one of the rare instances where external forces can selectively stabilize certain domains over others [278]. Transitions between states in different domains are triggered when the applied force creates a sufficient disparity in the stored free enthalpy between the domains, overcoming the energy barrier that separates them. This manifests as a change in sign in the optical activity tensor. Furthermore, although the activity tensor remains invariant under time inversion, its behavior can be modulated in magnetism through coupling with the magnetoelectric effect.

6. Chiral phonons

In an attempt to respond to the question of whether ‘if electrons can carry chirality at valleys in hexagonal 2D arrays, might photons do the same?’, Zhang and Niu [31] put the notion of phonon chirality in the spotlight in 2014 from a theoretical perspective. The experimental validation through an optical pump-probe technique and infrared CD came a few years later [30], which has pushed interest in chiral phonons to the forefront [32, 298–309]. Indeed, observing and manipulating chiral phonons has opened new research directions such as the phonon Hall effect, phonon Berry curvature [310–313], phonon effective magnetic field and induced orbital or spin magnetization [33, 302, 308, 314, 315], current induced by chiral phonons [306], axial thermal expansion [299] or even using chiral phonons as dark matter detectors [316], all of them extending the field of phononic applications to new horizons [317].

To qualify the phonon chirality, Zhang and Niu used the pseudo angular momentum (PAM) of the eigendisplacements associated with this phonons [318] (see figure 18). We point out that the concept of PAM was previously introduced in [319] in the context of electronic Bloch states at high symmetry points and hence characterized by a discrete rotational invariance. The PAM (both in the phonon and electron contexts) can be thought as the unitary generator of such point group rotation and is expected to be a conserved quantity. With reference to [31], it can be seen that the Zhang and Niu treatment allows the splitting of the phonon eigenvectors into right and left-handed sublattices and defines a circular

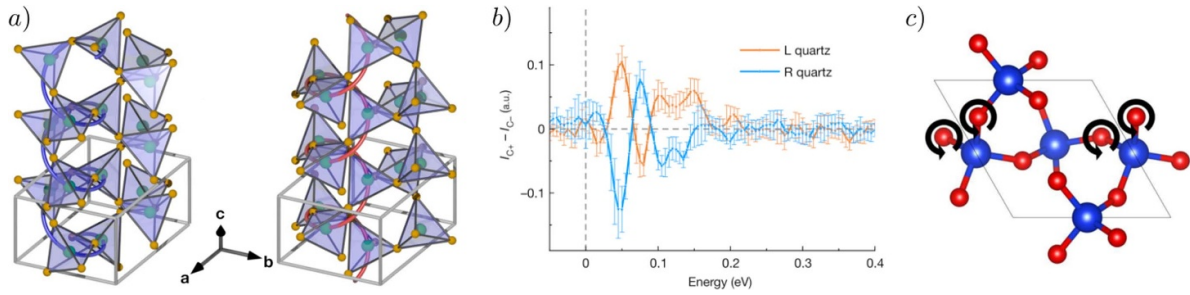


Figure 17. (a) Schematic picture of left ($P3_221$ space group) and right ($P3_121$ space group) handed quartz crystal structures. The tetrahedra represent the SiO₄ units. (b) Circular dichroism of the left and the right-handed quartz as extracted from the resonant x-ray scattering at the reciprocal lattice vector $q = (-0.25, 0, 0.32)$. (c) Schematic picture of the oxygen chiral motions of the phonon mode probed at $q = (-0.25, 0, 0.32)$. Red balls are for the O, and blue balls for the Si. Reproduced from [309]. CC BY 4.0.

polarization of the phonons. It is worth mentioning that while Zhang and Niu's paper refers to the phonon chirality in 2D, validation of such a concept requires its extension to 3D systems and in particular to the case of structures which symmetry operations belong to one of the enantiomorphic space groups. This extension has been recently provided in [320] with particular reference to the consequences of having non-symmorphic operations. The direct use of PAM was barely studied except when it interacts with the magnetic properties. Another interest for PAM is observing, characterizing, and exciting chiral phonons through polarized light. This was exemplified by Ishito *et al* in their polarized Raman scattering experiments to identify chiral phonons in cinnabar (α -HgS) [303]. They demonstrated the possibility of probing the chirality of the crystal domains through non-contact and non-destructive measurements. They showed that the conservation law of the pseudo-angular momentum between light and phonons allows momentum transfer, hence it is ideal for combined opto-phononic technological applications [321]. Clear experimental measurement of chiral phonons has recently been made in quartz through resonant inelastic x-ray scattering with circularly polarized x-rays [309]. By construction, the circularly polarized x-rays are chiral such that they can interact with chiral phonons of reciprocal space and, hence, dispersion of the chiral phonon modes can be obtained, see figure 17. The authors also performed DFT calculations and showed that the charge quadrupole of the O 2p orbitals in the chiral phonon eigenvector is the source of the dichroic x-ray signal detected experimentally.

In their article 'Orbital magnetic moments of phonons' [33], Juraschek and Spaldin made a systematic DFT calculation of the induced orbital magnetization coming from PAM in ionic crystals. Because chiral phonons will carry PAM by definition, they will naturally carry an orbital magnetic moment. In ionic crystals, the rotation of charged ions will induce magnetic moments through their gyromagnetic ratio. Hence, defining a phonon magneton as a unit measure of this effect is possible. Juraschek and Spaldin found that the order of magnitude of this phonon magneton is about $10^{-4} \mu_B$. This effect could be observed experimentally by ultrafast laser excitations of phonons.

The effect of chiral phonons on magnetism can be seen as an effective magnetic field on the system, also described as

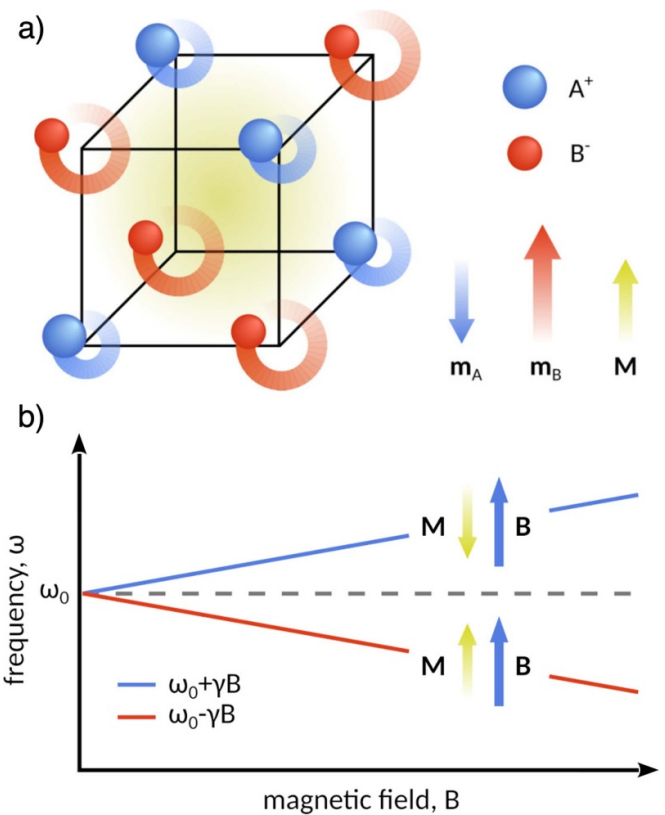


Figure 18. (a) Schematic picture of local circular motions of ions as present in chiral phonons, here for a hypothetical diatomic ionic crystal (e.g. PbTe [322]). The circular motions of the ions create local magnetic moments of different amplitudes m_A and m_B such that the total magnetic moment M is non-zero. Reprinted figure with permission from [322], Copyright (2022) by the American Physical Society. (b) Schematic picture showing the phonon Zeeman splitting of a degenerate mode. The phonon frequency (ω) is plotted concerning the magnetic field amplitude (B) where the phonon eigenvector with opposite magnetic moment to the field is shifted upward ($\omega_0 + \gamma B$). In contrast, the one with moment aligned with the field is shifted downward ($\omega_0 - \gamma B$) where γ would represent the gyromagnetic ratio of the phonon. Reprinted figure with permission from [323], Copyright (2017) by the American Physical Society.

a phonon analog of the inverse Faraday effect in optics [302, 314, 321, 324, 325]. Xiong *et al* [314] used a classical point charge model (using the Born effective charges of the atoms)

and a fundamental magnetostatic Biot and Savart law to show that the circular motion of charged atoms of chiral phonons will induce a local effective magnetic field. They show that in systems with time-reversal symmetry, chiral phonons' total induced effective field is zero but can be observed through temperature gradients. When applied to bulk tellurium, their model can give a total effective magnetic field of 0.01 Tesla at room temperature. They also show that this effective magnetic field from chiral phonons can renormalize the Curie temperature of ferromagnetic substances with Heisenberg model interactions. While this effective magnetic field of chiral phonons was reported to be relatively small, recently, Juraschek *et al* [302] have estimated from first-principles calculations and microscopic models that the effective magnetic field can be larger than 100 Tesla in rare earth trichlorides under the conditions of ultrafast laser excitation experiments. This can also explain the large phonon splitting between left and right circularly polarized eigenvectors under applied magnetic field reported by Schaack in the paramagnetic CeF_3 [326] or more recently in the DSM Cd_3As_2 [327] where a large phonon Zeeman effect was observed (with an effective phonon moment of $2.7\mu_B$). If such a giant magnetic effective field induced by ultrashort terahertz pulses is confirmed experimentally, this will put the field of phonomagnetism at a new scale with a high impact in materials science [328–330]. Such an effect being possible in non-magnetic insulators opens the way for inducing dynamical magnetoelectricity in non-magnetic non-polar materials through chiral phonons is now also at its infancy [308, 322, 323, 331, 332].

Another effect that has been raised by Geilhufe [333] is that the circular motion of ions introduces inertial effects on electrons, which can be seen as effective Zeeman-like splitting of the phonon frequencies.

The transfer of angular momentum between phonons, electrons, and magnetism (spin and/or orbital) relies on the electron-phonon coupling. However, its exact microscopic mechanism was not clearly defined until recently [334]. This transfer of angular momentum to magnetism is intimately linked to the Einstein/de Haas or Barnett effect, which highlights the fact that changing the magnetization of a material induces a mechanical rotation of the sample and the other way around, respectively [335, 336]. Recently, Mentink *et al* [337] have developed a microscopic theory of an 'angulon' quasiparticle to unify these effects. Through this theory, they show that new high-frequency effects should be observed in electron spin resonance that could help understand the transfer of angular momentum appearing in ultrafast experiments.

To conclude this section, we mention that the concept of chirality can be associated with zone-center phonons, although the corresponding modes must have zero angular momentum. Different metrics should be adopted in that case, such as the continuous chirality measure (CCM) [28] for example. Recently applied to the chiral eigendisplacements of $\text{Pb}_5\text{Ge}_3\text{O}_{11}$ at the Γ point, the CCM has been found to increase concerning the phonon frequency [156] due to the significant presence of oxygen in the unit cell. This suggests the use of high-frequency electric fields as a way to realize the control of this chiral degree of freedom through a fast-switching

mechanism [156]. Moreover, a $\Delta\mathbf{L}_{ph}$ difference—which could be interpreted as a torque—can be induced by a nonchiral to chiral phase transition as also reported in [156]. Again in the context of theoretical predictions, 3D chiral Weyl phonons have been recently predicted in elementary Te systems [338]. In particular, a relationship between the phonon PAM, angular momentum, structural symmetries and Weyl Chern number has been identified [338].

The chiral phonons field has been particularly active within the past few years, where a first dedicated CECAM workshop was organized in July 2023 [339]. Hence, we can expect more regarding chiral phonons in both fundamental research (chiral bosons) and new technological applications (phononics).

7. Chiral order parameter and control of structural chirality

An order parameter can be defined as a degree of freedom whose magnitude signifies the transition from one phase to another. Typically, these phases are distinguished by the presence or absence of specific symmetries. The existence of an order parameter is linked to the notion of (spontaneous) symmetry breaking (SSB), which aligns with the Landau theory of phase transitions [340], although several exceptions are known (e.g. topological [341], liquid-gas or reconstructive [342] phase transitions, for instance). The idea of a spontaneous order appearing below a critical temperature T_c is thus generally associated with the breaking of symmetry as a result of an instability of some kind in the system: a magnetic order breaks the $\text{SO}(3)$ rotation of the spin, a polarization breaks the inversion along some mirror plane (while leaving more than one position unmoved under point group operations, thus removing the inversion center) and so on. Hence, we can raise the following questions: Does the spontaneous emergence of a structural distortion from a high-symmetry achiral phase to a low-symmetry chiral phase produce an independent order parameter? And can we treat this distortion as an internal degree of freedom in a crystal?

If a crystal possesses an unstable phonon that drives a transition from an achiral to a chiral phase, it is natural to adopt the amplitude of the symmetry-lowering mode as the order parameter. In this case, the phase transition is displacive or order-disorder (i.e. not reconstructive) when a group-subgroup relation between the two phases exists, which also means it preserves the internal connectivity and does not break any bonds [343]. It can also be linked to a free energy double well, as illustrated in figure 19, where both the achiral and chiral configurations are energetically feasible within the solid-state transition. In such scenarios, we can classify this structural phase transition as primarily chiral, where chirality is the primary order parameter. As we have seen in section 4, a few examples of displacive chiral phase transitions are known (e.g. K_3NiO_2 [136]). While the distortion originating from the unstable mode drives the system to be chiral, there exists ambiguity regarding its classification as the chiral order parameter. Despite the distortion embodying chirality is coming from the soft phonon mode, determining it as the definitive

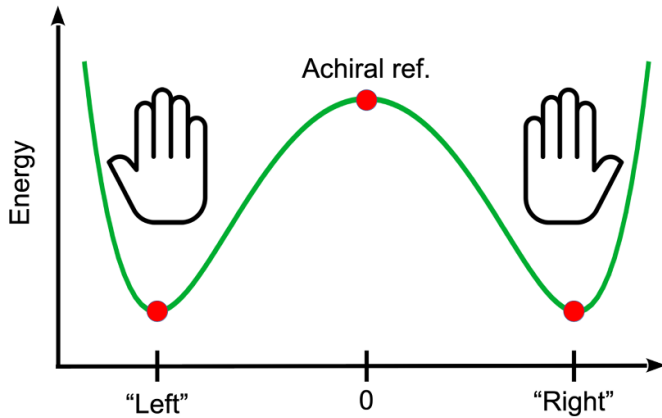


Figure 19. Schematic picture of a double well associated to a chiral structural instability coming from an achiral reference structure.

chiral order parameter requires a more profound investigation. Additionally, a close examination is essential to clarify whether the magnitude of this distortion inherently captures chirality to the degree that justifies its acknowledgment as the chiral order parameter.

This section delves into the current literature surrounding the definition of an order parameter for chirality in periodic crystals and the mechanisms by which external stimuli can trigger chirality flipping. Additionally, we investigate the case of coupled order parameters to chirality, in which enantiomorphic switching could occur by flipping those other order parameters. Controlling the associated structurally chiral domains by external means are enormously appealing as this would open materials science to new functionalities based on chirality. Defining an order parameter for chirality, quantifying it (see section 8), and having an associated conjugate field would also have substantial consequences in the fundamentals of solid state physics as chirality would enter as a new ferroic order aside to ferroelectricity, ferromagnetism, ferroelasticity, and ferrotoroidicity [344]. Furthermore and since the purpose of this section is to focus on chiral orders in periodic solids, we will not explore this concept in polar vortices in nanostructures or in stacked and twisted 2D layers, although we provide some references in appendices A and B.

7.1. Definition of a chiral order parameter

A crystal is chiral if its space group only contains proper operations [28]. Hence a straightforward definition of a chiral order parameter, associated with an achiral phase, would be that of a degree of freedom—for instance a phonon or symmetry adapted mode—which spontaneously breaks some improper (e.g. mirror) operations, thus inducing chirality in the system. Some additional restriction requires having the chiral order to belong to a non-invariant irreducible representation of an achiral space group, and the most logical choice is represented by the time-reversal even pseudoscalar representation. It has in fact been proven that every chiral space group possess the so called G_0 monopole [49], which is a pseudoscalar

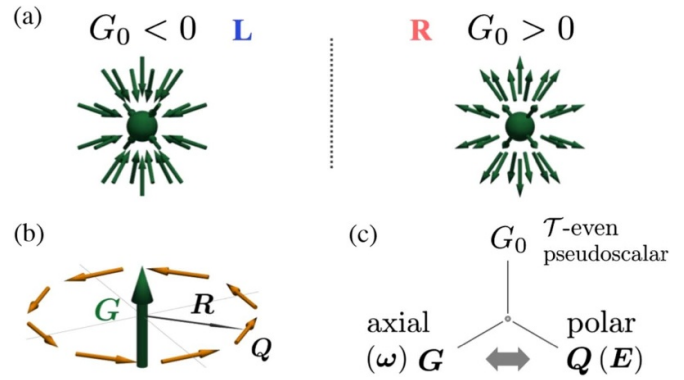


Figure 20. (a) Schematic picture of the left (L) and right (R) handed pseudoscalar electrotoroidal monopole G_0 where the green arrows represent the flux of electrotoroidal dipoles. (b) ‘Classical’ representation of the toroidal moment as a vortex-like configuration of dipoles Q . The axial-polar-chiral (pseudoscalar) interaction is represented in (c), where Q is the electrotoroidal dipole, E is the electric field and ω is an axial deformation of either electromagnetic or mechanical origin. Reprinted figure with permission from [345], Copyright (2022) by the American Physical Society.

property. One can associate the sign of G_0 with a specific handedness following a convention as in figure 20 from [345]. Naturally, many distinct properties may fulfill the requirement of being pseudoscalars and in several physical contexts. As explained in appendix C polar and axial components may be extracted from the multipole expansion of a generic observable operator. While neither is necessarily by itself chiral, assuming for example a polar vortex $\mathbf{P}(\mathbf{r})$ such that $\nabla \times \mathbf{P} \neq 0$, the dot product $\mathbf{P}(\mathbf{r}) \cdot (\nabla \times \mathbf{P}(\mathbf{r}))$ represents a local 3D formulation of G_0 , albeit not a unique one. While the specific formulation of a chiral order parameter depends on the problem under consideration and may change upon the context (with the sole requirement of being zero in space groups possessing improper symmetry operations), the possibility of a spontaneous transition from an achiral reference phase to a chiral state has been elucidated in several recent works [294, 346, 347]. In particular and with reference to the work of Hlinka [346], it is easy to spot that the chiral representation can be obtained as the product between the polar and the axial representations as also highlighted in the character table figure 21. This detail is crucial to define a so called enantioselective effect, namely an interaction between a chiral material and an external parameter capable of removing the degeneracy between states equidistant from a nonchiral reference but with opposite handedness.

7.1.1. Enantioselectivity mediated by physical effects. After defining the electric toroidal monopole as a chiral order parameter, Kishine *et al* [49] try to define an associated conjugate field. According to them, this conjugate field should be able to favor one or the other enantiomorphic phase through flipping the sign of G_0 , i.e. it should have the same symmetry transformation as G_0 (the field times G_0 should be an invariant of the Hamiltonian). One proposed example of such a field is the

| Irrep | E ∞ 2_{\parallel} | $\bar{1}$ $\bar{\infty}$ m_{\perp} | m_{\parallel} | 2_{\perp} | $1'$ ∞' $2'_{\parallel}$ | $\bar{1}'$ $\bar{\infty}'$ m'_{\perp} | m'_{\parallel} | $2'_{\perp}$ | Symbol |
|------------------------|------------------------------------|--------------------------------------------|-----------------|-------------|---------------------------------------|-----------------------------------------------|------------------|--------------|----------|
| $A_{1g}(\Sigma_g^+)$ | 1 | 1 | 1 | 1 | 1 | 1 | 1 | 1 | N |
| $A_{2g}(\Sigma_g^-)$ | 1 | 1 | -1 | -1 | 1 | 1 | -1 | -1 | G |
| $A_{1u}(\Sigma_u^+)$ | 1 | -1 | 1 | -1 | 1 | -1 | 1 | -1 | P |
| $A_{2u}(\Sigma_u^-)$ | 1 | -1 | -1 | 1 | 1 | -1 | -1 | 1 | C |
| $mA_{1g}(m\Sigma_g^+)$ | 1 | 1 | 1 | 1 | -1 | -1 | -1 | -1 | L |
| $mA_{2g}(m\Sigma_g^-)$ | 1 | 1 | -1 | -1 | -1 | -1 | 1 | 1 | M |
| $mA_{1u}(m\Sigma_u^+)$ | 1 | -1 | 1 | -1 | -1 | 1 | -1 | 1 | T |
| $mA_{2u}(m\Sigma_u^-)$ | 1 | -1 | -1 | 1 | -1 | 1 | 1 | -1 | F |

Figure 21. Character table of the point group $\infty/m\bar{1}$ point group from [346]. Here **N**, **G**, **P** and **C** represent the time-even nematic, axial, polar and chiral orders respectively. At the same time, **L**, **M**, **T** and **F** indicate the antiferromagnetic, magnetic, magneto-toroidal and time-odd chiral representations. Reprinted figure with permission from [346], Copyright (2014) by the American Physical Society.

so-called Lipkin ‘zilch’ ρ_{χ} [49, 348–350]:

$$\rho_{\chi} = \frac{\epsilon_0}{2} \mathbf{E} \cdot (\nabla \times \mathbf{E}) + \frac{1}{2\mu_0} \mathbf{B} \cdot (\nabla \times \mathbf{B}), \quad (9)$$

which can be a measure of the chirality of an electromagnetic field [349] (e.g. a circularly polarized wave) and where \mathbf{E} and \mathbf{B} are the electric and magnetic fields, respectively. This spacial-dependent zilch field is a conserved property of the electromagnetic fields in vacuum [348, 351]. Such an object may couple with the structural chirality of a crystal since the product between a vector (namely, the electric field) and a pseudovector (that is, $\nabla \times \mathbf{E}$) must contain the pseudoscalar irreducible representation. The electromagnetic force associated with circularly polarized waves contains a chiral contribution and produces a torque that can be used to trigger enantiomeric separation in, e.g. plasmonic nanoparticles [352, 353] or molecules [354]. While it has recently been proposed in the context of crystal enantioselectivity [136, 345], to the best of our current knowledge, no experiment in this sense has been performed.

If we define χ as the pseudoscalar gyrotropic order parameter, by a small modification of equation (3) of [345], we have the following interaction:

$$V = h_{ij} \chi \cdot P_i \cdot G_j - \mathbf{P} \cdot \mathbf{E} - \mathbf{G} \cdot (\nabla \times \mathbf{E}) \quad (10)$$

where \mathbf{G} is the axial electrotoroidal moment [355, 356] and h_{ij} a material-dependent coupling. If the polar and toroidal ‘auxiliary’ orders are non-spontaneous, we can recast the previous expression as $V = \chi h'_{ij} \cdot E_i \cdot (\nabla \times \mathbf{E})_j$. The expression of equation (10) can break the degeneracy between two opposite-handed crystal phases, hence allowing enantioselectivity. Naturally, this comes with the additional energy cost of creating auxiliary orders, specifically a polar order and an

electrotoroidal order, from the same electromagnetic perturbation. This strategy involving axial and vector fields has been explored for tuning chirality in [136]. Finally, along with the zilch, we ought to mention that electromechanical interactions may also couple with a chiral order. An axial configuration of dipoles can also be triggered by a rotational lattice deformation ($\nabla \times \mathbf{u}$, where \mathbf{u} is an ion displacement vector). Thus, such rotational distortion applied simultaneously with an electric field could be used to directly affect the chirality as much as the aforementioned zilch and as suggested by [136, 345]. This would also mean that an electric field could induce a rotation of the crystal and, the other way around, a rotation of the crystal could induce an electric polarization in chiral compounds (rotoelectricity [357], analogous to the Barnett and Einstein-de-Haas effects in magnets [335]). Interestingly, the character table of the parent phase of enantiomorphic compounds shows that tensors behaving as $[\mathbf{V}^2] \times \mathbf{V}$ (\mathbf{V} being a vector) – such as the strain gradient $\nabla \epsilon_{ij}$ – may contain the pseudoscalar IRREP, which would allow them to directly interact with χ without the need of an intermediary electromagnetic field [136]. This hypothetical phenomenon, dubbed ‘flexochirality’, remains completely unexplored.

7.2. Chirality coupled with other order parameters

Although a definition of a conjugate field for crystal (structural) chirality in a Landau theory sense (i.e. a field that strictly transforms as the chiral irreducible representation) has not yet been reported, the coupling of chirality with other order parameters that can be tuned by external fields can be considered.

Such a mechanism is well known in, e.g. ferroelectric crystals, such as improper, hybrid improper, or pseudoproper ferroelectricity [358–362]. In proper ferroelectrics, it is the polarization order parameter that drives the phase transition and it is said to be the primary order parameter. In the other ferroelectric cases, the primary order parameter is not the polarization itself but another non-polar order that couples with the polarization (if allowed by symmetry, i.e. the coupling is an invariant of the free energy [132, 133, 363, 364]). In this situation, the polarization arises from the presence of the non-polar order parameter and it is said to be the secondary order parameter (see table 3 of [365]). In those situations, an applied electric field can affect the non-polar order parameter through its coupling with the polarization. This situation is, e.g. sought after in magnetoelectric and multiferroic compounds, where the magnetic properties can be electrically tweaked [365]. Primary and secondary order parameter mechanisms can exist among all order parameters, providing their coupling is allowed by symmetry. Hence, looking at a similar mechanism for chirality seems natural.

Throughout the rest of this section, we will discuss such coupling mechanisms that may prove helpful concerning the switching and flipping of the chirality and show that, generally, an interaction between external parameters (namely, an electric field and/or lattice deformations) and the chirality can

exist and could induce enantioselectivity if certain conditions are met.

7.2.1. Coupling with other structural deformations. Before going through the proper coupling of chirality with other order parameters, we would like to discuss the case where chirality is described by the product between an axial pseudovector \mathbf{A} and a regular vector \mathbf{V} . While an irreducible representation solely associated with the chirality generally exists [346], it is also contained in the (generally reducible) product between a vector \mathbf{V} and an axial \mathbf{A} representation. Consequently, it is reasonable to consider such a product as an effective conjugate field for the chirality, although subject to competition with other phases as a consequence of its generally reducible character (see also section 7.1 and appendix A). We have discussed the example of $\text{Pb}_5\text{Ge}_3\text{O}_{11}$ (section 4.5) for which the handedness and optical activity can be flipped via an applied electric field (i.e. gyroelectricity, see section 5.3) in which the polar domains are spontaneously chiral and optically active since the polar soft mode driving the ferroelectric transition drives also the chirality [156]. In this case, the high symmetry phase already contains axiality \mathbf{A} such that when the polar vector \mathbf{P} develops in the crystal, the chirality is automatically induced through the presence of both \mathbf{A} and \mathbf{P} together. Hence, chirality is flipped when the polarization is reversed because the axial vector is frozen into the structure. Remarkably, the low symmetry ferroelectric phase of $\text{Pb}_5\text{Ge}_3\text{O}_{11}$ is at the same time axial, polar, and chiral, which, in a way, makes an electric field a conjugate field for chirality in this compound. This simple but essential fact is possibly the most efficient and unique way to control the global gyrotropic properties in chiral crystals. However, it requires the additional and spontaneous presence of a fixed-sign axiality. We note that Fabini *et al* [161] recently reported several possible chiral phases in the CsSnBr_3 perovskite crystal where chirality can be present with other structural distortions, like ferroelectric or antiferroelectric ones, and is hence a good case for looking at chirality coupling with other order parameters.

Another case of chirality driven by coupled orders has been reported in the afore-discussed $\text{Ba}(\text{TiO})\text{Cu}_4(\text{PO}_4)_4$ crystal (see section 4). With the help of x-ray diffraction, Hayashida *et al* [157] report a second-order ferrochiral transition at 710 °C, induced by the coupling between an antipolar and an antiferroaxial order as depicted in figure 22. Hence, strictly speaking, neither polar nor axial order exists in the high or low symmetry phases of $\text{Ba}(\text{TiO})\text{Cu}_4(\text{PO}_4)_4$. The chosen order parameter, in this case, is the staggered rotation of the antipolar structural Cu_4O_{12} units, and the phase transition appears to be a second-order one.

Very recently, proper ferroelectricity has been designed and observed in $\text{SrM}_2\text{V}_2\text{O}_8$ ($M = \text{Ni}, \text{Mg}$ and Co) and ascribed to the combination of chiral and axial structural units [366]. This mechanism is found to be independent from the chemical elements, such that the authors concluded a geometric origin of ferroelectricity in those compounds, which can be generalized to any crystal exhibiting a combination of rotational and chiral distortions.

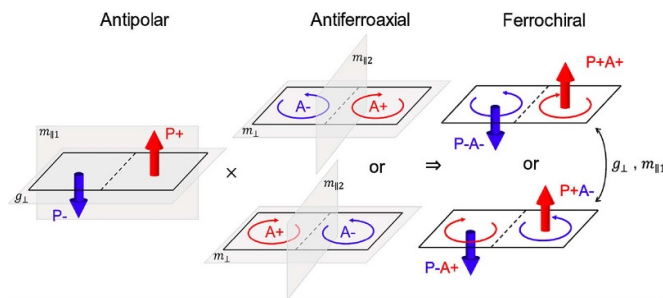


Figure 22. Illustration of chirality as a combination of antipolar and antiferroaxial orders. $A(\pm)$ represents a clockwise/counterclockwise axial order, while $P(\pm)$ is a positive/negative local polarization. The pairs $(-P, -A; P, A)$ and $(-P, A; P, -A)$ have opposite handedness. Reprinted (adapted) with permission from [157]. Copyright (2021) American Chemical Society.

In the case of K_3NiO_2 , CsCuCl_3 and MgTi_2O_4 crystals (see section 4), the chiral phase transition is coming from a zone boundary mode that does not involve a polar vector nor an axial distortion. This raises a significant question: is it possible to flip the gyrotropic properties of such nonpolar nonaxial systems possessing a chiral order, including materials crystallizing into enantiomorphic pairs, by external means? The case of K_3NiO_2 has been scrutinized from DFT calculations by Fava *et al* [136] where the chiral distortion can be seen as a helix of atomic displacements (see figure 5). Nevertheless, possible couplings with polar distortions have been explored, where it appeared that the first coupling with the chiral distortion would be at the fourth order in an energy expansion and involves a Raman mode together with the polar one. By symmetry analysis, the authors [136] could further infer that when the achiral phase belongs to the mmm point group or another with lower symmetry, no rotational external field is required to break the degeneracy between right- and left-handed configurations meaning that a constant bias could in principle flip the chirality in this scenario.

Additionally, as recently reported in [367] chirality can be enhanced by the coupling with a pair of infrared phonon modes, as shown in LiB_3O_5 , where activating a Γ_2 mode lowers the symmetry from $Pna2_1$ to $P2_1$, increasing the optical activity tensor's independent coefficients from 1 to 4 and defining an electro-chiral susceptibility. This would also mean that chirality could be dynamically tuned through non-linear phononic ultrafast laser excitation [329, 368, 369].

7.2.2. Coupling with strain. Another possible coupled order to chirality is strain. Chirality switching with strain has been demonstrated from DFT calculations in the NaCu_5S_3 crystal [288]. NaCu_5S_3 crystallizes in the space groups $P6_3/mcm$ and $P6_322$ (Sohncke non-enantiomorphic space group) in the high and low symmetry phases, respectively. The high symmetry $P6_3/mcm$ phase is described to be antichiral as it contains compensated opposite chirality. In comparison, the low symmetry $P6_322$ phase can be described as *ferrochiral* because the balance between opposite chiralities is broken as a result of the phase transition, leaving them uncompensated. In this

case, it has been demonstrated that a few percent of biaxial strain can tune and quench the barrier between the two ferri-chiral domains, hence inducing a switching between the two chiral cases. Another example of strain tuning chirality is the case of BiFeO₃ perovskite where it has been predicted numerically that (−110) epitaxial strain (of about 7%) can induce a gyrotropic phase transition from an achiral phase (of *Pnma* symmetry) to a phase of non-enantiomorphic Sohncke *P2₁2₁2₁* symmetry [370]. The associated distortions present in the *P2₁2₁2₁* phase can be described by interpenetrated arrays of ferroelectric vortices and antivortices such that the resulting distortion is chiral (the one induced by the vortices). However, the gyrotropic properties alone and the chirality flipping possibilities were not explored further in this case.

Another example of stress-induced control of chirality in crystals is the ferroelastic compound Ca₂Sr(C₂H₅CO₂)₆ [292, 293], as discussed in section 5.4. This material has a chiral tetragonal space group at room temperature, of *P4₁2₁2* symmetry (or its enantiomorph *P4₃2₁2*). For dicalcium propionate salts, Ca₂A(C₂H₅CO₂)₆ (*A* = Sr Pb, Ba), Ba exhibits only a cubic structure at room temperature, suggesting a potential cubic-to-chiral phase transition, although it has not been observed. A hypothetical transition driven by an *X₄* primary symmetry mode and a tetragonal strain ($\eta = c/a - \sqrt{2}$) could enable the Sr displacements to flip, converting left- to right-handed chirality. Specifically, the twin (0,1,1) planes' separate domains, with opposite 4₁ and 4₃ screw symmetries, show opposite optical powers. Applying deformation allows chirality control, with a critical stress that decreases as temperature drops. Stress favors 4₁ domains, enabling simultaneous ferroelastic and gyrogyrotropic switching [293].

7.2.3. Coupling with magnetism. As discussed in section 5.1.2, there can be an intimate link between magnetism and crystal chirality. Indeed, the structural chirality can dictate the helicity of the spin structure (e.g. langasite Ba₃NbFe₃Si₂O₁₄, section 5.1.4). The opposite scenario, of a chiral spin structure emerging on an achiral structure, is unusual but has been observed (e.g. Mn₃Sn, CaMn₇O₁₂, section 5.1.2). In this section, we discuss the coupling between chirality and magnetism from the perspective of an order parameter.

As discussed in section 7.2.1, chirality can arise from combining axiality (properties described by an axial vector **A**) and vector properties (such as polarization). In the context of magnetic order, Cu₃Nb₂O₈ provides an interesting example in which the paramagnetic crystal structure (of *P1* symmetry) supports an axial vector **A**, which allows a polarization **P** to develop along **A** at the onset of chiral, helical magnetic order [371]. Similarly in CaMn₇O₁₂ (with achiral but ferroaxial crystal structure), the helical spin order σ breaks inversion symmetry and induces a polarization **P** perpendicular to spin rotation plane as a result of ferroaxial coupling [233].

7.2.4. Coupling with electronic degrees of freedom. A general requirement for a quantity to be chiral is to be parity-odd and time-reversal even, according to Kelvin and Barron [49,

54, 372]. Since chirality is associated with the absence of improper operations (not simply the lack of inversion symmetry), it is natural to seek time-reversal-even pseudoscalar quantities as chiral objects. By studying the Fermi liquid instabilities of spin-orbit-coupled metals, Fu [373] demonstrated that the Ising parameter $\sum_{\mathbf{k}} \hat{\mathbf{k}} \cdot \mathbf{s}(\mathbf{k})$, where **s** is the wavevector dependent spin and $\hat{\mathbf{k}}$ its normalized momentum, corresponds to a pseudoscalar order parameter when nonzero. This occurs in an isotropic and gyrotropic liquid phase. This peculiar order can be extracted from the (*L*, *J*) decomposition of the electron-spin energy functional according to equation (10) of [373], and specifically by a Pomeranchuk instability at the (*L* = 1, *J* = 0) channel.

A gyrotropic order of electronic origin has been measured in the layered semimetal 1T-TiSe₂ [374]. In particular, near the critical temperature (~174 K), a circularly polarized mid-infrared light can favor one chiral domain over the other. The proposed energy invariant (δF), coupling matter and electromagnetic chiralities, in this case takes the form $\delta F \sim \phi_{\text{gyro}}[(\mathbf{E} \times \partial_z \mathbf{E}) \cdot \hat{\mathbf{z}}]$ where ϕ_{gyro} is the gyrotropic order parameter. However, due to the system's metallic nature, a gyrotropic switchable order cannot be detected via bulk optical activity measurement due to light absorption. Thus, the circular photogalvanic current generated by (and parallel to) the incident light perpendicular to the sample surface was used to detect the chirality and its flipping in this metallic compound. It is nevertheless important to realize that the measurements in [374] do not show any observable hysteresis upon thermal cycling, which means that the right-to-left/left-to-right permanent flip is probably not realized in the sample. Finally, while understanding the origin of the gyrotropic state requires further analysis, two possible mechanisms have been theorized: (i) the modulation of a charge density wave state (CDW) and (ii) the realization of a Pomeranchuk instability in the *p* channel [374]. Indeed, and since this material is layered, once formed at *T*_{CDW} = 198 K, the CDW direction can orient chirally for the propagation direction (e.g. perpendicular to each layer). The proposed gyrotropic invariant thus describes the interaction between the CDW's chirality and that of the incoming light. On the other hand, a chiral order generated by an instability in the Fermi surface would be unrelated to the CDW and coexist with it [374].

An equivalent to helical or helicoidal spin orders, but purely structural, chiral phase transition from an achiral reference has been identified in the doped BiMn₇O₁₂ [375] compound. The chirality, in this case, takes the form $\mathbf{k} \cdot (\mathbf{u}_i \times \mathbf{u}_j)$ where **k** is the modulation vector of the low-temperature phase and **u_i** is an atomic displacement, and can be identified as a helical configuration of electric dipoles, further stabilized by the competition between lone pairs and the orbital ordering, and with the mixing of *d*-orbitals along the direction of propagation [375].

7.2.5. Additional sources of chirality inversion through lasers. While circularly polarized femtosecond laser-induced enantioselectivity has been extensively used in solutions [376], this has been recently achieved in a dry state of NaClO₃ [377]. From a metastable *P2₁/a* phase, circularly polarized light can

achieve an enantiomeric excess of about 20%. More specifically, while heating can locally reduce the energy gap between achiral and chiral phases, a nonzero enantiomeric excess can only be created if circularly polarized light is employed. It is found that the transition proceeds in two steps, starting from the $P2_1/a$ reference structure. More specifically, the sliding of the unit cell by $c/4$ to form transient octahedral units occurs. As the light momentum is transferred to this intermediate phase, it determines the transition to either the right or left-handed chiral structure via twisting of the octahedra. The force associated with this twisting is proposed to result from combining a photon scattering term and the circularly polarized light's spin angular momentum. While the electromagnetic spin angular momentum alone cannot induce the chiral deformation, the occurrence of a spin-to-orbital conversion process [378, 379] generates an orbital angular momentum whose associated torque is likely to be responsible [377] for the observed structural enantioselectivity in NaClO_3 . It is worth mentioning that, when crystallized from an aqueous solution, Kondenpudi *et al* [380] have reported that a quasi-full enantioselection can be achieved by simply stirring the solution. This is an experimental demonstration that an axial macroscopic rotation can tune chirality during growth, and it would be interesting to test the same effect in a fully solid state case during the achiral to chiral phase transition [381].

Recent experiments performed on the previously discussed $\text{Ba}(\text{TiO})\text{Cu}_4(\text{PO}_4)_4$ crystal (sections 4 and 7.2) support the idea that chiral domains can also be flipped by a laser but via local heating and through handedness-independent source [382]. A laser wavelength associated with a peak in the material's absorption coefficient induces local and radial heating. If the power density is sufficiently high, chiral domains could be manipulated. Surprisingly, the switching process was observed to be independent from the polarization of the electromagnetic field and dominated by local heating. Domain reconstruction was explained in terms of domain boundary minimization. It is found under laser scanning, where the laser hitting point is moved from one domain to the other at constant power, and laser cooling, where the hitting point does not change but decreases the power step-wise.

8. Chirality measure and quantification

Whilst it is very tangible to consider chirality regarding the non-superimposability of mirror images [4], this simplistic approach fails to capture many subtleties and consequences.

This section addresses concerns regarding chirality and its measure or quantification. Primarily, it is crucial to consider the dimensionality of the ambient space, as chirality may only occur in the lowest dimension in which the object under study is embedded. Chiral objects in a given dimension n will lose their chirality when placed in an $(n + 1)$ -dimensional framework since the n -dimensional hyperplane accommodating them becomes a mirror symmetry hyperplane [383]. In figure 23, we show a schematic picture of this fact where a 1D

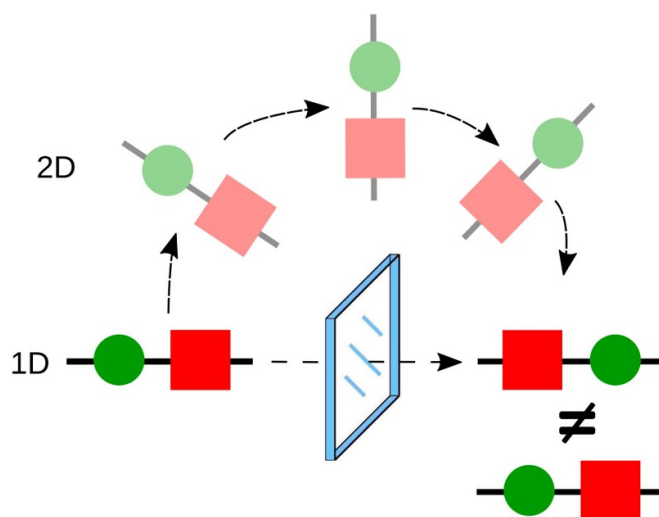


Figure 23. Schematic view of a one-dimensional asymmetric object. In 1D the object on the left is chiral since we cannot superimpose it with its mirror image (on the right). However, in 2D the additional (azimuthal) rotational symmetry allows the overlap of the object with its reflected image as depicted in the top transformation.

chiral object becomes achiral when considered in two dimensions. We will limit our discussion to 3D spaces for this review to avoid confusion.

Moreover, a binary chiral vs achiral classification sometimes proves inadequate, prompting significant efforts in the literature to develop methods for continuously quantifying chirality despite its inherent difficulty [384–386]. One would anticipate that a reliable chirality measure, ξ , should function to rank objects, denoted as x , within a given subset \mathcal{X} according to their degree of chirality i.e. the extent that they differ from an achiral analog. Additionally, as discussed in [384], it is important to impose certain natural requirements: (i) ξ is a continuous function on \mathcal{X} as two sufficiently close objects x_1 and x_2 are expected to show similar chiral responses; (ii) if an object in \mathcal{X} is achiral its degree of chirality should be zero. Conversely, if the degree of chirality of an object is zero, then it should be achiral; (iii) any two enantiomorphic pairs x, x' should have the same degree of chirality. Therefore, if ξ is a scalar function, $\xi(x) = \xi(x')$, and if ξ is a pseudoscalar function, $\xi(x) = -\xi(x')$.

The most common case of scalar chiral measures typically stems from distance functions relative to an achiral reference, as discussed in [387]. Concrete famous examples in the literature include Hausdorff distances [28, 388] or the CCM [154]. The former is based on the supremum of the distances between the atomic positions of the chiral and achiral structures, while the latter relies on the mean square of such distances. Careful definitions and examples can be found in [28]. As standard scalar measures, they assign identical values to both enantiomers, lacking the capacity to discern between them. Despite their widespread use, they might be troublesome and have been intensely debated [40, 385, 386, 389, 390]. This is due in

part to the difficulty in determining the absolute chirality of an object (see section 3.1): to determine whether an object is left or right-handed requires a pre-established definition of what we call left or right [2]. Nevertheless, determining an object's 'chiral strength' or chiral amplitude is unclear unless one pre-defines the reference to what is left or right-handedness. Indeed, one would first need an achiral reference to know the 'zero' and quantify the amount of chirality from it. However, defining a zero-reference may not be apparent depending on the object, and applying this concept to a realistic physical system would be hindered by the additional constraint of not breaking the bonds unless the phase transition is reconstructive. And even though a continuous deformation to an achiral reference may be possible in 3D, such transformation is often likely to be physically impossible [391]. This shows that despite its primary role in natural sciences, the chirality measure has evaded researchers so far. Exploring this problem in extended solids adds another difficulty due to the periodic boundary conditions [392].

Although almost unexplored in the context of structural chirality quantification, another way to measure chirality is through pseudoscalar functions. An example of a pseudoscalar measure could be the hydrodynamical helicity [393–395], which quantifies the handedness of the streamlines in a fluid and can be computed from the velocity field, \vec{v} , as

$$\mathcal{H} = \int d^3\vec{r} \vec{v} \cdot [\vec{\nabla} \times \vec{v}]. \quad (11)$$

This definition has recently been extended to solids by establishing the velocity field through the individual atomic displacements that drive the system from the high-symmetry phase to the low-symmetry chiral phase [396]. Moreover, it has recurrently been applied to quantify the handedness of polar vector fields in ferroelectric/dielectric superlattices [36, 41].

Another recent interesting example is based on the quantification of the electric toroidal monopole [397–399]. As a time-reversal even pseudoscalar (parity-odd) entity, it has been shown to effectively indicate the chirality state of twisted methane molecules [397]. The electric toroidal moments exhibited a finite value when the symmetry of the CH_4 molecule was reduced from T_d to D_2 , with their sign reversing in accordance with the molecule's handedness.

Although pseudoscalar functions can discriminate between enantiomers, more fundamental problems arise when considering them as chirality measures due to the chiral connectedness property [63, 383, 400, 401]. This property refers to the fact that a sufficiently complex chiral object x can be continuously transformed into its mirror image x' while being chiral throughout the entire transformation process as schematized in figure 24. Therefore, we can define a continuous chiral path γ such that $\gamma(0) = x$ and $\gamma(1) = x'$. As elucidated in [383, 400, 401], this poses challenges since our continuous pseudoscalar function ξ changes sign along

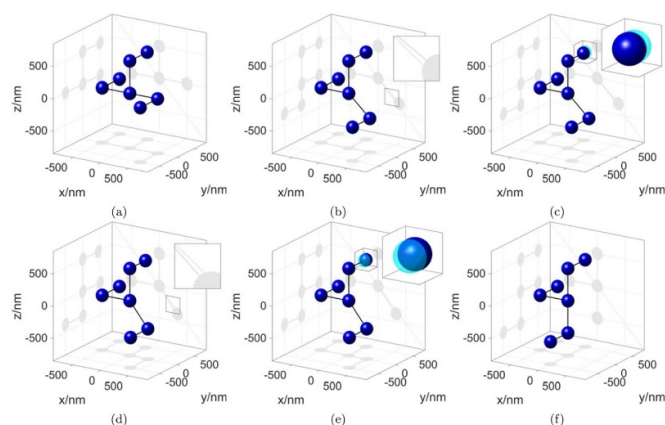


Figure 24. Continuous transformation of the initial chiral configuration (a) to its enantiomer (f) avoiding any intermediate achiral configuration. The achiral state is avoided as follows. First, the right leg is rotated about the y -axis by $9\pi/40$ (b). Note that we stop just before the $\pi/4$ which will create a symmetry plane in the molecule making it achiral. Then, the furthest top sphere is shifted by 50 nm along the negative direction of the y -axis (c) the transparent blue sphere depicts the sphere's position before the shift (also enlarged in the top right corner). Note that this small displacement is sufficient to break the $\pi/4$ mirror plane which allows us to continue the rotation of the right leg without falling in an achiral state. Then the right leg is rotated by an extra $2\pi/40$ (d). Afterward, the shifted top sphere is brought back to its initial position (e), and finally, the right leg is rotated by the remaining $9\pi/40$ onto the final configuration. All intermediate configurations are chiral as we have avoided the critical $\pi/4$ rotation by slightly moving the furthest top molecule and braking thus that mirror plane. This can be seen in the corresponding insets containing zoomed-in versions of the shadows of the right leg on the yz plane. In (b) and (e), such shadow does not coincide with the reference diagonal, breaking the mirror symmetry. Reproduced from [63]. © The Author(s). Published by IOP Publishing Ltd. CC BY 4.0.

the segment, necessitating the presence of a zero within it. Inevitably, ξ will assign a zero value to a chiral structure, leading to the problem of the *false zeros*. This observation also suggests the existence of chiral objects for which assigning a specific handedness may not be applicable, as pseudoscalar functions fail to determine the handedness of some chiral objects. A recent work [63], has addressed this problem by combining a pseudoscalar function with a scalar quantity as a phase factor introduced into a complex exponential. This way, they could distinguish between right-handed, left-handed, unchiral and non-chiral objects, avoiding the false-zeros problem.

A notable exception to the false-zeros problem occurs in sets where enantiomorphs are connected only through achiral states. An illustrative example, particularly relevant to this review, is the set of helices with variable pitch, as discussed in [402]. In such cases, pseudoscalar functions exclusively yield zero values for achiral objects, making them suitable chirality measures. Consequently, as presented in table 1, enantiomorphic space groups are unaffected by this issue and

can be classified according to their handedness. Conversely, non-enantiomorphic space groups exhibit chiral connectedness, making the presence of chiral non-handed configurations inevitable.

Another obvious problem related to the insofar proposed measures, such as the CCM [154], is that the quantification of chirality is tackled from a geometrical and symmetry point of view only, without a clear connection with a physical picture. Indeed, part of this reason is the apparent lack of a conjugate field associated with handedness or chirality. This is not at all what happens in the case of, e.g. electric polarization and magnetization, which are not just measurements of the breaking of an inversion or time-reversal symmetry but also well-defined system properties and linearly coupled with the electromagnetic field. Hence, it is not surprising that most of the experimental work aiming at detecting chirality in crystals focuses on the optical activity and dichroism, even though these properties can be non-zero in certain achiral systems as well (see section 3). Examples taking the NOA as the order parameter are known [126, 153, 403]. Nevertheless, these cases always assume a phenomenological relation between the gyrotropic tensor and, for instance, the electric polarization or the strain. It can be proven [289] that the first derivative of the dielectric tensor concerning a wave-vector \mathbf{q} produces no contribution to the free energy expansion, which means that the onset of an eventual ‘gyrotropic’ order is always a byproduct of a different order produced by an instability. These approaches do not, however, tackle *per se* the issue of defining a physically meaningful measure of chirality, nor its emergence from an achiral reference.

9. Discussion and perspectives

Chirality in inorganic solids is fruitful area of study due to the unique optical and electronic properties these materials can exhibit. Before concluding, let us explore additional challenges and perspectives. Regarding the question of whether chirality can be a new ferroic order parameter, a similar question has been raised for magnetic toroidal moments, i.e. if a magnetic toroidal moment can be a primary order parameter with its ferroic phase transition or if it is conditional on the magnetic order [204, 344, 404–408]. This question has been clarified with the demonstration that the toroidal moment can be defined as a ferroic order [407] and is, hence, the 4th ferroic order, i.e. ferrotoroidicity [344]. This has also been associated with a microscopic Berry phase theory of toroidization [409], showing that the quantification of the toroidal moment is a Berry phase problem as the polarization of ferroelectric is [410]. If we consider possible analogies with chirality, we can question whether the quantification of structural chirality would also be a Berry phase problem. There are parallels between the history of quantifying chirality [385], and the development of methods to quantify the polarization of ferroelectrics which have led to the modern theory of polarization [410]. The problem is that we do not have a mathematical formulation for quantifying chirality, and the attempts to date involve in one way or another the position operator (like the

CCM [154], or the Hausdorff distances [28]), which would require a Berry phase treatment in periodic boundary conditions. The fact that some crystals can exhibit a displacive (or order-disorder) phase transition (i.e. not reconstructive) from an achiral to a chiral structural phase (e.g. K_3NiO_2 , CsCuCl_3 or MgTi_2O_4 discussed at the beginning of this review) suggests that there is probably a way to quantify it through the amplitude of the distortion mode that describes the achiral-chiral phase transition if one has a precise formula. This suggestion that chirality can be quantified can be pursued further, the electrotoroidal monopole could also give some hints regarding this problem. It also means that we should be able to define linear responses from it, like the change of chirality concerning a strain perturbation would drive piezochirality or elastochirality and hence being more general than the piezogyratation or elastogyration effect [126]. Another physical property that could be defined is the notion of dynamical chiral effective charges, i.e. how much an atom motion changes the chirality of a crystal structure, i.e. similarly to the Born effective charges (reflecting the change of polarization of an atom motion) or the magnetic effective charges (reflecting the change of magnetization associated to an atom motion) [411]. This would also directly define phonon mode chiral effective charge (or oscillator strength), expressing how much chirality a phonon mode carries [156].

While no known conjugate field is associated with chirality in crystals to tune it, polarized light still could be of interest. Light intensity is presently insufficient to switch large domains as the magnetic field component of the light interacts weakly with the crystal and, hence, impedes the possibility of controlling structural chirality [412–414]. Despite this weak interaction, it would be possible to have a poling effect at displacive (or order-disorder) chiral phase transitions, i.e. doing a polarized light field cooling poling effect as reported in NaClO_3 [377]. Indeed, while the system is nearing a chiral phase transition, illuminating the sample with polarized light should favor the formation of one chiral domain over the other. Instead of switching chirality, this could selectively choose one of the two enantiomorphic phases, which is of primary interest for applications and fundamental research. Some theoretical solutions using the electric part of the light have been proposed through ultrafast laser excitation that could do the job at a more local level and short time [412, 413, 415]. As we have discussed in section 7, other regular fields like magnetic or electric field or strain should also be explored further.

On the other hand, there is a compelling need to intensify efforts to establish a more nuanced correlation between optical activity, chiral crystal purity, and CD [416–418]. These phenomena are not merely of academic interest but hold substantial promise for various applications, including enantiomeric sensing [419], chiral photonics [112], and the innovation of groundbreaking optical devices [420, 421]. A concerted push towards developing experimental methodologies is essential to unlocking potential applications of chiral materials [422–424]. This effort entails refining the techniques for measuring and quantifying these effects and devising new approaches for synthesizing materials with high enantiomeric purity and controlled optical properties. Advancements in this

area could lead to significant breakthroughs, enabling the precise manipulation of light and the creation of susceptible enantiomeric detection systems. Furthermore, by deepening our understanding of the interplay between enantiomeric purity and optical behavior, researchers can tailor materials to specific applications, enhancing the performance and efficiency of chiral photonic devices [425, 426]. Moreover, this endeavor will require a multidisciplinary approach, drawing on materials science, chemistry, physics, and engineering expertise. Collaborative research efforts that bridge these diverse fields can foster innovation and lead to the discovery of novel physics, materials, or fabrication techniques. For example, Romao *et al* recently proposed detecting dark matter through chiral phonons [316]. Additionally, integrating computational modeling with experimental research can expedite the design and testing of new chiral materials and predict their properties with greater accuracy and efficiency.

Exploring the intersection between chirality and various material properties represents a fertile ground for future research, offering a pathway to uncover novel phenomena and applications. In this review, we have delineated the current understanding of several couplings, such as gyroelectricity or magnetochirality, which illustrate the intricate interplay between chirality and material properties under the influence of external electric or magnetic fields. However, the scope for investigation extends far beyond these initial studies, with several other possible couplings to be explored. The concept of coupling external fields to chiral materials' electronic and structural response opens up a vast landscape for scientific inquiry. These couplings can manifest in myriad ways, potentially leading to new classes of responsive materials that exhibit unprecedented behaviors. For instance, applying electric or magnetic fields could induce or modulate chirality in materials, leading to reversible changes in their optical, magnetic, or electronic properties. This responsiveness deepens our fundamental understanding of chirality and paves the way for innovative applications, such as tunable optical filters [427, 428], switchable catalysts [429, 430], or data storage devices [431, 432] that leverage chiral materials' unique properties. To harness these opportunities, focused research is needed to systematically explore how different external fields can interact with chiral materials' electronic and structural aspects. High-resolution imaging, spectroscopic techniques, and advanced microscopy methods will allow for the direct observation and manipulation of chiral structures at the nanoscale, providing invaluable insights into their behavior under external stimuli.

Exploring hybrid materials presents an exciting frontier for future research in chiral materials [433–435]. This approach strategically integrates inorganic chiral structures with organic components or other inorganic elements to forge hybrid materials [38, 433]. The essence of this strategy lies in its potential to amalgamate the superior qualities of both inorganic and organic worlds, thereby designing materials that exhibit enhanced or entirely novel properties [433, 436, 437]. Combining different materials could create a synergy that leads to breakthroughs in material properties such as increased mechanical strength, enhanced electrical conductivity, or

improved thermal stability, each tailored for specific application needs. Concurrently, we must advance our computational methods and machine learning capabilities. These technological tools are set to play a pivotal role in the future of chiral materials research. By harnessing the power of computational simulations and machine learning algorithms, researchers can leapfrog the conventional trial-and-error approach, enabling the rapid prediction and identification of new chiral inorganic structures. Moreover, integrating computational models with experimental research is anticipated to tighten the correlation between theoretical definitions of chirality and their experimental counterparts. This harmonization is crucial for advancing our theoretical frameworks of chirality, ensuring that they are robust, predictive, and reflective of observable phenomena. By enhancing the dialogue between theory and experiment, researchers can achieve a more comprehensive understanding of chirality, which, in turn, will inform the design and synthesis of novel chiral materials with precision and purpose.

10. Conclusion

This review article provides a comprehensive overview of the enantiomorphic crystal structural chirality observed in periodic inorganic solids and the associated properties arising from their structural characteristics. Given the promising potential of these materials, the review aims to stimulate further research efforts in this domain. Specifically, it encourages experimental studies focused on the synthesis, discovery, and characterization of new chiral inorganic solids and computational investigations employing high-throughput machine learning techniques for materials discovery and theoretical approaches to understand and quantify the coupled properties arising from structural chirality. We also reviewed the different definitions of crystal chirality and in particular, we make a distinction between chiral axis and absolute chirality that has been sometimes incorrectly identified in some publications. We noted the need for more significant efforts to provide a unique method that defines crystal chirality. While the literature on chiral crystals continues to grow, our discussion primarily focuses on existing studies examining crystal phase transitions within this domain. We observed that only a limited number of systems have been thoroughly characterized, underscoring a significant gap in our understanding of how these transitions occur and how they relate across enantiomer subgroups to the supergroup. This observation highlights the need for a concerted effort to expand our understanding of chirality control by external fields. The review delves into established phenomena like optical activity, electrogyration, and magnetochirality and emerging fields such as chiral phonons and altermagnetism, which remain largely unexplored in enantiomorphic chiral crystals. These nascent areas hint at novel behaviors awaiting thorough investigation, emphasizing the need to discover new chiral materials that could host these intriguing properties and phenomena. Hence, chirality in extended solids is a rich and fruitful research area with high potential for new fundamental studies (topology, quantification problems, new ferroic order and related order parameter

and conjugate field) and new technological applications (tuning optical activity from external means for, e.g. photonics and other chiroptical applications [112, 353, 438, 439] or exciting and controlling chiral phonons for phononics [304, 440]). Our review is also an invitation/appeal for further studies of chirality in periodic crystals to design and find new properties of matter.

Data availability statement

No new data were created or analysed in this study.

Acknowledgments

MF, FGO & EB acknowledge the Fonds de la Recherche Scientifique (FNRS) for support, the PDR Project CHRYSLID No. 40003544 and the Consortium des Équipements de Calcul Intensif (CÉCI), funded by the F.R.S.-FNRS under Grant No. 2.5020.11 and the Tier-1 Lucia supercomputer of the Walloon Region, infrastructure funded by the Walloon Region under the Grant Agreement No. 1910247. FGO also acknowledges financial support from MSCA-PF 101148906 funded by the European Union and the Fonds de la Recherche Scientifique (FNRS) through the Grant FNRS-CR 1.B.227.25F. The work in West Virginia was supported by the U.S. Department of Energy (DOE), Office of Science, Basic Energy Sciences (BES), under Award DE-SC0021375. This work used Bridges2 and Expanse at the Pittsburgh Supercomputer and the San Diego Supercomputer Center through allocation DMR140031 from the Advanced Cyberinfrastructure Coordination Ecosystem: Services & Support (ACCESS) program, which National Science Foundation supports Grants 2138259, 2138286, 2138307, 2137603, and 2138296. Certain images in this publication have been obtained by the author(s) from the Wikipedia/Wikimedia website, where they were made available under a Creative Commons licence or stated to be in the public domain. Please see individual figure captions in this publication for details. To the extent that the law allows, IOP Publishing disclaim any liability that any person may suffer as a result of accessing, using or forwarding the image(s). Any reuse rights should be checked and permission should be sought if necessary from Wikipedia/Wikimedia and/or the copyright owner (as appropriate) before using or forwarding the image(s).

Appendix A. Chirality in polar nanostructures

Although this review is focused on bulk systems, it is interesting to mention some recent work investigating the realization of chiral structures in nano- and heterostructures because some of these results could be extended/exploited at the bulk level. The observation of polar vortices rotating both clockwise and anticlockwise and antivortices has recently been reported in oxide superlattices $\text{SrTiO}_3/\text{PbTiO}_3$ [41, 441, 442]. The coexistence between polar and toroidal order was

observed in this system [443], and the chirality of the vortices was shown to be controllable with an electric field [444]. A recent theoretical analysis [445] has further proven that this chiral state undergoes a double phase transition as the temperature increases, from a regular crystal-like state composed by alternating clockwise/counterclockwise vortices—with a definite handedness—to a state where the vortices form a handed liquid structure deprived of its long-range order, to, finally, a non-handed state. It is essential to realize that the symmetry-based definition of chirality is also fulfilled by objects such as $\mathbf{p} \cdot (\nabla \times \mathbf{p}) = \mathbf{p} \cdot \mathbf{g}$ (\mathbf{p} and \mathbf{g} being a local dipole and a local toroidal field, respectively) and a net and electric-field switchable chirality has been detected via SHGs in tri-layers superlattice oxides [444] and ferroelectric nanodots [446]. In such cases, the switching via an electric field naturally stems from the local polar-axial coupling in these systems. An intriguing development in chiral switching involves altering the sense of rotation of vortices using twisted light as explored in [447], where the interaction between polar skyrmions and a non-zero electric field curl is simulated.

In recent years, there has also been a great deal of interest in understanding electro-toroidal orders, mainly at the interface between insulators and ferroelectrics and nano-systems [448–450]. In these scenarios, the control of the electro-toroidal order is numerically simulated via coupling with a polar state [448] and/or a torque [449]. At the same time, the issue of having a nonzero electric field curl can be circumvented with non-homogeneous electric fields [450]. The effect of a homogeneous field is instead that of favoring a polar state and to suppress any dipole-vortices, with $\Delta \mathbf{G}_z \sim -\mathbf{E}^2$ as realized in $\text{Pb}(\text{Zr,Ti})\text{O}_3$ nanoparticles [451]. In this case, the role of the vortex states in nucleating the polarization is also significant. Incipient phase transitions have also been analyzed in KTaO_3 nanodots, where the G-order is suppressed at low-temperature by fluctuations [452]. Furthermore, the electro-toroidal order is shown to couple to the stress, thus producing a new kind of electro-mechanical interaction [453]. $\nabla \times \mathbf{E}$ -induced susceptibilities are also discussed and numerically analyzed via second-principles Hamiltonians [452, 453]. A comprehensive review on these dipole vortices in nanosystems, mimicking their magnetic equivalent, is given in [454].

These polar vortices share many features with their magnetic counterparts, skyrmions [25, 26]. Thus, exploring their origin, stability, and topological properties comes naturally [213]. Skyrmions of electric origin and with a topological invariant given by $q = \frac{1}{4\pi} \mathbf{u} \cdot (\partial_x \mathbf{u} \times \partial_y \mathbf{u})$ have been theoretically studied [455] and experimentally observed [456] (\mathbf{u} is a normalized local dipole moment) and while from early studies, it seemed that their stability was the result of geometry confinement and dipolar interaction (due to the apparent lack of a (chiral) DMI as it happens in the magnetic case), the existence of an electric equivalent of the DMI (eDMI) $\sim \mathbf{D}_{ij}'(\mathbf{u}_i \times \mathbf{u}_j)$ has recently been established [457–459]. It has been further shown that this electric DMI is an electronic effect associated with a hopping process (induced by local inversion breaking) and related to the anti-symmetric part of the interatomic force constants [460]. The aforementioned literature and examples

concerning chiral order parameters focus on dipole vortices in low-dimensional systems, and thus, the control of chirality stems from a polar-axial coupling. A similar mechanism, also based on the ferroaxial $\sigma\mathbf{AP}$ coupling (where σ represents a time-even structural or spin chirality and \mathbf{A} is an axial, not necessarily electro-toroidal, degree of freedom), has been observed in bulk systems as well (see section 7.2.3).

Appendix B. Chirality in twisted bilayers

The realization of a chiral degree of freedom in materials may also be achieved by stacking 2D layers—interacting via Van Der Waals forces—on top of each other. The chirality and associated gyrotropic properties would be controlled by changing the twisting angle. It has been recently shown in CrI_3 [46] through density functional theory and tight-binding calculations, that the activation, magnitude and sign of both the ferroelectric polarization and magneto-optical Kerr effect depend on the twisting angle between two stacked monolayers and that an interplay between the ‘global’ chirality and the so called ‘octahedral chirality’ (associated with each monolayer) occurs. Finally, while chirality in stacked layers is not the focus of this review, we mention the recent appearances of an editorial [461] and of a perspective [462] article which may likely spark a future research interest on this subject.

Appendix C. Toroidal Monopole and other potential chirality order parameter

As we have discussed in this review and in particular in section 8, a proper measurement of chirality has not been yet established. Though several efforts have been proposed, we will discuss the most convenient one introduced in this appendix and some additional symmetry vectorlike quantities that can be used for such a purpose.

C.1. Multipole expansion and electric toroidal monopole

In this section, we discuss some relevant literature to describe wave function descriptors of chirality, notably drawing from the referenced works [49, 346]. Our framework is structured around the foundational concept of electronic multipoles, serving as a pivotal instrument for delineating the differentiation between chiral and other point groups. The distinction between chiral and non-chiral point groups is inherently reflected in the distinctive attributes of their respective wave functions and associated electronic degrees of freedom. Elucidating the specific nature of the wave function in these frameworks proves invaluable in representing electronic degrees of freedom using a comprehensive symmetry-adapted basis set encompassing multipole components.

The concept of electronic multipoles, encompassing electric, magnetic, electric toroidal, and magnetic toroidal monopoles, offers a comprehensive framework for scrutinizing the electronic structure of materials, as well as it can also be used for other properties. We need to include the electric toroidal

and magnetic toroidal in the multipole description because the electric dipole is even under time reversal but odd with spatial inversion. In contrast, the magnetic dipole is odd under time reversal and even under spatial inversion. Therefore, there is a need for two additional multipoles that expand all possible combinations of dependence concerning parity and time reversal, in particular, even under both or odd under both transformations. Of particular intrigue are the electric toroidal and magnetic toroidal multipoles, representing axial (pseudo) and polar (true) tensors, respectively, acting as counterparts to the conventional electric and magnetic multipoles concerning parity. It is important to note that the main mathematical difference between ‘pseudo’ and ‘true’ tensors comes when a unitary transformation U is performed. True and pseudo tensors transform as $T_{\alpha\beta\dots} = U_{\alpha i}U_{\beta j}\dots T_{ij\dots}$, and $PT_{\alpha\beta\dots} = \det(U)U_{\alpha i}U_{\beta j}\dots T_{ij\dots}$ respectively. Each multipole is distinguished by its rank, designated as k , where the monopole corresponds to $k=0$, the dipole to $k=1$, the quadrupole to $k=2$, and so forth. Notably, the polar (true) tensor exhibits parity $(-1)^k$, while the axial (pseudo) tensor demonstrates parity $(-1)^{k+1}$ under inversion operations. Consequently, multipole tensors with even ranks exhibit even parity, while those with odd ranks showcase odd parity. It is imperative to underscore that these four distinct multipoles constitute a complete basis set, enabling them to comprehensively depict any symmetry-adapted electronic state that characterizes materials’ electronic behavior across diverse symmetry scenarios. This approach has been used in other contexts, such as exploring the electronic landscape of materials [463], and classifying magneto-electricity in topological magnetic structures such as skyrmions [464].

The derivation of the multipole expansion can be found in several electromagnetic references such as [355, 356]. In conventional treatments commonly found in textbooks, electromagnetic field scalar and vector components are typically expanded using Cartesian coordinates. However, this traditional method overlooks the existence of electric and magnetic toroidal terms, limiting its relevance in specific contexts. Two alternative methodologies have been proposed to address or work around these limitations. The first approach, which upholds Cartesian coordinates, is grounded on the principle that physically significant multipole moments should exhibit proper behavior under parity and rotations. This approach necessitates that such moments be symmetric and traceless. While this method effectively tackles issues related to non-traceless tensors, it is restricted by the need for spatially confined sources. Nevertheless, it presents a viable solution within its defined scope, making it particularly useful in practical scenarios where spatial confinement is feasible. Conversely, based on spherical coordinates, the second approach offers a different perspective. It decomposes the current density in momentum space, making it viable to compute multipole moments based on angular momentum eigenstates. With its focus on spherical symmetry or momentum-space considerations, this approach provides a unique advantage in scenarios where these factors are pertinent, enhancing its appeal to researchers. While some literature discusses the effect of each approach, here we only present the main results obtained using

the expansion spherical coordinates and discuss the implications on chirality.

First, let us define the quantity $O_{lm} = \sqrt{4\pi/(2+1)}r^l Y_{lm}^*(\hat{\mathbf{r}})$, where $\hat{\mathbf{r}}$ is the unitary vector position, Y_{lm}^* is the complex conjugate of the lm spherical harmonics and where l and m are the azimuthal and magnetic quantum numbers, respectively. Therefore, the multipole expansions would have the form:

$$Q_{lm} = \int d\mathbf{r} \mathbf{P}(\mathbf{r}) \cdot \nabla Q_{lm}(\mathbf{r}), \quad (\text{C1})$$

$$M_{lm} = \int d\mathbf{r} \mathbf{M}(\mathbf{r}) \cdot \nabla Q_{lm}(\mathbf{r}), \quad (\text{C2})$$

$$T_{lm} = \int d\mathbf{r} \mathbf{T}(\mathbf{r}) \cdot \nabla Q_{lm}(\mathbf{r}), \quad (\text{C3})$$

$$G_{lm} = \int d\mathbf{r} \mathbf{G}(\mathbf{r}) \cdot \nabla Q_{lm}(\mathbf{r}), \quad (\text{C4})$$

where Q_{lm} are the electric multipoles, M_{lm} are the magnetic multipoles and T_{lm} are the magnetic toroidal multipoles and G_{lm} is the electric toroidal multipoles, that corresponds to a time-reversal-even axial tensor. These quantities are given as functions of \mathbf{P} , the electric polarization, \mathbf{M} , magnetization, \mathbf{T} magnetic toroidalization (related to the magnetization as $\mathbf{M} = \nabla \times \mathbf{T}$ and \mathbf{G} , the electric toroidalization and that is related to the electric polarization as $\mathbf{P} = \nabla \times \mathbf{G}$. Equations (C1)–(C4) were taken from [465], where a detailed discussion on how these equations are obtained can be found.

For chiral materials, the difference between chiral and other point groups must be reflected in the character of their wave functions and associated electronic degrees of freedom. To extract the specific character of the wave function, it is helpful to express any electronic degrees of freedom in terms of the complete symmetry-adapted (multipole) basis set. For instance, an electric dipole moment distinguishes a polar wave function from a non-polar one. Using four types of multipoles (monopole, dipole, quadrupole, and octupole), all point groups can be uniquely classified by the active multipole moments. In the language of group theory, any active moments belong to the symmetric (identity) irreducible representations, and they are so-called order parameters in Landau's theory of phase transitions. Notably, in [345], it is shown that the monopole moment (G_0) captures the manifestation of chirality. The sign of the monopole represents the two possible handednesses.


While the electric toroidal monopole captures chirality in an electronic system, other possible vectorlike quantities can be used similarly. This is detailed in [346]. This paper discusses the symmetry properties of various vectorlike physical quantities under the non-relativistic space-time rotation group. The author discussed eight symmetrically distinct classes of stationary physical quantities defined by a magnitude, an axis or direction, and a geometric sign (+ or −). These classes are specified by their transformation properties under the operations of the group $O(3) \times \{1, 1'\}$ (where $1'$ is the time-reversal operation) and are represented by 1D irreducible representations of this group. The eight classes include two kinds of polar vectors (e.g. electric dipole moment \mathbf{P} , magnetic toroidal moment \mathbf{T}), two kinds of axial vectors (e.g. magnetization \mathbf{M} , electric toroidal moment \mathbf{G}), two chiral 'bidirectors' (\mathbf{C} and \mathbf{F}

associated with true and false chirality respectively), and two achiral bidirectors (\mathbf{N} and \mathbf{L}). The symmetry properties distinguish these quantities from the conventional polar and axial vectors. For example, \mathbf{C} and \mathbf{F} describe chiral objects without mirror symmetry. The paper provides the geometric meaning of the parity signs for these quantities. It examines the possibilities of extending algebraic operations to vectors and directors. This classification is potentially helpful for symmetry analysis in various areas like multiferroics, chiral systems, topological defects in vector fields, and long-wavelength excitations in crystals. Therefore, they represent an extension of what has been discussed in this review that needs to be explored.

ORCID iDs

Eric Bousquet  <https://orcid.org/0000-0002-9290-3463>

Mauro Fava  <https://orcid.org/0000-0002-3461-1585>

Zachary Romestan  <https://orcid.org/0000-0001-5582-4515>

Fernando Gómez-Ortiz  <https://orcid.org/0000-0002-7203-8476>

Emma E McCabe  <https://orcid.org/0000-0001-5868-4570>

Aldo H Romero  <https://orcid.org/0000-0001-5968-0571>

References

- [1] Curie P 1894 Sur la symétrie dans les phénomènes physiques, symétrie d'un champ électrique et d'un champ magnétique *J. Phys. Theor. Appl.* **3** 393
- [2] Cintas P 2007 Tracing the origins and evolution of chirality and handedness in chemical language *Angew. Chem., Int. Ed.* **46** 4016
- [3] Dezarnaud-Dandine C, Sevin A and Piem A 2007 *Symétrie M'était Contée... Histoires de Symétries* (Ed. Ellipses)
- [4] Thompson W 1894 *The Molecular Tactics of a Crystal* (Clarendon: Robert Boyle Lecture)
- [5] Shalygin V A, Sofronov A N, Vorob'ev L E and Farbshtein I I 2012 Current-induced spin polarization of holes in tellurium *Phys. Solid State* **54** 2362
- [6] Cai R-G and Yang R-Q 2015 Holographic model for the paramagnetism/antiferromagnetism phase transition *Phys. Rev. D* **91** 086001
- [7] Yamamoto H and Carreira E M 2012 *Comprehensive Chirality* vol 1 (Newnes)
- [8] Mauskopf S 2006 A history of chirality *Chiral Analysis* (Elsevier) pp 3–24
- [9] Biot J B 1812 Sur de nouveaux rapports qui existent entre la réflexion et la polarisation de la lumière des corps cristallisés *Mem. Cl. Sci. Math. Phys. Inst.* **13** 1
- [10] Pasteur L 1848 Sur les relations qui peuvent exister entre la forme cristalline, la composition chimique et le sens de la polarization rotatoire *Ann. Chim. Phys.* **24** 442
- [11] Kelvin W T B 1894 *The Molecular Tactics of a Crystal* (Clarendon)
- [12] Fischer E and Fischer E 1909 Über die konfiguration des traubenzuckers und seiner isomeren. I *Untersuchungen Über Kohlenhydrate und Fermente (1884–1908)* (Springer) p 417
- [13] Kelvin L W T 1904 *Baltimore Lectures on Molecular Dynamics and the Wave Theory of Light* (CUP Archive)
- [14] Weller M G 2024 The mystery of homochirality on earth *Life* **14** 341

- [15] Morrow S, Bisette A and Fletcher S 2017 Transmission of chirality through space and across length scales *Nat. Nanotechnol.* **12** 410
- [16] Glazer A M and Stadnicka K 1986 On the origin of optical activity in crystal structures *J. Appl. Crystallogr.* **19** 108
- [17] Thomas P 1988 The crystal structure and absolute optical chirality of paratellurite, α -TeO₂ *J. Phys. C: Solid State Phys.* **21** 4611
- [18] Stadnicka K, Glazer A M and Arzt S 1993 The absolute optical chirality of KLiSO₄ *J. Appl. Crystallogr.* **26** 555
- [19] Stadnicka K, Glazer A M and Moxon J R L 1985 The structural chirality and optical activity of α -LiIO₃ *J. Appl. Crystallogr.* **18** 237
- [20] Schröter N B M *et al* 2019 Chiral topological semimetal with multifold band crossings and long Fermi arcs *Nat. Phys.* **15** 759
- [21] Chang G *et al* 2018 Topological quantum properties of chiral crystals *Nat. Mater.* **17** 978
- [22] Sanchez D S *et al* 2019 Topological chiral crystals with helicoid-arc quantum states *Nature* **567** 500
- [23] Zhou X, Feng W, Li Y and Yao Y 2023 Spin-chirality-driven quantum anomalous and quantum topological Hall effects in chiral magnets *Nano Lett.* **23** 5680
- [24] Mazzola F *et al* 2024 Signatures of a surface spin-orbital chiral metal *Nature* **626** 752–8
- [25] Mühlbauer S, Binz B, Jonietz F, Pfleiderer C, Rosch A, Neubauer A, Georgii R and Böni P 2009 Skyrmion lattice in a chiral magnet *Science* **323** 915
- [26] Zhang X, Xia J, Tretiakov O A, Ezawa M, Zhao G, Zhou Y, Liu X and Mochizuki M 2023 Chiral skyrmions interacting with chiral flowers *Nano Lett.* **23** 11793
- [27] Schaibley J, Yu H, Clark G, Rivera P, Ross J S, Seyler K L, Yao W and Xu X 2016 Valleytronics in 2D materials *Nat. Rev. Mater.* **1** 16055
- [28] Fecher G H, Kübler J and Felser C 2022 Chirality in the solid state: chiral crystal structures in chiral and achiral space groups *Materials* **15** 5812
- [29] Chen X, Lu X, Dubey S, Yao Q, Liu S, Wang X, Xiong Q, Zhang L and Srivastava A 2019 Entanglement of single-photons and chiral phonons in atomically thin WSe₂ *Nat. Phys.* **15** 221
- [30] Zhu H, Yi J, Li M-Y, Xiao J, Zhang L, Yang C-W, Kaindl R A, Li L-J, Wang Y and Zhang X 2018 Observation of chiral phonons *Science* **359** 579
- [31] Zhang L and Niu Q 2015 Chiral phonons at high-symmetry points in monolayer hexagonal lattices *Phys. Rev. Lett.* **115** 115502
- [32] Chen H, Wu W, Yang S A, Li X and Zhang L 2019 Chiral phonons in kagome lattices *Phys. Rev. B* **100** 094303
- [33] Juraschek D M and Spaldin N A 2019 Orbital magnetic moments of phonons *Phys. Rev. Mater.* **3** 064405
- [34] Johnson R D, Chapon L C, Khalyavin D D, Manuel P, Radaelli P G and Martin C 2012 Giant improper ferroelectricity in the ferroaxial magnet CaMn₇O₁₂ *Phys. Rev. Lett.* **108** 067201
- [35] Johnson R D, Cao K, Chapon L C, Fabrizio F, Perks N, Manuel P, Yang J J, Oh Y S, Cheong S-W and Radaelli P G 2013 MnSb₂O₆: a polar magnet with a chiral crystal structure *Phys. Rev. Lett.* **111** 017202
- [36] Shafer P *et al* 2018 Emergent chirality in the electric polarization texture of titanate superlattices *Proc. Natl Acad. Sci. USA* **115** 915
- [37] Avnir D 2024 Chiral Minerals *Minerals* **14** 995
- [38] Lou F, Gu T, Ji J, Feng J, Xiang H and Stroppa A 2020 Tunable spin textures in polar antiferromagnetic hybrid organic-inorganic perovskites by electric and magnetic fields *npj Comput. Mater.* **6** 114
- [39] Jana M K, Song R, Liu H, Khanal D R, Janke S M, Zhao R, Liu C, Valy Vardeny Z, Blum V and Mitzi D B 2020 Organic-to-inorganic structural chirality transfer in a 2D hybrid perovskite and impact on Rashba-Dresselhaus spin-orbit coupling *Nat. Commun.* **11** 4699
- [40] Jenkins S J 2018 *Chirality at Solid Surfaces* (Wiley) (<https://doi.org/10.1002/9781118880173.ch1>)
- [41] Junquera J *et al* 2023 Topological phases in polar oxide nanostructures *Rev. Mod. Phys.* **95** 025001
- [42] Shao Y-T *et al* 2023 Emergent chirality in a polar meron to skyrmion phase transition *Nat. Commun.* **14** 1355
- [43] McCarter M R *et al* 2022 Structural chirality of polar skyrmions probed by resonant elastic x-ray scattering *Phys. Rev. Lett.* **129** 247601
- [44] Prosandeev S, Malashevich A, Gui Z, Louis L, Walter R, Souza I and Bellaiche L 2013 Natural optical activity and its control by electric field in electrotoroidic systems *Phys. Rev. B* **87** 195111
- [45] Yananose K, Cantele G, Lucignano P, Cheong S-W, Yu J and Stroppa A 2021 Chirality-induced spin texture switching in twisted bilayer graphene *Phys. Rev. B* **104** 075407
- [46] Yananose K, Radaelli P G, Cuoco M, Yu J and Stroppa A 2022 Activating magnetoelectric optical properties by twisting antiferromagnetic bilayers *Phys. Rev. B* **106** 184408
- [47] Togawa Y, Koyama T, Takayanagi K, Mori S, Kousaka Y, Akimitsu J, Nishihara S, Inoue K, Ovchinnikov A and Kishine J-I 2012 Chiral magnetic soliton lattice on a chiral helimagnet *Phys. Rev. Lett.* **108** 107202
- [48] Volkov O M, Sheka D D, Gaididei Y, Kravchuk V P, Röbber U K, Fassbender J and Makarov D 2018 Mesoscale Dzyaloshinskii-Moriya interaction: geometrical tailoring of the magnetochirality *Sci. Rep.* **8** 866
- [49] Kishine J-I, Kusunose H and Yamamoto H M 2022 On the definition of chirality and enantioselective fields *Isr. J. Chem.* **62** e202200049
- [50] Hearmon A J, Fabrizio F, Chapon L C, Johnson R, Prabhakaran D, Streltsov S V, Brown P and Radaelli P G 2012 Electric field control of the magnetic chiralities in ferroaxial multiferroic RbFe(MoO₄)₂ *Phys. Rev. Lett.* **108** 237201
- [51] Cheong S-W and Xu X 2022 Magnetic chirality *npj Quantum Mater.* **7** 40
- [52] Simonet V, Loire M and Ballou R 2012 Magnetic chirality as probed by neutron scattering *Eur. Phys. J. Spec. Top.* **213** 5
- [53] Tanygin B 2011 Magnetic symmetry based definition of the chirality in the magnetically ordered media *Physica B* **406** 3423
- [54] Barron L D 1986 True and false chirality and absolute asymmetric synthesis *J. Am. Chem. Soc.* **108** 5539
- [55] Ishizuka H and Nagaosa N 2018 Impurity-induced vector spin chirality and anomalous Hall effect in ferromagnetic metals *New J. Phys.* **20** 123027
- [56] Ishizuka H and Nagaosa N 2020 Anomalous electrical magnetochiral effect by chiral spin-cluster scattering *Nat. Commun.* **11** 2986
- [57] Kawamura H 2011 The ordering of XY spin glasses *J. Phys.: Condens. Matter* **23** 164210
- [58] Chan E *et al* 2022 Neutron diffraction in MnSb₂O₆: magnetic and structural domains in a helicoidal polar magnet with coupled chiralities *Phys. Rev. B* **106** 064403
- [59] Udagawa M and Moessner R 2013 Anomalous Hall effect from frustration-tuned scalar chirality distribution in Pr₂Ir₂O₇ *Phys. Rev. Lett.* **111** 036602
- [60] Schopper H 2020 *Particle Physics Reference Library: Volume 1: Theory and Experiments* (Springer) (https://doi.org/10.1007/978-3-030-38207-0_1)
- [61] Tamura S, Hoshino S and Tanaka Y 2019 Odd-frequency pairs in chiral symmetric systems: spectral bulk-boundary correspondence and topological criticality *Phys. Rev. B* **99** 184512

- [62] Daido A and Yanase Y 2019 Chirality polarizations and spectral bulk-boundary correspondence *Phys. Rev. B* **100** 174512
- [63] Vavilin M and Fernandez-Corbaton I 2022 Multidimensional measures of electromagnetic chirality and their conformal invariance *New J. Phys.* **24** 033022
- [64] Burns A M and Glazer G 1990 *Space Groups for Solid State Scientists* (Academic)
- [65] Nespolo M, Aroyo M I and Souvignier B 2018 Crystallographic shelves: space-group hierarchy explained *J. Appl. Crystallogr.* **51** 1481
- [66] Nespolo M and Benahsene A H 2021 Symmetry and chirality in crystals *J. Appl. Crystallogr.* **54** 1594
- [67] Lu X, Wang X, Wang S and Ding T 2023 Polarization-directed growth of spiral nanostructures by laser direct writing with vector beams *Nat. Commun.* **14** 1422
- [68] Glazer A M and Stadnicka K 1989 On the use of the term 'absolute' in crystallography *Acta Crystallogr. A* **45** 234
- [69] Mason S 1986 The origin of chirality in nature *Trends Pharmacol. Sci.* **7** 20
- [70] Arago F 1811 Mémoire sur la polarisation colorée *Œuvres Complètes de François Arago*
- [71] Maddox J and Zimmer C 1998 What remains to be discovered: mapping the secrets of the universe, the origins of life, and the future of the human race (Martin Kessler Books)
- [72] Soai K and Kawasaki T 2008 Asymmetric autocatalysis with amplification of chirality *Amplification of Chirality* ed K Soai (Springer) pp 1–33 (https://doi.org/10.1007/128_2007_138)
- [73] Condon E U 1937 Theories of optical rotatory power *Rev. Mod. Phys.* **9** 432
- [74] Bondo Pedersen T and Hansen A E 1995 *Ab initio* calculation and display of the rotary strength tensor in the random phase approximation. Method and model studies *Chem. Phys. Lett.* **246** 1
- [75] Varsano D, Espinosa-Leal L A, Andrade X, Marques M A L, di Felice R and Rubio A 2009 Towards a gauge invariant method for molecular chiroptical properties in TDDFT *Phys. Chem. Chem. Phys.* **11** 4481
- [76] Yabana K and Bertsch G F 1999 Application of the time-dependent local density approximation to optical activity *Phys. Rev. A* **60** 1271
- [77] Zhong H, Levine Z H, Allan D C and Wilkins J W 1993 Optical activity of selenium: a nearly first-principles calculation *Phys. Rev. Lett.* **70** 1032
- [78] Zhong H, Levine Z H, Allan D C and Wilkins J W 1993 Band-theoretic calculations of the optical-activity tensor of α -quartz and trigonal Se *Phys. Rev. B* **48** 1384
- [79] Malashevich A and Souza I 2010 Band theory of spatial dispersion in magnetoelectrics *Phys. Rev. B* **82** 245118
- [80] Ocaña O P and Souza I 2023 Multipole theory of optical spatial dispersion in crystals *SciPost Phys.* **14** 118
- [81] Wang X and Yan Y 2023 Optical activity of solids from first principles *Phys. Rev. B* **107** 045201
- [82] Jönsson L, Levine Z H and Wilkins J W 1996 Large local-field corrections in optical rotatory power of quartz and selenium *Phys. Rev. Lett.* **76** 1372
- [83] Zabalo A and Stengel M 2023 Natural optical activity from density-functional perturbation theory *Phys. Rev. Lett.* **131** 086902
- [84] Ramberg P J 2017 *Chemical Structure, Spatial Arrangement: The Early History of Stereochemistry, 1874–1914* (Routledge)
- [85] Ceramella J, Iacopetta D, Franchini A, De Luca M, Saturnino C, Andreu I, Sinicropi M S and Catalano A 2022 A look at the importance of chirality in drug activity: some significative examples *Appl. Sci.* **12** 10909
- [86] Authier A 2013 International tables for crystallography *Int. Tab. Crystall.* (<https://doi.org/10.1107/9780955360206000>)
- [87] Caticha-Ellis S and Taylor C A 1981 *Anomalous Dispersion of X-Rays in Crystallography* vol 8 (University College Cardiff Press Wales)
- [88] Halasyamani P S and Poeppelmeier K R 1998 Noncentrosymmetric oxides *Chem. Mater.* **10** 2753
- [89] Newnham R E 2005 *Properties of Materials: Anisotropy, Symmetry, Structure* (Oxford University Press)
- [90] International Union of Crystallography 2019 IUCr online dictionary (available at: <https://dictionary.iucr.org/Crystal>) (Last edit 23 March 2021)
- [91] Claborn K, Isborn C, Kaminsky W and Kahr B 2008 Optical rotation of achiral compounds *Angew. Chem., Int. Ed.* **47** 5706
- [92] Nomura K C 1960 Optical activity in tellurium *Phys. Rev. Lett.* **5** 500
- [93] Versteeg R B, Vergara I, Schäfer S D, Bischoff D, Aqeel A, Palstra T T M, Grüninger M and van Loosdrecht P H M 2016 Optically probed symmetry breaking in the chiral magnet Cu_2OSeO_3 *Phys. Rev. B* **94** 094409
- [94] Byers J, Yee H, Petralli-Mallow T and Hicks J 1994 Second-harmonic generation circular-dichroism spectroscopy from chiral monolayers *Phys. Rev. B* **49** 14643
- [95] Hauptert L M and Simpson G J 2009 Chirality in nonlinear optics *Annu. Rev. Phys. Chem.* **60** 345
- [96] Baiker A 1998 Chiral catalysis on solids *Curr. Opin. Solid State Mater. Sci.* **3** 86
- [97] Song C E and Lee S-G 2002 Supported chiral catalysts on inorganic materials *Chem. Rev.* **102** 3495
- [98] Mallat T, Orglmeister E and Baiker A 2007 Asymmetric catalysis at chiral metal surfaces *Chem. Rev.* **107** 4863
- [99] Nafie L A 2011 *Vibrational Optical Activity: Principles and Applications* (Wiley)
- [100] Zheng Z-G, Lu Y-Q and Li Q 2020 Photoprogrammable mesogenic soft helical architectures: a promising avenue toward future chiro-optics *Adv. Mater.* **32** 1905318
- [101] Bahar E 2008 Detection and identification of optical activity using polarimetry—applications to biophotonics, biomedicine and biochemistry *J. Biophotonics* **1** 230
- [102] Rochat E, Walker S D and Parker M C 2004 Polarisation and wavelength division multiplexing at 1.55 μm for bandwidth enhancement of multimode fibre based access networks *Opt. Express* **12** 2280
- [103] Gisin N and Thew R 2007 Quantum communication *Nat. Photon.* **1** 165
- [104] Liao S-K *et al* 2018 Satellite-relayed intercontinental quantum network *Phys. Rev. Lett.* **120** 030501
- [105] Humphreys P C, Kalb N, Morits J P J, Schouten R N, Vermeulen R F L, Twitchen D J, Markham M and Hanson R 2018 Deterministic delivery of remote entanglement on a quantum network *Nature* **558** 268
- [106] Quan L N, Kang J, Ning C-Z and Yang P 2019 Nanowires for photonics *Chem. Rev.* **119** 9153
- [107] Fang L, Luo H-Z, Cao X-P, Zheng S, Cai X-L and Wang J 2019 Ultra-directional high-efficiency chiral silicon photonic circuits *Optica* **6** 61
- [108] Yang Y, da Costa R C, Fuchter M J and Campbell A J 2013 Circularly polarized light detection by a chiral organic semiconductor transistor *Nat. Photon.* **7** 634
- [109] Li W, Coppens Z J, Besteiro L V, Wang W, Govorov A O and Valentine J 2015 Circularly polarized light detection with hot electrons in chiral plasmonic metamaterials *Nat. Commun.* **6** 8379

- [110] Schulz M, Balzer F, Scheunemann D, Arteaga O, Lützen A, Meskers S C J and Schiek M 2019 Chiral excitonic organic photodiodes for direct detection of circular polarized light *Adv. Funct. Mater.* **29** 1900684
- [111] Service R F 2001 Lighting the way to a quantum computer *Science* **292** 2412
- [112] Lodahl P, Mahmoodian S, Stobbe S, Rauschenbeutel A, Schneeweiss P, Volz J, Pichler H and Zoller P 2017 Chiral quantum optics *Nature* **541** 473
- [113] Wang J *et al* 2019 Spin-optoelectronic devices based on hybrid organic-inorganic trihalide perovskites *Nat. Commun.* **10** 129
- [114] Abendroth J M, Stemer D M, Bloom B P, Roy P, Naaman R, Waldeck D H, Weiss P S and Mondal P C 2019 Spin selectivity in photoinduced charge-transfer mediated by chiral molecules *ACS Nano* **13** 4928
- [115] Long G *et al* 2018 Spin control in reduced-dimensional chiral perovskites *Nat. Photon.* **12** 528
- [116] Han J, Guo S, Lu H, Liu S, Zhao Q and Huang W 2018 Recent progress on circularly polarized luminescent materials for organic optoelectronic devices *Adv. Opt. Mater.* **6** 1800538
- [117] Wu Z-G, Han H-B, Yan Z-P, Luo X-F, Wang Y, Zheng Y-X, Zuo J-L and Pan Y 2019 Chiral octahydro-binaphthol compound-based thermally activated delayed fluorescence materials for circularly polarized electroluminescence with superior EQE of 32.6% and extremely low efficiency roll-off *Adv. Mater.* **31** 1900524
- [118] Zinna F, Pasini M, Galeotti F, Botta C, Di Bari L and Giovanella U 2017 Design of lanthanide-based OLEDs with remarkable circularly polarized electroluminescence *Adv. Funct. Mater.* **27** 1603719
- [119] Zinna F, Albano G, Taddeucci A, Colli T, Aronica L A, Pescitelli G and Di Bari L 2020 Emergent nonreciprocal circularly polarized emission from an organic thin film *Adv. Mater.* **32** 2002575
- [120] Yang Y, da Costa R C, Smilgies D-M, Campbell A J and Fuchter M J 2013 Induction of circularly polarized electroluminescence from an achiral light-emitting polymer via a chiral small-molecule dopant *Adv. Mater.* **25** 2624
- [121] Bisoyi H K and Li Q 2014 Light-directing chiral liquid crystal nanostructures: from 1D to 3D *Acc. Chem. Res.* **47** 3184
- [122] Heffern M C, Matosziuk L M and Meade T J 2014 Lanthanide probes for bioresponsive imaging *Chem. Rev.* **114** 4496
- [123] Kissick D J, Wanapun D and Simpson G J 2011 Second-order nonlinear optical imaging of chiral crystals *Annu. Rev. Anal. Chem.* **4** 419
- [124] Lee H, Huttunen M J, Hsu K-J, Partanen M, Zhuo G-Y, Kauranen M and Chu S-W 2013 Chiral imaging of collagen by second-harmonic generation circular dichroism *Biomed. Opt. Express* **4** 909
- [125] Flack H D and Bernardinelli G 2008 The use of x-ray crystallography to determine absolute configuration *Chirality* **20** 681
- [126] Konak C, Kopsky V and Smutny F 1978 Gyrotropic phase transitions *J. Phys. C: Solid State Phys.* **11** 2493
- [127] Le Guennec P 1998 On the concept of chirality *J. Math. Chem.* **23** 429
- [128] Le Guennec P 2000 Two-dimensional theory of chirality. I. Absolute chirality *J. Math. Phys.* **41** 5954
- [129] Le Guennec P 2000 Two-dimensional theory of chirality. II. Relative chirality and the chirality of complex fields *J. Math. Phys.* **41** 5986
- [130] Isobe M and Ueda Y 2002 Observation of phase transition from metal to spin-singlet insulator in MgTi_2O_4 with $S = 1/2$ pyrochlore lattice *J. Phys. Soc. Japan* **71** 1848
- [131] Schmidt M, Ratcliff W, Radaelli P G, Refson K, Harrison N M and Cheong S W 2004 Spin singlet formation in MgTi_2O_4 : evidence of a helical dimerization pattern *Phys. Rev. Lett.* **92** 056402
- [132] Campbell B J, Stokes H T, Tanner D E and Hatch D M 2006 *ISODISPLACE*: a web-based tool for exploring structural distortions *J. Appl. Crystallogr.* **39** 607
- [133] Stokes H T, Hatch D M and Campbell B J 2007 Isotropy software suite p 171 (available at: <http://iso.byu.edu>)
- [134] Ivanov V V, Talanov V M, Shirokov V B and Talanov M V 2011 Crystal chemistry and formation mechanism of tetragonal MgTi_2O_4 *Inorg. Mater.* **47** 990
- [135] Đuriš K, Müller U and Jansen M 2012 K_3NiO_2 revisited, phase transition and crystal structure refinement *Z. Anorg. Allg. Chem.* **638** 737
- [136] Fava M, McCabe E, Romero A H and Bousquet E 2024 A phonon-driven mechanism for an emergent and reversible chirality in crystals (arXiv:2405.12696 [cond-mat.mtrl-sci])
- [137] Schlueter A W, Jacobson R A and Rundle R E 1966 A redetermination of the crystal structure of CsCuCl_3 *Inorg. Chem.* **5** 277
- [138] Hirotsu S 1975 Some optical and thermal properties of CsCuCl_3 and its phase transition near 423K *J. Phys. C: Solid State Phys.* **8** L12
- [139] Hirotsu S 1977 Jahn-teller induced phase transition in CsCuCl_3 : structural phase transition with helical atomic displacements *J. Phys. C: Solid State Phys.* **10** 967
- [140] Kousaka Y *et al* 2017 Monochiral helimagnetism in homochiral crystals of CsCuCl_3 *Phys. Rev. Mater.* **1** 071402
- [141] Adachi K, Achiwa N and Mekata M 1980 Helical magnetic structure in CsCuCl_3 *J. Phys. Soc. Japan* **49** 545
- [142] Yosida K 1996 *Theory of Magnetism* (Springer)
- [143] Moskvina A 2019 Dzyaloshinskii-Moriya coupling in 3D insulators *Condens. Matter* **4** 84
- [144] Syromyatnikov A V 2005 Chiral fluctuations in triangular antiferromagnets at $T \ll T_N$ *Phys. Rev. B* **71** 144408
- [145] Maki I and Sugimura T 1968 Metasilicates in the ternary system $\text{Na}_2\text{O}-\text{CaO}-\text{SiO}_2$ *J. Ceram. Soc. Jpn.* **76** 144
- [146] Fischer R X and Tillmanns E 1987 Revised data for combeite, $\text{Na}_2\text{Ca}_2\text{Si}_3\text{O}_9$ *Acta Crystallogr. C* **43** 1852
- [147] Ohsato H, Takéuchi Y and Maki I 1990 Structural study of the phase transition of $\text{Na}_4\text{Ca}_4[\text{Si}_6\text{O}_{18}]$ *Acta Crystallogr. B* **46** 125
- [148] Kahlenberg V 2023 Concerning the incorporation of potassium in the crystal structure of combeite ($\text{Na}_2\text{Ca}_2\text{Si}_3\text{O}_9$) *Mineral. Petrol.* **117** 293
- [149] Yamada T and Koizumi H 1983 Czochralski growth of $\text{Ag}_4\text{P}_2\text{O}_7$ crystals *J. Cryst. Growth* **64** 558
- [150] Newnham R, Wolfe R and Darlington C 1973 Prototype structure of $\text{Pb}_5\text{Ge}_3\text{O}_{11}$ *J. Solid State Chem.* **6** 378
- [151] Iwata Y 1977 Neutron diffraction study of the structure of paraelectric phase of $\text{Pb}_5\text{Ge}_3\text{O}_{11}$ *J. Phys. Soc. Japan* **43** 961
- [152] Iwasaki H and Sugii K 2003 Optical activity of ferroelectric $5(\text{PbO}_3\text{GeO}_2)$ single crystals *Appl. Phys. Lett.* **19** 92
- [153] Iwasaki H, Miyazawa S, Koizumi H, Sugii K and Niizeki N 1972 Ferroelectric and optical properties of $\text{Pb}_5\text{Ge}_3\text{O}_{11}$ and its isomorphous compound $\text{Pb}_5\text{Ge}_2\text{SiO}_{11}$ *J. Appl. Phys.* **43** 4907
- [154] Zabrodsky H and Avnir D 1995 Continuous symmetry measures. 4. Chirality *J. Am. Chem. Soc.* **117** 462
- [155] Fava M, Lafargue-Dit-Hauret W, Romero A H and Bousquet E 2023 Large and tunable spin-orbit effect of $6p$ orbitals through structural cavities in crystals *Phys. Rev. B* **108** L201112

- [156] Fava M, Lafargue-Dit-Hauret W, Romero A H and Bousquet E 2024 Ferroelectricity and chirality in the $\text{Pb}_5\text{Ge}_3\text{O}_{11}$ crystal *Phys. Rev. B* **109** 024113
- [157] Hayashida T, Kimura K, Urushihara D, Asaka T and Kimura T 2021 Observation of ferrochiral transition induced by an antiferroaxial ordering of antipolar structural units in $\text{Ba}(\text{TiO})\text{Cu}_4(\text{PO}_4)_4$ *J. Am. Chem. Soc.* **143** 3638
- [158] Misawa R, Ueda H, Kimura K, Tanaka Y and Kimura T 2021 Chirality and magnetic quadrupole order in $\text{Pb}(\text{TiO})\text{Cu}_4(\text{PO}_4)_4$ probed by interference scattering in resonant x-ray diffraction *Phys. Rev. B* **103** 174409
- [159] Kato Y *et al* 2019 Magnetoelectric behavior from cluster multipoles in square cupolas: study of $\text{Sr}(\text{BO})\text{Cu}_4(\text{PO}_4)_4$ in comparison with Ba and Pb isostructurals *Phys. Rev. B* **99** 024415
- [160] Kimura K, Sera M and Kimura T 2016 A^{2+} cation control of chiral domain formation in $\text{A}(\text{TiO})\text{Cu}_4(\text{PO}_4)_4$ ($\text{A} = \text{Ba}, \text{Sr}$) *Inorg. Chem.* **55** 1002
- [161] Fabini D H *et al* 2024 Noncollinear electric dipoles in a polar chiral phase of CsSnBr_3 perovskite *J. Am. Chem. Soc.* **146** 15701
- [162] Walsh A, Payne D J, Egdell R G and Watson G W 2011 Stereochemistry of post-transition metal oxides: revision of the classical lone pair model *Chem. Soc. Rev.* **40** 4455
- [163] Groom C R and Allen F H 2014 The Cambridge structural database in retrospect and prospect *Angew. Chem., Int. Ed.* **53** 662
- [164] Groom C R, Bruno I J, Lightfoot M P and Ward S C 2016 The Cambridge structural database *Acta Crystallogr. B* **72** 171
- [165] Hellenbrandt M 2004 The inorganic crystal structure database (ICSD)—present and future *Crystallogr. Rev.* **10** 17
- [166] Allmann R and Hinek R 2007 The introduction of structure types into the inorganic crystal structure database ICSD *Acta Crystallogr. A* **63** 412
- [167] Jain A *et al* 2013 Commentary: The materials project: a materials genome approach to accelerating materials innovation *APL Mater.* **1** 011002
- [168] Gražulis S, Daškevič A, Merkys A, Chateigner D, Lutterotti L, Quiros M, Serebryanaya N R, Moeck P, Downs R T and Le Bail A 2012 Crystallography Open Database (COD): an open-access collection of crystal structures and platform for world-wide collaboration *Nucleic Acids Res.* **40** D420
- [169] Calderon C E *et al* 2015 The aflow standard for high-throughput materials science calculations *Comput. Mater. Sci.* **108** 233
- [170] Draxl C and Scheffler M 2019 The NOMAD laboratory: from data sharing to artificial intelligence *J. Phys.: Mater.* **2** 036001
- [171] Merchant A, Batzner S, Schoenholz S S, Aykol M, Cheon G and Cubuk E D 2023 Scaling deep learning for materials discovery *Nature* **624** 80–85
- [172] Szymanski N J *et al* 2023 An autonomous laboratory for the accelerated synthesis of novel materials *Nature* **624** 86–91
- [173] Pizzi G, Cepellotti A, Sabatini R, Marzari N and Kozinsky B 2016 AiiDA: automated interactive infrastructure and database for computational science *Comput. Mater. Sci.* **111** 218
- [174] Ong S P, Richards W D, Jain A, Hautier G, Kocher M, Cholia S, Gunter D, Chevrier V L, Persson K A and Ceder G 2013 Python Materials Genomics (pymatgen): a robust, open-source Python library for materials analysis *Comput. Mater. Sci.* **68** 314
- [175] Gražulis S, Chateigner D, Downs R T, Yokochi A, Quirós M, Lutterotti L, Manakova E, Butkus J, Moeck P and Le Bail A 2009 Crystallography open database—an open-access collection of crystal structures *J. Appl. Crystallogr.* **42** 726
- [176] Belsky A, Hellenbrandt M, Karen V L and Luksch P 2002 New developments in the inorganic crystal structure database (ICSD): accessibility in support of materials research and design *Acta Crystallogr. B* **58** 364
- [177] Yang S-H, Naaman R, Paltiel Y and Parkin S S P 2021 Chiral spintronics *Nat. Rev. Phys.* **3** 328
- [178] Lenz J and Edelstein S 2006 Magnetic sensors and their applications *IEEE Sens. J.* **6** 631
- [179] Li C, Cui H and Zhang X 2017 Optical magnetic field sensor based on electrogyratory and electrooptic compensation in single quartz crystal *IEEE Sens. J.* **18** 1427
- [180] Nye J F 1985 *Physical Properties of Crystals: Their Representation by Tensors and Matrices* (Oxford University Press)
- [181] Caldwell D 1966 Some observations of the Faraday effect *Proc. Natl Acad. Sci.* **56** 1391
- [182] Pershan P S 1967 Magneto-optical effects *J. Appl. Phys.* **38** 1482
- [183] Rikken G and Raupach E 1997 Observation of magneto-chiral dichroism *Nature* **390** 493
- [184] Wagnière G and Meier A 1983 The influence of a static magnetic field on the absorption coefficient of a chiral molecule *Chem. Phys. Lett.* **93** 78
- [185] Wagnière G 1984 Magneto-chiral dichroism in emission. Photoselection and the polarization of transitions *Chem. Phys. Lett.* **110** 546
- [186] Barron L D and Vrbancich J 1984 Magneto-chiral birefringence and dichroism *Mol. Phys.* **51** 715
- [187] Atzori M, Rikken G L J A and Train C 2020 Magneto-chiral dichroism: a playground for molecular chemists *Chem. Eur. J.* **26** 9784
- [188] Atzori M, Train C, Hillard E A, Avarvari N and Rikken G L J A 2021 Magneto-chiral anisotropy: from fundamentals to perspectives *Chirality* **33** 844
- [189] Atzori M, Breslavetz I, Paillot K, Inoue K, Rikken G L J A and Train C 2019 A chiral Prussian blue analogue pushes magneto-chiral dichroism limits *J. Am. Chem. Soc.* **141** 20022
- [190] Pointillart F, Atzori M and Train C 2024 Magneto-chiral dichroism of chiral lanthanide complexes *Inorg. Chem. Front.* **11** 1313
- [191] Ishii K, Hattori S and Kitagawa Y 2020 Recent advances in studies on the magneto-chiral dichroism of organic compounds *Photochem. Photobiol. Sci.* **19** 9
- [192] Perez-Mato J, Gallego S, Tasci E, Elcoro L, de la Flor G and Aroyo M 2015 Symmetry-based computational tools for magnetic crystallography *Ann. Rev. Mater. Res.* **45** 217
- [193] Perez-Mato J M, Gallego S V, Elcoro L, Tasci E and Aroyo M I 2016 Symmetry conditions for type II multiferroicity in commensurate magnetic structures *J. Phys.: Condens. Matter* **28** 286001
- [194] Zheludev I S 1986 Space and time inversion in physical crystallography *Acta Crystallogr. A* **42** 122
- [195] Inoue K 2021 Chiral magnetism: coupling static and dynamic chirality *Chem. Lett.* **50** 742
- [196] Kaplan T A and Menyuk N 2007 Spin ordering in three-dimensional crystals with strong competing exchange interactions *Phil. Mag.* **87** 3711
- [197] Qureshi N *et al* 2020 Absolute crystal and magnetic chiralities in the langasite compound $\text{Ba}_3\text{NbFe}_3\text{Si}_2\text{O}_{14}$ determined by polarized neutron and x-ray scattering *Phys. Rev. B* **102** 054417
- [198] Marty K, Simonet V, Ressouche E, Ballou R, Lejay P and Bordet P 2008 Single domain magnetic helicity and triangular chirality in structurally enantiopure $\text{Ba}_3\text{NbFe}_3\text{Si}_2\text{O}_{14}$ *Phys. Rev. Lett.* **101** 247201
- [199] Stock C, Chapon L C, Schneidewind A, Su Y, Radaelli P G, McMorro D F, Bombardi A, Lee N and Cheong S-W 2011 Helical spin waves, magnetic order and fluctuations

- in the langasite compound $\text{Ba}_3\text{NbFe}_3\text{Si}_2\text{O}_{14}$ *Phys. Rev. B* **83** 104426
- [200] Faure Q, Dashwood C D, Colin C V, Johnson R D, Ressouche E, Stenning G B G, Spratt J, McMorro D F and Perry R S 2023 Magnetic structure and field dependence of the cycloid phase mediating the spin reorientation transition in $\text{Ca}_3\text{Ru}_2\text{O}_7$ *Phys. Rev. Res.* **5** 013040
- [201] Pop F, Auban-Senzier P, Canadell E, Rikken G L J A and Avarvari N 2014 Electrical magnetochiral anisotropy in a bulk chiral molecular conductor *Nat. Commun.* **5** 3757
- [202] Morimoto T and Nagaosa N 2016 Chiral anomaly and giant magnetochiral anisotropy in noncentrosymmetric Weyl semimetals *Phys. Rev. Lett.* **117** 146603
- [203] Saito M, Ishikawa K, Taniguchi K and Arima T 2008 Magnetic control of crystal chirality and the existence of a large magneto-optical dichroism effect in CuB_2O_4 *Phys. Rev. Lett.* **101** 117402
- [204] Van Aken B B, Rivera J-P, Schmid H and Fiebig M 2007 Observation of ferrotoroidic domains *Nature* **449** 702
- [205] Reimers J, Greedan J and Subramanian M 1989 Crystal structure and magnetism in MnSb_2O_6 : incommensurate long-range order *J. Solid State Chem.* **79** 263
- [206] Kinoshita M, Seki S, Sato T J, Nambu Y, Hong T, Matsuda M, Cao H B, Ishiwata S and Tokura Y 2016 Magnetic reversal of electric polarization with fixed chirality of magnetic structure in a chiral-lattice helimagnet MnSb_2O_6 *Phys. Rev. Lett.* **117** 047201
- [207] Hulliger F and Pobitschka E 1970 On the magnetic behavior of new 2H NbS_2 -type derivatives *J. Solid State Chem.* **1** 117
- [208] Dyadkin V, Mushenok F, Bosak A, Menzel D, Grigoriev S, Pattison P and Chernyshov D 2015 Structural disorder versus chiral magnetism in $\text{Cr}_{1/3}\text{NbS}_2$ *Phys. Rev. B* **91** 184205
- [209] Miyadai T, Kikuchi K, Kondo H, Sakka S, Arai M and Ishikawa Y 1983 Magnetic properties of $\text{Cr}_{1/3}\text{NbS}_2$ *J. Phys. Soc. Japan* **52** 1394
- [210] Kousaka Y, Nakao Y, Kishine J, Akita M, Inoue K and Akimitsu J 2009 Chiral helimagnetism in $\text{T}_{1/3}\text{NbS}_2$ ($\text{T}=\text{Cr}$ and Mn) *Nucl. Instrum. Methods Phys. Res. A* **600** 250
- [211] Tsuruta K, Mito M, Deguchi H, Kishine J, Kousaka Y, Akimitsu J and Inoue K 2016 Phase diagram of the chiral magnet $\text{Cr}_{1/3}\text{NbS}_2$ in a magnetic field *Phys. Rev. B* **93** 104402
- [212] Yonemura J-I *et al* 2017 Magnetic solitons and magnetic phase diagram of the hexagonal chiral crystal CrNb_3S_6 in oblique magnetic fields *Phys. Rev. B* **96** 184423
- [213] Tokura Y and Kanazawa N 2021 Magnetic skyrmion materials *Chem. Rev.* **121** 2857
- [214] Boren B 1934 Roentgenuntersuchung der legierungen von silicium mit chrom, mangan, kobalt und nickel *Ark. Kemi Mineral. Geol.* **11** 1
- [215] Dyadkin V, Wright J, Pattison P and Chernyshov D 2016 Probing structural chirality with high-energy synchrotron radiation *J. Appl. Crystallogr.* **49** 918
- [216] Grigoriev S *et al* 2010 Interplay between crystalline chirality and magnetic structure in $\text{Mn}_{1-x}\text{Fe}_x\text{Si}$ *Phys. Rev. B* **81** 012408
- [217] Lebech B, Harris P, Skov Pedersen J, Mortensen K, Gregory C, Bernhoeft N, Jermy M and Brown S 1995 Magnetic phase diagram of MnSi *J. Magn. Magn. Mater.* **140–144** 119
- [218] Bauer A and Pfleiderer C 2012 Magnetic phase diagram of MnSi inferred from magnetization and ac susceptibility *Phys. Rev. B* **85** 214418
- [219] Grigoriev S V, Maleyev S V, Okorokov A I, Chetverikov Y O, Böni P, Georgii R, Lamago D, Eckerlebe H and Pranzas K 2006 Magnetic structure of MnSi under an applied field probed by polarized small-angle neutron scattering *Phys. Rev. B* **74** 214414
- [220] Skyrme T H R and Schonland B F J 1961 A non-linear field theory *Proc. R. Soc. A* **260** 127
- [221] Skyrme T H R 1962 A unified field theory of mesons and baryons *Nucl. Phys.* **31** 556
- [222] Bogdanov A and Hubert A 1994 Thermodynamically stable magnetic vortex states in magnetic crystals *J. Magn. Magn. Mater.* **138** 255
- [223] Kézsmárki I *et al* 2015 Néel-type skyrmion lattice with confined orientation in the polar magnetic semiconductor GaV_4S_8 *Nat. Mater.* **14** 1116
- [224] Kurumaji T *et al* 2019 Skyrmion lattice with a giant topological Hall effect in a frustrated triangular-lattice magnet *Science* **365** 914
- [225] Hirschberger M *et al* 2019 Skyrmion phase and competing magnetic orders on a breathing kagomé lattice *Nat. Commun.* **10** 5831
- [226] Krén E and Kádár G 1970 Neutron diffraction study of Mn_3Ga *Solid State Commun.* **8** 1653
- [227] Tomiyoshi S, Yamaguchi Y and Nagamiya T 1983 Triangular spin configuration and weak ferromagnetism of Mn_3Ge *J. Magn. Magn. Mater.* **31–34** 629
- [228] Tomiyoshi S and Yamaguchi Y 1982 Magnetic structure and weak ferromagnetism of Mn_3Sn studied by polarized neutron diffraction *J. Phys. Soc. Japan* **51** 2478
- [229] Pradhan S, Samanta K, Saha K and Nandy A K 2023 Vector-chirality driven topological phase transitions in noncollinear antiferromagnets and its impact on anomalous Hall effect *Commun. Phys.* **6** 272
- [230] Nakatsuji S, Kiyohara N and Higo T 2015 Large anomalous Hall effect in a non-collinear antiferromagnet at room temperature *Nature* **527** 212–5
- [231] Johnson R D, Khalyavin D D, Manuel P, Bombardi A, Martin C, Chapon L C and Radaelli P G 2016 Modulated spin helicity stabilized by incommensurate orbital density waves in a quadruple perovskite manganite *Phys. Rev. B* **93** 180403
- [232] Ślawiński W, Przeniosło R, Sosnowska I, Bieringer M, Margiolaki I and Suard E 2009 Modulation of atomic positions in $\text{CaCu}_x\text{Mn}_{7-x}\text{O}_{12}$ ($x \leq 0.1$) *Acta Crystallogr. B* **65** 535
- [233] Perks N, Johnson R D, Martin C, Chapon L C and Radaelli P G 2012 Magneto-orbital helices as a route to coupling magnetism and ferroelectricity in multiferroic $\text{CaMn}_7\text{O}_{12}$ *Nat. Commun.* **3** 1277
- [234] Zhang G, Dong S, Yan Z, Guo Y, Zhang Q, Yunoki S, Dagotto E and Liu J-M 2011 Multiferroic properties of $\text{CaMn}_7\text{O}_{12}$ *Phys. Rev. B* **84** 174413
- [235] Ślawiński W, Przeniosło R, Sosnowska I and Bieringer M 2010 Structural and magnetic modulations in $\text{CaCu}_x\text{Mn}_{7-x}\text{O}_{12}$ *J. Phys.: Condens. Matter* **22** 186001
- [236] Hlinka J, Privratska J, Ondrejčková P and Janovec V 2016 Symmetry guide to ferroaxial transitions *Phys. Rev. Lett.* **116** 177602
- [237] Bhim A, Sutter J-P, Gopalakrishnan J and Natarajan S 2021 Stuffed tridymite structures: synthesis, structure, second harmonic generation, optical and multiferroic properties *Chem. Eur. J.* **27** 1995
- [238] Xu X, Huang F-T, Admasu A S, Kratochvílová M, Chu M-W, Park J-G and Cheong S-W 2022 Multiple ferroic orders and toroidal magnetoelectricity in the chiral magnet BaCoSiO_4 *Phys. Rev. B* **105** 184407
- [239] Ding L *et al* 2021 Field-tunable toroidal moment in a chiral-lattice magnet *Nat. Commun.* **12** 5339
- [240] Šmejkal L, Sinova J and Jungwirth T 2022 Emerging research landscape of altermagnetism *Phys. Rev. X* **12** 040501

- [241] Turek I 2022 Altermagnetism and magnetic groups with pseudoscalar electron spin *Phys. Rev. B* **106** 094432
- [242] Cheong S-W and Huang F-T 2024 Altermagnetism with non-collinear spins *npj Quantum Mater.* **9** 13
- [243] Mazin I 2024 Altermagnetism then and now *Physics* **17** 4
- [244] Šmejkal L, González-Hernández R, Jungwirth T and Sinova J 2020 Crystal time-reversal symmetry breaking and spontaneous Hall effect in collinear antiferromagnets *Sci. Adv.* **6** eaaz8809
- [245] Adhikari Y, Liu T, Wang H, Hua Z, Liu H, Lochner E, Schlottmann P, Yan B, Zhao J and Xiong P 2023 Interplay of structural chirality, electron spin and topological orbital in chiral molecular spin valves *Nat. Commun.* **14** 5163
- [246] Wieder B J *et al* 2022 Topological materials discovery from crystal symmetry *Nat. Rev. Mater.* **7** 196
- [247] Lv B, Qian T and Ding H 2021 Experimental perspective on three-dimensional topological semimetals *Rev. Mod. Phys.* **93** 025002
- [248] Yang X-F, Liu Q-B, Wang Z-Q and Fu H-H 2023 Unconventional charge-two Weyl phonons in high-symmetry lines *Adv. Phys. Res.* **2** 2300004
- [249] Hasan M Z, Chang G, Belopolski I, Bian G, Xu S-Y and Yin J-X 2021 Weyl, Dirac and high-fold chiral fermions in topological quantum matter *Nat. Rev. Mater.* **6** 784
- [250] Thouless D J, Kohmoto M, Nightingale M P and den Nijs M 1982 Quantized Hall conductance in a two-dimensional periodic potential *Phys. Rev. Lett.* **49** 405
- [251] Simon B 1983 Holonomy, the quantum adiabatic theorem and Berry's phase *Phys. Rev. Lett.* **51** 2167
- [252] Bradlyn B, Cano J, Wang Z, Vergniory M, Felser C, Cava R J and Bernevig B A 2016 Beyond Dirac and Weyl fermions: unconventional quasiparticles in conventional crystals *Science* **353** aaf5037
- [253] Sadhukhan B and Nag T 2021 Electronic structure and unconventional nonlinear response in double Weyl semimetal SrSi_2 *Phys. Rev. B* **104** 245122
- [254] Yu Z-M, Zhang Z, Liu G-B, Wu W, Li X-P, Zhang R-W, Yang S A and Yao Y 2022 Encyclopedia of emergent particles in three-dimensional crystals *Sci. Bull.* **67** 375
- [255] Sreeparvathy P, Mondal C, Barman C K and Alam A 2022 Coexistence of multifold and multidimensional topological phonons in KMgBO_3 *Phys. Rev. B* **106** 085102
- [256] Wang X, Zhou F, Zhang Z, Wu W, Yu Z-M and Yang S A 2022 Single pair of multi-Weyl points in nonmagnetic crystals *Phys. Rev. B* **106** 195129
- [257] Juneja R *et al* 2021 Quasiparticle twist dynamics in non-symmorphic materials *Mater. Today Phys.* **21** 100548
- [258] Juneja R, Li X, Thebaud S, Moseley D, Cheng Y, Manley M, Hermann R and Lindsay L 2022 Phonons in complex twisted crystals: angular momenta, interactions and topology *Phys. Rev. B* **106** 094310
- [259] Wu P, Liu G, Hu X and Xu H 2023 Paired charge-2 Weyl-Dirac phonons in tetragonal crystals *Phys. Rev. B* **108** 054305
- [260] Liu Q-B, Yang X-F, Lou A and Fu H-H 2022 Beyond no-go theorem' Weyl phonons (arXiv:2203.04596 [cond-mat.mes-hall])
- [261] Liu G, Huang Z, Chen Z, Jin Y, He C and Xu H 2022 Coexistence of charge-2 Dirac and Weyl phonons in chiral space groups *Phys. Rev. B* **106** 054306
- [262] Aizu K 1964 Reversal in optical rotatory power—"gyroelectric" crystals and "hypergyroelectric" crystals *Phys. Rev.* **133** A1584
- [263] Zheludev I S 1976 Optical activity of crystals under the action of an electric field (electrogyration) *Sov. Phys. - Usp.* **19** 1029
- [264] Stasyuk I V and Kotsur S S 1983 The microscopic theory of the gyration and electrogyration in dielectric crystals *Phys. Status Solidi b* **117** 557
- [265] Kobayashi J 1983 Optical gyration and electrogyration effects of some ferroelectrics *Ferroelectrics* **50** 53
- [266] Koralewski M 1984 Magnitude of electrogyration effect in crystals *Ferroelectr. Lett. Sect.* **2** 77
- [267] Vlokh O G 1987 Electrogyration properties of crystals *Ferroelectrics* **75** 119
- [268] Uesu Y, Okada N, Inoue M and Hara S 1990 Circular dichroism of ferroelectrics and origin of the electrogyration effect *Ferroelectrics* **107** 33
- [269] Gunning M J and Raab R E 1997 Electric-field-induced optical activity in nonmagnetic crystals *J. Opt. Soc. Am. B* **14** 1692
- [270] Vlokh O G 2001 The historical background of finding of electrogyration *Ukr. J. Phys. Opt.* **2** 53
- [271] Buckingham A, Graham C and Raab R 1971 On the theory of linear electro-optical rotation *Chem. Phys. Lett.* **8** 622
- [272] Futama H and Pepinsky R 1962 Optical activity in ferroelectric $\text{LiH}_3(\text{SeO}_3)_2$ *J. Phys. Soc. Japan* **17** 725
- [273] Hayashida T, Uemura Y, Kimura K, Matsuoka S, Hagihara M, Hirose S, Morioka H, Hasegawa T and Kimura T 2021 Phase transition and domain formation in ferroaxial crystals *Phys. Rev. Mater.* **5** 124409
- [274] Iwasaki H, Sugii K, Niizeki N and Toyoda H 1972 Switching of optical rotatory power in ferroelectric $5\text{PbO} \cdot 3\text{GeO}_2$ single crystal *Ferroelectrics* **3** 157
- [275] Shopa M, Ftomyn N and Shopa Y 2021 High-accuracy polarimetric studies on lead germanate single crystals *J. Appl. Crystallogr.* **54** 1615
- [276] Adamenko D, Klymiv I, Duda V M, Vlokh R and Vlokh O 2008 Electrogyration and faraday rotation in pure and Cr-doped lead germanate crystals *J. Phys.: Condens. Matter* **20** 075201
- [277] Kizel' V A, Krasilov Y I and Burkov V I 1975 Experimental studies of gyrotropy of crystals *Sov. Phys. - Usp.* **17** 745
- [278] Wadhawan V K 1979 Gyrotropy: an implicit form of ferroicity *Acta Crystallogr. A* **35** 629
- [279] Wadhawan V K 1982 Ferroelasticity and related properties of crystals *Phase Transit.* **3** 3
- [280] Kobayashi J and Yamada N 1962 Optical activity in ferroelectric $\text{Ca}_2\text{Sr}(\text{C}_2\text{H}_3\text{CO}_2)_6$ *J. Phys. Soc. Japan* **17** 876
- [281] Takahashi N, Tomizawa M and Kobayashi J 1992 Optical activity and electrogyration effect of $\text{Co}_3\text{B}_7\text{O}_{13}\text{I}$ and $\text{Cu}_3\text{B}_7\text{O}_{13}\text{Cl}$ *Japan. J. Appl. Phys.* **31** 3209
- [282] Deliolanis N C, Kourmoulis I M, Asimellis G, Apostolidis A G, Vanidhis E D and Vainos N A 2004 Direct measurement of the dispersion of the electrogyration coefficient of photorefractive $\text{Bi}_{12}\text{GeO}_{20}$ crystals *J. Appl. Phys.* **97** 023531
- [283] Deliolanis N C, Vanidhis E D and Vainos N A 2006 Dispersion of electrogyration in sillenite crystals *Appl. Phys. B* **85** 591
- [284] Vlokh R, Mys O, Grabar A and Vysochanskii Y 2008 Optical activity of $\text{Sn}_2\text{P}_2\text{S}_6$ crystals at the phase transition *Ukr. J. Phys. Opt.* **9** 1
- [285] Novikov M A, Stepanov A A and Khyshov A A 2017 An electric sensor based on the electrogyration effect in a lead tungstate crystal *Tech. Phys. Lett.* **43** 372
- [286] Hayashida T, Uemura Y, Kimura K, Matsuoka S, Morikawa D, Hirose S, Tsuda K, Hasegawa T and Kimura T 2020 Visualization of ferroaxial domains in an order-disorder type ferroaxial crystal *Nat. Commun.* **11** 4582
- [287] Ben-Haïm E, Lesne A and Victor J-M 2001 Chromatin: a tunable spring at work inside chromosomes *Phys. Rev. E* **64** 051921

- [288] Huang P, Xia Z, Gao X, Rondinelli J M, Zhang X, Zhang H, Poeppelmeier K R and Zunger A 2020 Ferri-chiral compounds with potentially switchable Dresselhaus spin splitting *Phys. Rev. B* **102** 235127
- [289] Wadhawan V 2000 *Introduction to Ferroic Materials* (CRC Press)
- [290] Zhang C, dos Reis R, Poeppelmeier K and Dravid V 2021 Show me your “hand”: direct determination of “handedness” in NaCu_5S_3 chiral crystal via aberration-corrected scanning transmission electron microscopy *Microsc. Microanal.* **27** 2652
- [291] Singh A K, Wang W, Panda D P, Bagchi D, Goud D, Ray B, He J and Peter S C 2022 Cobalt-induced phase transformation of Ni_3Ga_4 generates chiral intermetallic $\text{Co}_3\text{Ni}_3\text{Ga}_8$ *J. Am. Chem. Soc.* **145** 1433
- [292] Sawada A, Ishibashi Y and Takagi Y 1977 Ferroelasticity and the origin of optical activity of $\text{Ca}_2\text{Sr}(\text{C}_2\text{H}_5\text{CO}_2)_6$ (DSP) *J. Phys. Soc. Japan* **43** 195
- [293] Glazer A M, Stadnicka K and Singh S 1981 The structure and optical activity of the paraelectric phase of dicalcium strontium propionate *J. Phys. C: Solid State Phys.* **14** 5011
- [294] Erb K and Hlinka J 2020 Vector, bidirector and bloch skyrmion phases induced by structural crystallographic symmetry breaking *Phys. Rev. B* **102** 024110
- [295] Srinivasan G, Rasmussen E, Bush A, Kamentsev K, Meshcheryakov V and Fetisov Y 2004 Structural and magnetoelectric properties of MFe_2O_4 -PZT ($\text{M} = \text{Ni, Co}$) and $\text{La}_x(\text{Ca, Sr})_{1-x}\text{MnO}_3$ -PZT multilayer composites *Appl. Phys. A* **78** 721
- [296] Zhang S, van der Laan G and Hesjedal T 2017 Direct experimental determination of spiral spin structures via the dichroism extinction effect in resonant elastic soft x-ray scattering *Phys. Rev. B* **96** 094401
- [297] Nomura T, Zhang X-X, Zherlitsyn S, Wosnitza J, Tokura Y, Nagaosa N and Seki S 2019 Phonon magnetochiral effect *Phys. Rev. Lett.* **122** 145901
- [298] Kishine J, Ovchinnikov A S and Tereshchenko A A 2020 Chirality-induced phonon dispersion in a noncentrosymmetric micropolar crystal *Phys. Rev. Lett.* **125** 245302
- [299] Romao C P 2019 Anomalous thermal expansion and chiral phonons in BiB_3O_6 *Phys. Rev. B* **100** 060302
- [300] Ptok A, Kobińska A, Sternik M, Łażewski J, Jochym P T, Oleś A M, Stankov S and Piekarczyk P 2021 Chiral phonons in the honeycomb sublattice of layered CoSn -like compounds *Phys. Rev. B* **104** 054305
- [301] Suri N, Wang C, Zhang Y and Xiao D 2021 Chiral phonons in moiré superlattices *Nano Lett.* **21** 10026
- [302] Juraschek D M, Neuman T C V and Narang P 2022 Giant effective magnetic fields from optically driven chiral phonons in $4f$ paramagnets *Phys. Rev. Res.* **4** 013129
- [303] Ishito K, Mao H, Kousaka Y, Togawa Y, Iwasaki S, Zhang T, Murakami S, Kishine J-I and Satoh T 2023 Truly chiral phonons in α - HgS *Nat. Phys.* **19** 35
- [304] Chen H, Wu W, Zhu J, Yang Z, Gong W, Gao W, Yang S A and Zhang L 2022 Chiral phonon diode effect in chiral crystals *Nano Lett.* **22** 1688
- [305] Xiong G, Yu Z and Zhang L 2022 Interband chiral phonon transfer in a magnetic field *Phys. Rev. B* **105** 024312
- [306] Yao D and Murakami S 2022 Chiral-phonon-induced current in helical crystals *Phys. Rev. B* **105** 184412
- [307] Tsunetsugu H and Kusunose H 2023 Theory of energy dispersion of chiral phonons *J. Phys. Soc. Japan* **92** 023601
- [308] Geilhufe R M and Hergert W 2023 Electron magnetic moment of transient chiral phonons in KTaO_3 *Phys. Rev. B* **107** L020406
- [309] Ueda H, García-Fernández M, Agrestini S, Romao C P, van den Brink J, Spaldin N A, Zhou K-J and Staub U 2023 Chiral phonons in quartz probed by x-rays *Nature* **618** 946
- [310] Qin T, Zhou J and Shi J 2012 Berry curvature and the phonon Hall effect *Phys. Rev. B* **86** 104305
- [311] Saito T, Misaki K, Ishizuka H and Nagaosa N 2019 Berry phase of phonons and thermal Hall effect in nonmagnetic insulators *Phys. Rev. Lett.* **123** 255901
- [312] Park S and Yang B-J 2020 Phonon angular momentum Hall effect *Nano Lett.* **20** 7694
- [313] Saparov D, Xiong B, Ren Y and Niu Q 2022 Lattice dynamics with molecular Berry curvature: chiral optical phonons *Phys. Rev. B* **105** 064303
- [314] Xiong G, Chen H, Ma D and Zhang L 2022 Effective magnetic fields induced by chiral phonons *Phys. Rev. B* **106** 144302
- [315] Fransson J 2023 Chiral phonon induced spin polarization *Phys. Rev. Res.* **5** L022039
- [316] Romao C P, Catena R, Spaldin N A and Matas M 2023 Chiral phonons as dark matter detectors *Phys. Rev. Res.* **5** 043262
- [317] Maldovan M 2013 Sound and heat revolutions in phononics *Nature* **503** 209
- [318] Streib S 2021 Difference between angular momentum and pseudoangular momentum *Phys. Rev. B* **103** L100409
- [319] Yao W, Xiao D and Niu Q 2008 Valley-dependent optoelectronics from inversion symmetry breaking *Phys. Rev. B* **77** 235406
- [320] Zhang T and Murakami S 2022 Chiral phonons and pseudoangular momentum in nonsymmorphic systems *Phys. Rev. Res.* **4** L012024
- [321] Juraschek D M, Narang P and Spaldin N A 2020 Phono-magnetic analogs to opto-magnetic effects *Phys. Rev. Res.* **2** 043035
- [322] Baydin A *et al* 2022 Magnetic control of soft chiral phonons in PbTe *Phys. Rev. Lett.* **128** 075901
- [323] Juraschek D M, Fechner M, Balatsky A V and Spaldin N A 2017 Dynamical multiferroicity *Phys. Rev. Mater.* **1** 014401
- [324] van der Ziel J P, Pershan P S and Malmstrom L D 1965 Optically-induced magnetization resulting from the inverse Faraday effect *Phys. Rev. Lett.* **15** 190
- [325] Popova D, Bringer A and Blügel S 2011 Theory of the inverse Faraday effect in view of ultrafast magnetization experiments *Phys. Rev. B* **84** 214421
- [326] Schaaack G 1976 Observation of circularly polarized phonon states in an external magnetic field *J. Phys. C: Solid State Phys.* **9** L297
- [327] Cheng B, Schumann T, Wang Y, Zhang X, Barbalas D, Stemmer S and Armitage N P 2020 A large effective phonon magnetic moment in a Dirac semimetal *Nano Lett.* **20** 5991
- [328] Nova T F, Cartella A, Cantaluppi A, Först M, Bossini D, Mikhaylovskiy R V, Kimel A V, Merlin R and Cavalleri A 2017 An effective magnetic field from optically driven phonons *Nat. Phys.* **13** 132
- [329] Afanasiev D, Hortensius J R, Ivanov B A, Sasani A, Bousquet E, Blanter Y M, Mikhaylovskiy R V, Kimel A V and Caviglia A D 2021 Ultrafast control of magnetic interactions via light-driven phonons *Nat. Mater.* **20** 607
- [330] Kimel A *et al* 2022 The 2022 magneto-optics roadmap *J. Phys. D: Appl. Phys.* **55** 463003
- [331] Geilhufe R M, Juričić V, Bonetti S, Zhu J-X and Balatsky A V 2021 Dynamically induced magnetism in KTaO_3 *Phys. Rev. Res.* **3** L022011
- [332] Bossini D *et al* 2023 Magnetoelectrics and multiferroics: theory, synthesis, characterisation, preliminary results and perspectives for all-optical manipulations *J. Phys. D: Appl. Phys.* **56** 273001

- [333] Geilhufe R M 2022 Dynamic electron-phonon and spin-phonon interactions due to inertia *Phys. Rev. Res.* **4** L012004
- [334] Hamada M and Murakami S 2020 Conversion between electron spin and microscopic atomic rotation *Phys. Rev. Res.* **2** 023275
- [335] Barnett S J 1935 Gyromagnetic and electron-inertia effects *Rev. Mod. Phys.* **7** 129
- [336] Zhang C, Yuan H, Tang Z, Quan W and Fang J C 2016 Inertial rotation measurement with atomic spins: from angular momentum conservation to quantum phase theory *Appl. Phys. Rev.* **3** 041305
- [337] Mentink J H, Katsnelson M I and Leshchko M 2019 Quantum many-body dynamics of the Einstein–de Haas effect *Phys. Rev. B* **99** 064428
- [338] Zhang T, Huang Z, Pan Z, Du L, Zhang G and Murakami S 2023 Weyl phonons in chiral crystals *Nano Lett.* **23** 7561
- [339] Geilhufe M, Juraschek D and Zhu H 2023 Chiral phonons in quantum materials (available at: www.cecam.org/workshop-details/1202)
- [340] Toledano P and Toledano J 1987 *Landau Theory of Phase Transitions, The: Application to Structural, Incommensurate, Magnetic and Liquid Crystal Systems* (World Scientific Lecture Notes in Physics) (World Scientific Publishing Company) (available at: <https://books.google.be/books?id=6gU8DQAAQBAJ>)
- [341] Brink L, Gunn M, José J V, Kosterlitz J M and Phua K K 2018 *Topological Phase Transitions and New Developments* (World Scientific) (<https://doi.org/10.1142/11016>)
- [342] Dmitriev V and Toledano P 1996 *Reconstructive Phase Transitions: In Crystals and Quasicrystals* (World Scientific Publishing Company) (available at: <https://books.google.be/books?id=T-3sCgAAQBAJ>)
- [343] Dove M T 1997 Theory of displacive phase transitions in minerals *Am. Mineral.* **82** 213
- [344] Gnewuch S and Rodriguez E E 2019 The fourth ferroic order: current status on ferrotoroidic materials *J. Solid State Chem.* **271** 175
- [345] Oiwa R and Kusunose H 2022 Rotation, electric-field responses and absolute enantioselection in chiral crystals *Phys. Rev. Lett.* **129** 116401
- [346] Hlinka J 2014 Eight types of symmetrically distinct vectorlike physical quantities *Phys. Rev. Lett.* **113** 165502
- [347] Erb K C and Hlinka J 2018 Symmetry guide to chiroaxial transitions *Phase Transit.* **91** 953
- [348] Lipkin D M 2004 Existence of a new conservation law in electromagnetic theory *J. Math. Phys.* **5** 696
- [349] Tang Y and Cohen A E 2010 Optical chirality and its interaction with matter *Phys. Rev. Lett.* **104** 163901
- [350] Proskurin I, Ovchinnikov A S, Nosov P and ichiro Kishine J 2017 Optical chirality in gyrotropic media: symmetry approach *New J. Phys.* **19** 063021
- [351] Philbin T G 2013 Lipkin's conservation law, Noether's theorem and the relation to optical helicity *Phys. Rev. A* **87** 043843
- [352] Rukhlenko I D, Teplov N V, Baimuratov A S, Andronaki S A, Gun'ko Y K, Baranov A V and Fedorov A V 2016 Completely chiral optical force for enantioseparation *Sci. Rep.* **6** 36884
- [353] Mun J, Kim M, Yang Y, Badloe T, Ni J, Chen Y, Qiu C-W and Rho J 2020 Electromagnetic chirality: from fundamentals to nontraditional chiroptical phenomena *Light Sci. Appl.* **9** 139
- [354] Genet C 2022 Chiral light-chiral matter interactions: an optical force perspective *ACS Photon.* **9** 319
- [355] Dubovik V M and Tugushev V V 1990 Toroid moments in electrodynamics and solid-state physics *Phys. Rep.* **187** 145–202
- [356] Dubovik V and Tugushev V 1990 Toroid moments in electrodynamics and solid-state physics *Phys. Rep.* **187** 145
- [357] Gopalan V and Litvin D B 2011 Rotation-reversal symmetries in crystals and handed structures *Nat. Mater.* **10** 376
- [358] Levanyuk A P and Sannikov D G 1974 Reviews of Topical Problems: Improper ferroelectrics *Sov. Phys. - Usp.* **17** 199
- [359] Bousquet E, Dawber M, Stucki N, Lichtensteiger C, Hermet P, Gariglio S, Triscone J-M and Ghosez P 2008 Improper ferroelectricity in perovskite oxide artificial superlattices *Nature* **452** 732
- [360] Cano A and Levanyuk A P 2010 Pseudoproper ferroelectricity in thin films *Phys. Rev. B* **81** 172105
- [361] Benedek N A and Fennie C J 2011 Hybrid improper ferroelectricity: a mechanism for controllable polarization-magnetization coupling *Phys. Rev. Lett.* **106** 107204
- [362] Benedek N A and Hayward M A 2022 Hybrid improper ferroelectricity: a theoretical, computational and synthetic perspective *Annu. Rev. Mater. Res.* **52** 331
- [363] Dresselhaus M, Dresselhaus G and Jorio A 2007 *Group Theory: Application to the Physics of Condensed Matter* (Springer) (available at: <https://books.google.be/books?id=sKaH8vrfmnQC>)
- [364] Hatch D M and Stokes H T 2003 Invariants: program for obtaining a list of invariant polynomials of the order-parameter components associated with irreducible representations of a space group *J. Appl. Crystallogr.* **36** 951
- [365] Bousquet E and Cano A 2016 Non-collinear magnetism in multiferroic perovskites *J. Phys.: Condens. Matter* **28** 123001
- [366] Nagai T, Hagihara M, Yokoi R, Moriwake H and Kimura T 2024 Ferroelectricity induced by a combination of crystallographic chirality and axial vector *J. Am. Chem. Soc.* **146** 23348
- [367] Romao C P and Juraschek D M 2024 Phonon-induced geometric chirality (arXiv:2311.00824 [cond-mat.mtrl-sci])
- [368] Juraschek D M, Fechner M and Spaldin N A 2017 Ultrafast structure switching through nonlinear phononics *Phys. Rev. Lett.* **118** 054101
- [369] Buzzi M, Först M, Mankowsky R and Cavalleri A 2018 Probing dynamics in quantum materials with femtosecond x-rays *Nat. Rev. Mater.* **3** 299
- [370] Prosandeev S, Kornev I A and Bellaiche L 2011 Phase transitions in epitaxial (–110) BiFeO₃ films from first principles *Phys. Rev. Lett.* **107** 117602
- [371] Johnson R D, Nair S, Chapon L C, Bombardi A, Vecchini C, Prabhakaran D, Boothroyd A T and Radaelli P G 2011 Cu₃Nb₂O₈: a multiferroic with chiral coupling to the crystal structure *Phys. Rev. Lett.* **107** 137205
- [372] Barron L D 1986 Symmetry and molecular chirality *Chem. Soc. Rev.* **15** 189
- [373] Fu L 2015 Parity-breaking phases of spin-orbit-coupled metals with gyrotropic, ferroelectric and multipolar orders *Phys. Rev. Lett.* **115** 026401
- [374] Xu S-Y *et al* 2020 Spontaneous gyrotropic electronic order in a transition-metal dichalcogenide *Nature* **578** 545
- [375] Khalyavin D D, Johnson R D, Orlandi F, Radaelli P G, Manuel P and Belik A A 2020 Emergent helical texture of electric dipoles *Science* **369** 680
- [376] Korede V, Nagalingam N, Penha F M, van der Linden N, Padding J T, Hartkamp R and Eral H B 2023 A review of laser-induced crystallization from solution *Cryst. Growth Des.* **23** 3873

- [377] Wang S-F and Sugiyama T 2023 Femtosecond laser-driven enantioselectivity on achiral-chiral polymorphic transition *Cell Rep. Phys. Sci.* **4** 101323
- [378] Zhao Y, Edgar J S, Jeffries G D M, McGloin D and Chiu D T 2007 Spin-to-orbital angular momentum conversion in a strongly focused optical beam *Phys. Rev. Lett.* **99** 073901
- [379] Bliokh K Y, Rodríguez-Fortuño F J, Nori F and Zayats A V 2015 Spin-orbit interactions of light *Nat. Photon.* **9** 796
- [380] Kondepudi D K, Kaufman R J and Singh N 1990 Chiral symmetry breaking in sodium chlorate crystallization *Science* **250** 975
- [381] Niinomi H, Miura H, Kimura Y, Uwaha M, Katsuno H, Harada S, Ujihara T and Tsukamoto K 2014 Emergence and amplification of chirality via achiral-chiral polymorphic transformation in sodium chlorate solution growth *Cryst. Growth Des.* **14** 3596
- [382] Hayashida T, Kimura K and Kimura T 2022 Switching crystallographic chirality in $\text{Ba}(\text{TiO})\text{Cu}_4(\text{PO}_4)_4$ by laser irradiation *J. Phys. Chem. Lett.* **13** 3857
- [383] Mezey P G 1995 Rules on chiral and achiral molecular transformations *J. Math. Chem.* **17** 185
- [384] Weinberg N and Mislow K 2000 On chirality measures and chirality properties *Can. J. Chem.* **78** 41
- [385] Petitjean M 2003 Chirality and symmetry measures: a transdisciplinary review *Entropy* **5** 271
- [386] Fowler P W 2005 Quantification of chirality: attempting the impossible *Symmetry: Cult. Sci.* **16** 321
- [387] Weinberg N and Mislow K 1993 Distance functions as generators of chirality measures *J. Math. Chem.* **14** 427
- [388] Buda A B and Mislow K 1992 A Hausdorff chirality measure *J. Am. Chem. Soc.* **114** 6006
- [389] Buda A B, der Heyde T A and Mislow K 1992 On quantifying chirality *Angew. Chem., Int. Ed. Engl.* **31** 989
- [390] Gilat G 1994 On quantifying chirality—obstacles and problems towards unification *J. Math. Chem.* **15** 197
- [391] Flapan E 2000 *When Topology Meets Chemistry: A Topological Look at Molecular Chirality (Outlooks)* (Cambridge University Press) (<https://doi.org/10.1017/CBO9780511626272>)
- [392] Resta R 1998 Quantum-mechanical position operator in extended systems *Phys. Rev. Lett.* **80** 1800
- [393] Moreau J J 1961 Constantes d'un flot tourbillonnaire en fluide parfait barotrope *C. R. Hebd. Seances Acad. Sci.* **252** 2810
- [394] Moffatt H and Ricca R 1992 Helicity and the Călugăreanu invariant *Proc. R. Soc. A* **439** 411
- [395] Moffatt H K 2014 Helicity and singular structures in fluid dynamics *Proc. Natl Acad. Sci. USA* **111** 3663
- [396] Gómez-Ortiz F, Fava M, McCabe E E, Romero A H and Bousquet E 2024 Structural chirality measurements and computation of handedness in periodic solids *Phys. Rev. B* **110** 174112
- [397] Inda A, Oiwa R, Hayami S, Yamamoto H M and Kusunose H 2024 Quantification of chirality based on electric toroidal monopole *J. Chem. Phys.* **160** 184117
- [398] Hayami S and Kusunose H 2024 Unified description of electronic orderings and cross correlations by complete multipole representation *J. Phys. Soc. Japan* **93** 072001
- [399] Kusunose H, Oiwa R and Hayami S 2020 Complete multipole basis set for single-centered electron systems *J. Phys. Soc. Japan* **89** 104704
- [400] Weinberg N and Mislow K 1997 On chiral pathways in E^n : a dimensional analysis *Theor. Chim. Acta* **95** 63
- [401] Banik M, Rodríguez K, Hulkko E and Apkarian V A 2016 Orientation-dependent handedness of chiral plasmons on nanosphere dimers: how to turn a right hand into a left hand *ACS Photon.* **3** 2482
- [402] Mislow K 1999 Molecular chirality *Topics in Stereochemistry* (Wiley) pp 1–82 (<https://doi.org/10.1002/9780470147313.ch1>)
- [403] Cuevas A G, Mato J M P, Tello M J, Madariaga G, Fernández J, Echarri L, Zuñiga F J and Chapuis G 1984 Gyrotropic phase transition in the layer crystal $(\text{C}_5\text{H}_{11}\text{NH}_3)_2\text{ZnCl}_4$ at 249 K *Phys. Rev. B* **29** 2655
- [404] Ederer C and Spaldin N A 2007 Towards a microscopic theory of toroidal moments in bulk periodic crystals *Phys. Rev. B* **76** 214404
- [405] Spaldin N A, Fiebig M and Mostovoy M 2008 The toroidal moment in condensed-matter physics and its relation to the magnetoelectric effect *J. Phys.: Condens. Matter* **20** 434203
- [406] Zimmermann A S, Meier D and Fiebig M 2014 Ferroic nature of magnetic toroidal order *Nat. Commun.* **5** 4796
- [407] Tolédano P, Ackermann M, Bohatý L, Becker P, Lorenz T, Leo N and Fiebig M 2015 Primary ferrotoroidicity in antiferromagnets *Phys. Rev. B* **92** 094431
- [408] Hayashida T, Misawa R, Fiebig M and Kimura T 2024 Observation of ferrotoroidic domains in a metal *Phys. Rev. B* **109** L100401
- [409] Gao Y, Vanderbilt D and Xiao D 2018 Microscopic theory of spin toroidization in periodic crystals *Phys. Rev. B* **97** 134423
- [410] King-Smith R D and Vanderbilt D 1993 Theory of polarization of crystalline solids *Phys. Rev. B* **47** 1651
- [411] Íñiguez J 2008 First-principles approach to lattice-mediated magnetoelectric effects *Phys. Rev. Lett.* **101** 117201
- [412] Ayuso D, Neufeld O, Ordóñez A F, Decleva P, Lerner G, Cohen O, Ivanov M and Smirnova O 2019 Synthetic chiral light for efficient control of chiral light-matter interaction *Nat. Photon.* **13** 866
- [413] Mahmoodian S 2019 Chiral light-matter interaction beyond the rotating-wave approximation *Phys. Rev. Lett.* **123** 133603
- [414] Poulikakos L V, Dionne J A and García-Etxarri A 2019 Optical helicity and optical chirality in free space and in the presence of matter *Symmetry* **11** 1113
- [415] Owens A, Yachmenev A, Yurchenko S N and Küpper J 2018 Climbing the rotational ladder to chirality *Phys. Rev. Lett.* **121** 193201
- [416] Polavarapu P L 2016 Structural analysis using chiroptical spectroscopy: insights and cautions *Chirality* **28** 445
- [417] Polavarapu P L 2006 Determination of molecular stereochemistry using optical rotatory dispersion, vibrational circular dichroism and vibrational raman optical activity *Chiral Analysis* (Elsevier) pp 461–504 (<https://doi.org/10.1016/B978-0-444-51669-5/50014-4>)
- [418] Crassous J, Fuchter M J, Freedman D E, Kotov N A, Moon J, Beard M C and Feldmann S 2023 Materials for chiral light control *Nat. Rev. Mater.* **8** 365
- [419] Pu L 2017 Simultaneous determination of concentration and enantiomeric composition in fluorescent sensing *Acc. Chem. Res.* **50** 1032
- [420] Huang S and Xu X 2021 Optical chirality detection using a topological insulator transistor *Adv. Opt. Mater.* **9** 2002210
- [421] Neubrech F, Hentschel M and Liu N 2020 Reconfigurable plasmonic chirality: fundamentals and applications *Adv. Mater.* **32** 1905640
- [422] Castiglioni E, Abbate S and Longhi G 2011 Experimental methods for measuring optical rotatory dispersion: survey and outlook *Chirality* **23** 711
- [423] Fernandez-Corbaton I, Rockstuhl C, Ziemke P, Gumbsch P, Albiez A, Schwaiger R, Frenzel T, Kadac M and Wegener M 2019 New twists of 3D chiral metamaterials *Adv. Mater.* **31** 1807742
- [424] Qian F *et al* 2018 New magnetic phase of the chiral skyrmion material Cu_2OSeO_3 *Sci. Adv.* **4** eaat7323

- [425] Duan Y and Che S 2023 Chiral mesostructured inorganic materials with optical chiral response *Adv. Mater.* **35** 2205088
- [426] Solomon M L, Saleh A A E, Poulidakos L V, Abendroth J M, Tadesse L F and Dionne J A 2020 Nanophotonic platforms for chiral sensing and separation *Acc. Chem. Res.* **53** 588
- [427] Kobrinski H and Cheung K-W 1989 Wavelength-tunable optical filters: applications and technologies *IEEE Commun. Mag.* **27** 53
- [428] Kenanakis G, Zhao R, Katsarakis N, Kafesaki M, Soukoulis C and Economou E 2014 Optically controllable THz chiral metamaterials *Opt. Express* **22** 12149
- [429] Romanazzi G, Degennaro L, Mastroilli P and Luisi R 2017 Chiral switchable catalysts for dynamic control of enantioselectivity *ACS Catal.* **7** 4100
- [430] Blanco V, Leigh D A and Marcos V 2015 Artificial switchable catalysts *Chem. Soc. Rev.* **44** 5341
- [431] Firouzeh S, Hossain M A, Cuerva J M, de Cienfuegos L A and Pramanik S 2024 Chirality-induced spin selectivity in composite materials: a device perspective *Acc. Chem. Res.* **57** 1478–87
- [432] Aiello C D *et al* 2022 A chirality-based quantum leap *ACS Nano* **16** 4989
- [433] Zhao B, Yang S, Deng J and Pan K 2021 Chiral graphene hybrid materials: structures, properties and chiral applications *Adv. Sci.* **8** 2003681
- [434] Tan L, Yu S-J, Jin Y, Li J and Wang P-P 2022 Inorganic chiral hybrid nanostructures for tailored chiroptics and chirality-dependent photocatalysis *Angew. Chem., Int. Ed.* **61** e202112400
- [435] Zhong H, Zhao B and Deng J 2021 Chiral magnetic hybrid materials constructed from macromolecules and their chiral applications *Nanoscale* **13** 11765
- [436] Altaf A, Hassan S, Pejic B, Baig N, Hussain Z and Sohail M 2022 Recent progress in the design, synthesis and applications of chiral metal-organic frameworks *Front. Chem.* **10** 1014248
- [437] Cho N H, Guerrero-Martínez A, Ma J, Bals S, Kotov N A, Liz-Marzán L M and Nam K T 2023 Bioinspired chiral inorganic nanomaterials *Nat. Rev. Bioeng.* **1** 88
- [438] Zhang Y, Arias-Muñoz J C, Cui X and Sun Z 2023 Prospect of optical chirality logic computing *Appl. Phys. Lett.* **123** 240501
- [439] Zhang Y *et al* 2022 Chirality logic gates *Sci. Adv.* **8** eabq8246
- [440] Chen H, Wu W, Zhu J, Yang S A and Zhang L 2021 Propagating chiral phonons in three-dimensional materials *Nano Lett.* **21** 3060
- [441] Yadav A K *et al* 2016 Observation of polar vortices in oxide superlattices *Nature* **530** 198
- [442] Kim K T *et al* 2022 Chiral structures of electric polarization vectors quantified by x-ray resonant scattering *Nat. Commun.* **13** 1769
- [443] Damodaran A R *et al* 2017 Phase coexistence and electric-field control of toroidal order in oxide superlattices *Nat. Mater.* **16** 1003
- [444] Behera P *et al* 2022 Electric field control of chirality *Sci. Adv.* **8** eabj8030
- [445] Gómez-Ortiz F, García-Fernández P, López J M and Junquera J 2022 Melting of crystals of polarization vortices and chiral phase transitions in oxide superlattices *Phys. Rev. B* **105** L220103
- [446] Tikhonov Y *et al* 2020 Controllable skyrmion chirality in ferroelectrics *Sci. Rep.* **10** 8657
- [447] Gao L, Prokhorenko S, Nahas Y and Bellaiche L 2024 Dynamical control of topology in polar skyrmions via twisted light *Phys. Rev. Lett.* **132** 026902
- [448] Chen W J, Zheng Y and Wang B 2015 Large and tunable polar-toroidal coupling in ferroelectric composite nanowires toward superior electromechanical responses *Sci. Rep.* **5** 11165
- [449] Liu J, Ji Y, Yuan S, Ding L, Chen W and Zheng Y 2018 Controlling polar-toroidal multi-order states in twisted ferroelectric nanowires *npj Comput. Mater.* **4** 78
- [450] Prosandeev S, Ponomareva I, Kornev I, Naumov I and Bellaiche L 2006 Controlling toroidal moment by means of an inhomogeneous static field: an *ab initio* study *Phys. Rev. Lett.* **96** 237601
- [451] Naumov I and Fu H 2007 Vortex-to-polarization phase transformation path in ferroelectric Pb(ZrTi)O₃ nanoparticles *Phys. Rev. Lett.* **98** 077603
- [452] Prosandeev S, Akbarzadeh A R and Bellaiche L 2009 Discovery of incipient ferrotoroidics from atomistic simulations *Phys. Rev. Lett.* **102** 257601
- [453] Prosandeev S, Kornev I and Bellaiche L 2007 Tensors in ferroelectric nanoparticles: first-principles-based simulations *Phys. Rev. B* **76** 012101
- [454] Prosandeev S, Ponomareva I, Naumov I, Kornev I and Bellaiche L 2008 Original properties of dipole vortices in zero-dimensional ferroelectrics *J. Phys.: Condens. Matter* **20** 193201
- [455] Nahas Y, Prokhorenko S, Louis L, Gui Z, Kornev I and Bellaiche L 2015 Discovery of stable skyrmionic state in ferroelectric nanocomposites *Nat. Commun.* **6** 8542
- [456] Das S *et al* 2019 Observation of room-temperature polar skyrmions *Nature* **568** 368
- [457] Stengel M 2023 Macroscopic polarization from nonlinear gradient couplings (arXiv:2304.06613 [cond-mat.mtrl-sci])
- [458] Zhao H J, Chen P, Prosandeev S, Artyukhin S and Bellaiche L 2021 Dzyaloshinskii–Moriya-like interaction in ferroelectrics and antiferroelectrics *Nat. Mater.* **20** 341
- [459] Junquera J 2021 Dzyaloshinskii–Moriya interaction turns electric *Nat. Mater.* **20** 291
- [460] Chen P, Zhao H J, Prosandeev S, Artyukhin S and Bellaiche L 2022 Microscopic origin of the electric Dzyaloshinskii–Moriya interaction *Phys. Rev. B* **106** 224101
- [461] 2024 Crafting moiré and chirality in two dimensions *Nat. Mater.* **23** 301
- [462] Zhu H and Yakobson B I 2024 Creating chirality in the nearly two dimensions *Nat. Mater.* **23** 316
- [463] Schaufelberger L, Merkel M E, Tehrani A M, Spaldin N A and Ederer C 2023 Exploring energy landscapes of charge multipoles using constrained density functional theory *Phys. Rev. Res.* **5** 033172
- [464] Bhowal S and Spaldin N A 2022 Magnetoelectric classification of skyrmions *Phys. Rev. Lett.* **128** 227204
- [465] Hayami S and Kusunose H 2018 Microscopic description of electric and magnetic toroidal multipoles in hybrid orbitals *J. Phys. Soc. Japan* **87** 033709